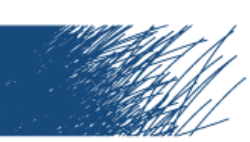


UNIVERSITEIT GENT

FACULTY OF SCIENCES

SYSTEMATIC STUDIES OF ELECTROCHEMICAL NUCLEATION AND GROWTH OF COPPER ON RU-BASED SUBSTRATES FOR DAMASCENE PROCESS.

Magi Margalit Nagar

Promotor: Prof. Dr. Katrien Strubbe
Supervisors: Prof. Dr. Philippe M. Vereecken
Dr. Aleksandar Radisic

Dissertation presented in fulfillment of the requirements for the degree of Doctor of Science: Chemistry.

October 2013

Gent University
Department of Inorganic and physical chemistry,
Krijgslaan 281 S3, 9000 Gent, Belgium.

SYSTEMATIC STUDIES OF ELECTROCHEMICAL NUCLEATION AND GROWTH OF COPPER ON RU-BASED SUBSTRATES FOR DAMASCENE PROCESS.

Magi Margalit Nagar

Members of the Examination Committee:
Prof. Dr. Klaartje De Buysser
Prof. Dr. Christophe Detavernier
Prof. Dr. Philippe Vereecken
Dr. Aleksandar Radisic
Prof. Dr. Katrien Strubbe
Dr. Petra Lommens
Prof. Dr. Zeger Hens
Dr. Edward Matthijs
Dr. Johan De Baets

Dissertation presented in fulfillment
of the requirements for the degree of
Doctor of Science: Chemistry.
Magi Margalit Nagar

In collaboration with IMEC , Interuniversity Microelectronics Centre,
Kapeldreef 75, B-3001 Heverlee, Belgium.

“I'd rather be in the mountains thinking of God than in church thinking about the mountains"

-John Muir (1838-1914)

Dedicated to people I have in my life, to people I’ve lost and to people I’ve found, who help me to understand that everything around me invites me to grow.

LIST OF ABBREVIATIONS

DP	direct plating
AFM	atomic force microscopy
ECD	electrochemical deposition
PVD	physical vapor deposition
PEG	polyethylene glycol
RDE	rotating disk electrode
RE	reference electrode
CE	counter electrode
WE	working electrode
SEM	scanning electron microscope
SHE	standard hydrogen electrode
ICs	integrated circuits
SSI	small-scale integration
ULSI	ultra-large-scale integration
CMP	chemical mechanical planarization
Ru	ruthenium
CV	cyclic voltammetry
GS	galvanostatic measurements
CA	chronoamperometry
CVD	chemical vapor deposition
ALD	atomic layer deposition
UPD	underpotential deposition
SE	secondary electrons
TOF-SIMS	time-of-flight secondary ion mass spectrometry
PCB	printed circuit board
EIS	electrochemical impedance spectroscopy
OCP	open-circuit potential
Mw	molecular weight
SERS	surface enhanced raman spectroscopy
ZCP	zero-current potentials
3D	three-dimensional
OPD	overpotential deposition

LIST OF SYMBOLS

N_p	cm^{-2}	island density
N_{Nucl}	cm^{-2}	the island density at η_{IRNuc}
U	V	electrode potential
$U_{(Cu^{2+}/Cu),eq}$	V	equilibrium potential difference
η	V	overpotential for copper deposition
η_{IR}	V	overpotential corrected for IR drop for copper deposition
η_{IRNucl}	V	overpotential corrected for IR drop for copper nucleation
$\eta_{IRCu/RuTa}$	V	capture overpotential region for growth of 3D copper islands on RuTa electrode in the absence of suppressor
η_{IRCu}	V	capture overpotential region for deposition of copper on copper electrode in the absence of suppressor
$\eta_{IRCuSup/RuTa}$	V	capture overpotential region for growth of 3D copper islands on RuTa electrode in the presence of suppressor
$\eta_{IRCuSup}$	V	capture overpotential region for deposition of copper on copper electrode in the presence of suppressor
i	$A\ cm^{-2}$	current density
I	A	current
F	$96{,}485\ C\ mol^{-1}$	Faraday constant
n	dimensionless	number of electrons
D	$cm^2\ s^{-1}$	diffusion coefficient
R_s	Ω	series resistance
C_b	$mol\ cm^{-3}$	bulk concentration
C_s	$mol\ cm^{-3}$	Surface concentration
Mw	$g\ mol^{-1}$	molecular weight
ρ	$g\ cm^{-3}$	copper density
t_{coal}	s	time when the copper islands coalesce
t_c	s	critical time for the potential drop seen in the galvanostatic measurements
t'_c	s	critical time for 100% copper coverage at the RuTa electrode observed in SEM
q_{Cu}	$C\ cm^{-2}$	charge density for copper deposition
$A_{p\ (Cu)}$	cm^2	surface area of one copper island
A_{Cu}	dimensionless	effective surface area of total deposited copper
A_{eff}	dimensionless	total effective electrode area
K	$C\ cm^{-3}$	material constant

d	cm	island diameter
d_{coal}	cm	island diameter at coalescence
b_{coal}	nm	coalescence thickness
T	kelvin	temperature
x	dimensionless	shape factor
α	dimensionless	transfer coefficient
R	8.314 $J \cdot mol^{-1} \cdot K^{-1}$	universal gas constant

LIST OF PUBLICATIONS

Conference proceedings

1. **M. Nagar**, A. Radisic, K. Strubbe, P.M. Vereecken, Tailoring copper island density for copper plating on a RuTa substrate, ECS Transactions, 28(29) (2010) 9.
2. **M. Nagar**, A. Radisic, K. Strubbe, P.M. Vereecken, Nucleation and growth of copper on Ru-based substrates, I: the effect of the inorganic components, ECS Transactions, 41(35) (2012) 75.
3. **M. Nagar**, A. Radisic, K. Strubbe, P.M. Vereecken, Nucleation and growth of copper on Ru-based substrates, II: the effect of the suppressor additive, ECS Transactions, 41(35) (2012) 99.

Journal papers

1. **M. Nagar**, A. Radisic, K. Strubbe, P.M. Vereecken, The effect of cupric ion concentration on the nucleation and growth of copper on RuTa seeded substrates, Electrochimica Acta 92 (2013) 474.
2. **M. Nagar**, A. Radisic, K. Strubbe, P.M. Vereecken, The Effect of Polyether Suppressors on the Nucleation and Growth of Copper on RuTa Seeded Substrate for Direct Copper Plating, under preparation.

ABSTRACT

The integration of copper in the IC manufacturing process is implemented by a Dual Damascene technology, where copper is electrochemically deposited on a conductive Cu seed layer. The continuing trend toward dimensional shrinkage in the Cu metallization technology requires alternative integration schemes, where the Cu seed layer is eliminated entirely, and platable barrier materials or alternative seed layers are introduced. Direct plating (DP) is one of the alternative approaches introduced in the damascene interconnects technology to overcome issues arising due to the continuous shrinkage in interconnect line dimensions. According to DP approach, copper electrodeposition (ECD) is performed directly on a thin resistive barrier or alternative seed material i.e. not on a Cu seed as it is conventionally performed within the damascene process.

Copper ECD on top of a foreign substrate is a well-known process and there is a vast amount of information available about it. However, there are several challenges to overcome when performing the process on a wafer level. Copper ECD on substrates other than copper involves electrochemical nucleation and growth processes. This has a significant impact when characteristic dimensions of the features to be filled are below 30 nm. In order to fill features with such small dimensions, a continuous copper thin film must first be formed in-situ inside the small features and across the whole 300 nm wafer. This in-situ formed seed layer then serves as a wetting layer for the copper ECD process and enables void-free filling. To achieve void-free filling, a high island density and quasi 2D growth of Cu islands are necessary. Therefore, a control over the island density, N_p, and the growth mode is essential for DP to succeed.

The main goal of this work was to gain a fundamental understanding of the nucleation and growth phenomena during galvanostatic deposition of copper on RuTa. This knowledge was used to explore the conditions that can best increase nucleation and promote quasi 2D growth of Cu islands leading to rapid coalescence into a continuous film on Ru-based layers with the hope of filling narrow features. The nucleation and growth of Cu was investigated as a function of various factors, including different substrates, solution composition, surface pre-treatment methods, and deposition parameters. The thinnest continuous Cu film on RuTa was found using high current density (-5 to -10 mA cm^{-2}), low Cu^{2+} concentration (0.01 M $CuSO_4$) and

Polyoxyethylene cetyl ether (Mw 1124) suppressor. It was also shown that an electrochemical clean with 10% Vol. H_2SO_4 can give N_p much closer to the one observed for Pt due to oxide removal. Finally, successful filling of 20 nm trenches was demonstrated using a two-step process from the same bath. The optimal conditions for seed formation was -5 mA cm^{-2} to grow ~2.5 nm seed layer. Then switching to a -1.2 mA cm^{-2} current density for filling the 20 nm trench.

Furthermore, electrochemical experimental techniques, such as cyclic voltammetry and chronopotentiometry, were combined with surface characterization technique, such as scanning electron microscopy, to examine the relationship between the overpotential, and the island density, island shape, and coalescence thickness. Based on these results, a method was developed to interpret the galvanostatic transients in order to correlate N_p with deposition overpotential.

TABLE OF CONTENTS

CHAPTER 1: INTRODUCTION

1.1 Microelectronics: evolution in interconnects technology

The use of complex electronic systems evolved throughout the last decade due to developments in integrated circuits (ICs) technology. The integrated circuit (IC) is a device that combines electronic components (such as transistors, resistors, diodes etc.) to perform a specific electronic function. This IC is embedded on a small silicon plate, also known as a "chip", with typical dimensions between a few millimeters and a few centimeters. The interesting history of ICs began in the late 50's when the first germanium-based and silicon-based ICs were invented [1-3]. These very simple ICs consisted of only a few transistors and thus their performance was relatively simple [1-3]. The desire to increase the IC performance, i.e. to have a chip that performs multiple tasks and calculations, required more electronic components in one chip. The term "downscaling" was coined when the components density in one chip increased. And so, over time, the ICs technology advanced from small-scale integration (SSI), consisting up to 100 components per interconnect (in the early 60s) to ultra-large-scale integration (ULSI)**,** consisting more than 1 million components per chip (nowadays). The rapid growth in IC technology towards ULSI required a larger number of metal lines per interconnect level, more interconnect levels, and at the same time a reduction in the interconnect line critical dimensions [1-3]. The aluminum-based interconnects technology, which was the dominant technology in the early days of modern microelectronics, could not have provided the desired circuit performance (e.g., speed, number of devices, chip area) due to the aluminum resistivity (2.65 μΩ) [1-3]. And thus, due to the continuous shrinkage in interconnect line dimensions, other materials were required to replace the aluminum-based interconnects. Copper was found a suitable substitute due to its low resistivity (1.68 μΩ) and better electromigration resistance.

1.2 Copper interconnect technology

The fabrication of copper interconnects was first introduced into manufacturing in 1997 by IBM [4]. The fabrication of copper interconnects is achieved by a damascene process. Figure 1.1

shows a flow chart diagram of the dual damascene process. The fabrication begins with deposition of a dielectric material such as SiO_2, followed by the etching of trench line or via-holes into the layer by lithography methods. Subsequently, a thin layer of barrier material such as TaN or TiN, is formed by a dry process such as physical vapor deposition (PVD). After the formation of the barrier layer, a thin copper seed layer is deposited on top of the barrier material by means of PVD. The diffusion barrier is required to prevent copper from diffusing into the silicon transistor, while the copper seed layer provides a good electrical contact and adhesion to the diffusion barrier layer. After that, copper is electrodeposited in order to fill the trenches and via holes. After the copper filling process, the excessive metal deposited outside the trenches and vias is removed by using chemical mechanical planarization (CMP) process. These steps are repeated until the required number of metallization layers is achieved (see Figure 1.2).

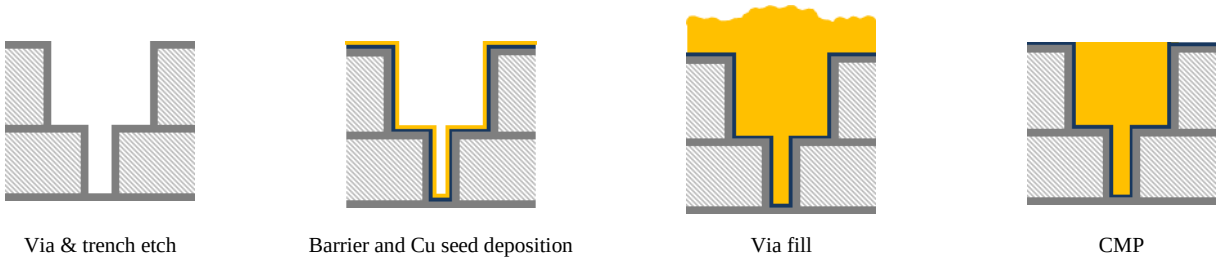

Figure 1.1: Flow chart diagram of a single Cu-damascene process.

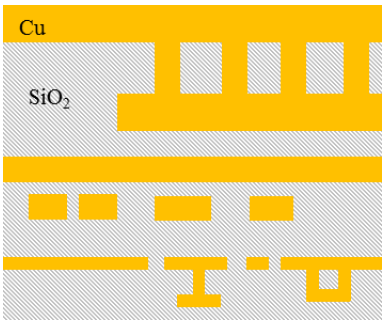

Figure 1.2: Schematic of a 6-level Cu wiring structure exhibiting the wiring hierarchy [5].

However, as the feature sizes decrease and aspect ratios increase, new challenges arise in obtaining conformal and continuous barrier/seed layers with the current PVD deposition methods. Besides that, the barrier/copper seed layers occupy a larger area fraction with respect to the trench and via openings. This could lead to pinch off at the feature opening during electrodeposition and consequently to void formation in the inlaid trench and via features. With

each advanced technology node, the thickness of barrier and copper seed layers are therefore scaled down as well. Armini and Vereecken [6,7] performed full wafer copper plating experiments on Cu seed layers with varied thicknesses between 5 and 150 nm. They showed that the minimum Cu seed layer thickness is limited by seed corrosion, as the severe potential drop across the resistive substrate, the so-called terminal effect, does not longer provide sufficient cathodic protection of the copper seed in the center of the wafer [6,7]. Therefore, alternative integration schemes are investigated where the Cu seed layer is eliminated altogether and platable materials (novel barrier or alternative seed layers) are introduced [8-10]. Figure 1.3 illustrates the challenges arising due to the shrinkage in interconnect size and direct plating (DP), as an alternative path to overcome these issues.

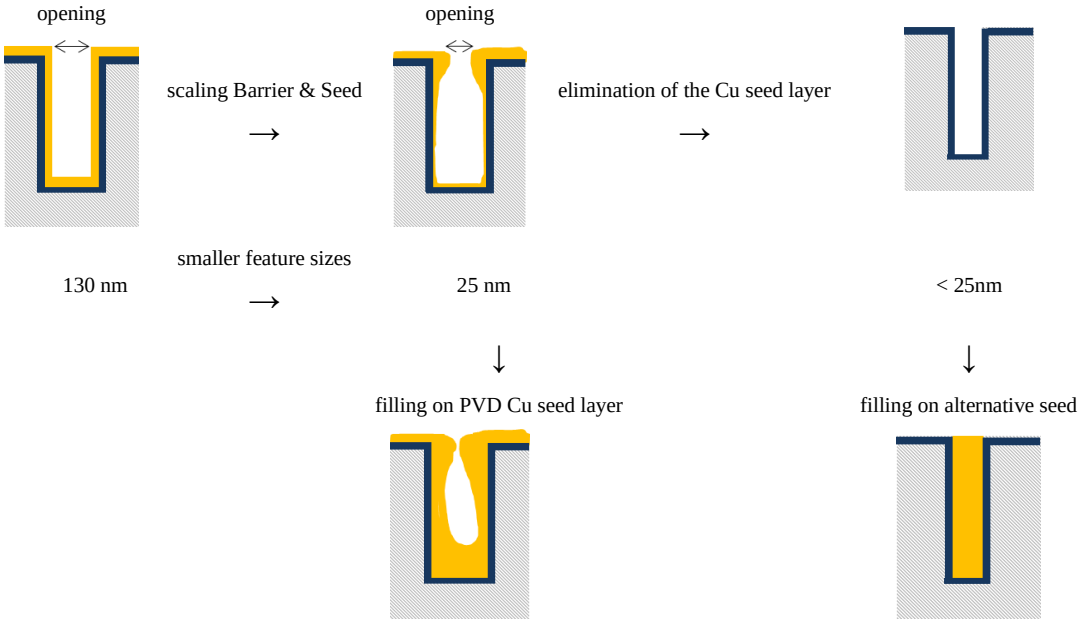

Figure 1.3: Schematic view of the challenges arising due to the shrinkage in interconnect size and DP, as an alternative path to overcome these issues.

1.3 Direct plating approach and requirements

The term “direct plating” (DP) was coined, when the downscaling technology required alternative integration schemes for the damascene process. In the case of direct plating, copper electrodeposition proceeds directly on the platable barrier/seed. The conductive Cu seed layer could be replaced, for example by a noble metal such as Ruthenium (Ru). In the effort to reduce

the area fraction of the barrier and seed layers with respect to the feature size, Ru alloys such as RuTa and RuTiN are also investigated [11,12]. Electrodeposition of copper on a foreign substrate proceeds through electrochemical nucleation and growth processes. In general, three different growth modes can be identified (Figure 1.4): layer by layer (Frank-van der Merwe growth), 3D island formation (Volmer-Weber growth) and 2D layer deposition followed by the growth of 3D islands (Stranski-Krastanov growth) [13].

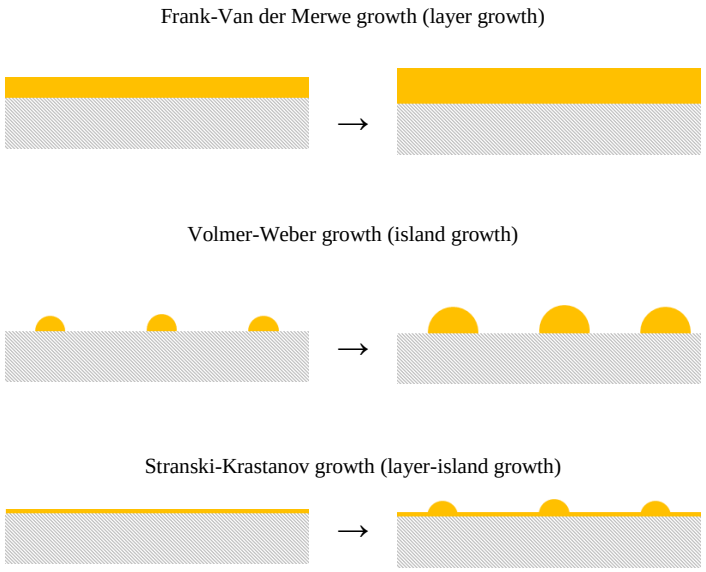

Figure 1.4: Thin film growth modes.

In many cases, deposition of copper onto foreign substrates follows a 3D island growth mechanism [8,14] i.e. either Volmer–Weber or Stranski-Krastanov growth modes. For both cases, Cu islands are formed and grow until they coalesce into a continuous film. The coalescence thickness, b_{coal}, is defined as the equivalent film thickness when islands coalesce into a continuous film for a certain deposited charge. Figure 1.5 shows two extreme cases for copper deposition on RuTa to illustrate the dependency of b_{coal} on the island density, N_p. In case (a), the island density was high and the electrodeposited Cu islands coalesced after a deposition time of 10*s* with b_{coal} equal to 70 nm. In case (b) the N_p was too low and the electrodeposited Cu islands did not coalesce within 50*s* of deposition. Instead, sphere-like Cu islands with average diameter of about 700 nm were formed on the RuTa surface.

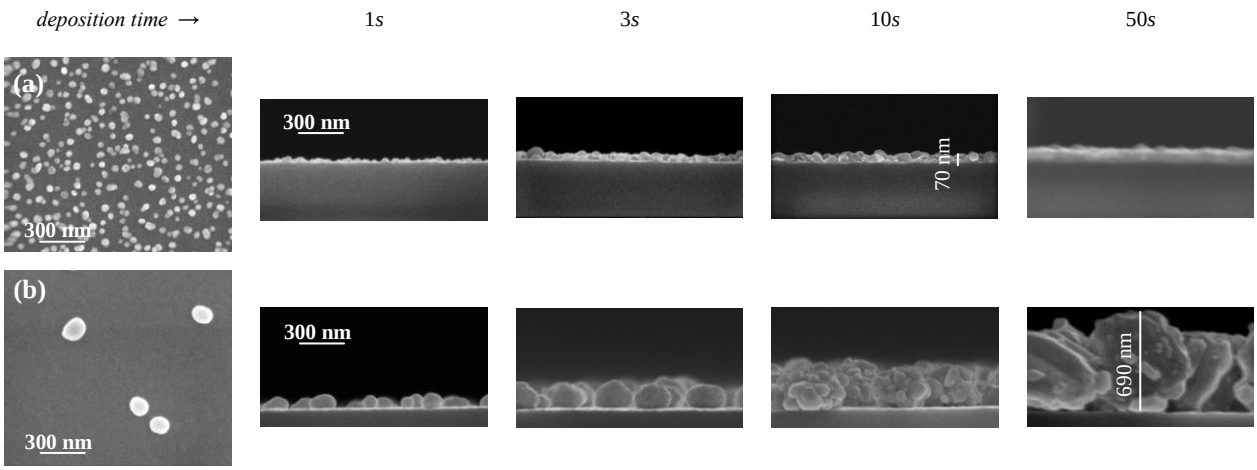

Figure 1.5: Top-view and cross sessional SEM images illustrating N_p, shape and coalescence of the Cu islands subsequent to copper deposition on RuTa from a solution of 1.8 M H_2SO_4, 1.4×10^{-3} M HCl and (a) 0.01 M $CuSO_4$ (b) 0.6 M $CuSO_4$ at current density of -10 mA cm^{-2} for different deposition times (1, 3, 10 and 50*s*).

The theoretical coalescence thickness can, for different island shapes, be calculated when assuming the ideal case of a hexagonal closed pack stacking for the Cu islands (see also Appendix). Figure 1.6 shows the b_{coal} dependency on N_p for 3D hemispherical islands (open squares) and for flattened islands towards 2D or "pancake-shaped" particles (open circles). From fig. 1.6 it can be seen that, in order to achieve a 5 nm continuous Cu film, N_p of about ~10^{12} cm^{-2} is required in the case of 3D hemispherical islands. However, the requirements for N_p can be lowered if a quasi 2D growth is promoted (see Figure 1.6). Thus, the coalescence thickness depends not only on the island density, N_p, but also on the geometry of the islands.

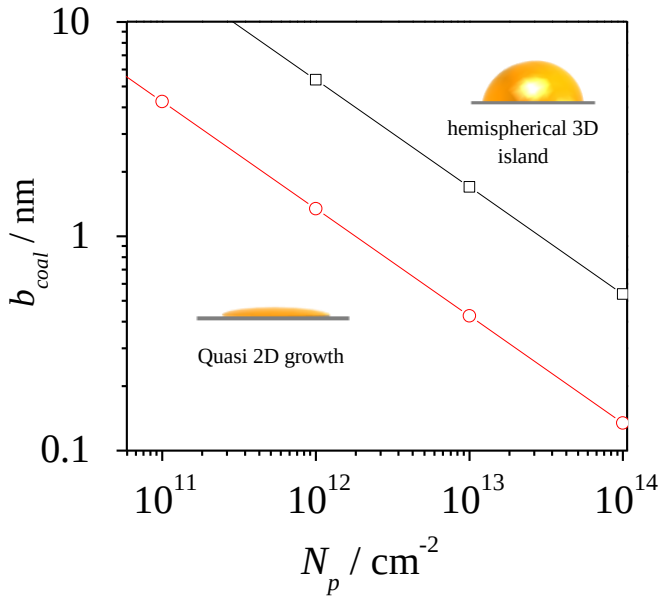

Figure 1.6: Coalescence thickness as a function of island density when an ideal case of hexagonal stacking of Cu islands is assumed. (□) for hemispherical islands with ratio between the island diameter, *d*, and its height, *h*, equal to 2 and (○) for quasi 2D growth with *d/h* ratio equal to 16 (see also Appendix).

In order to fill sub-30 nm features with copper efficiently by DP, a continuous Cu film with thickness of about 3 nm is required. The coalescence of copper nuclei with formation of this 3 nm thin continuous copper layer (in-situ formed wet seed) should be fast and within the small feature opening. Figure 1.7 illustrates the importance of a high N_p and a coalescence thickness that is sufficiently small during the plating of narrow trenches with a RuTa seeded substrate. In Figure 1.7(a), the island density is high, which leads to coalescence of the islands inside the feature. Figure 1.7(b) shows an extreme case where the island density, N_p is too low to form a coalesced copper film. In conclusion, for direct plating to succeed, the copper seed layer needs to be formed in-situ during the first stages of the plating process when targetting the fill from the same Cu bath. To meet this requirement, it is necessary to find a way to achieve island densities higher than 10^{13} cm^{-2}, in case of 3D hemispherical islands or alternatively to find a way to promote quasi 2D growth. For that purpose, it is essential to understand the phenomena of nucleation and growth of copper on RuTa, and the influence of parameters such as potential and bath composition in a profound way. This knowledge will allow better control and may lead to void-free filling of sub-30 nm features.

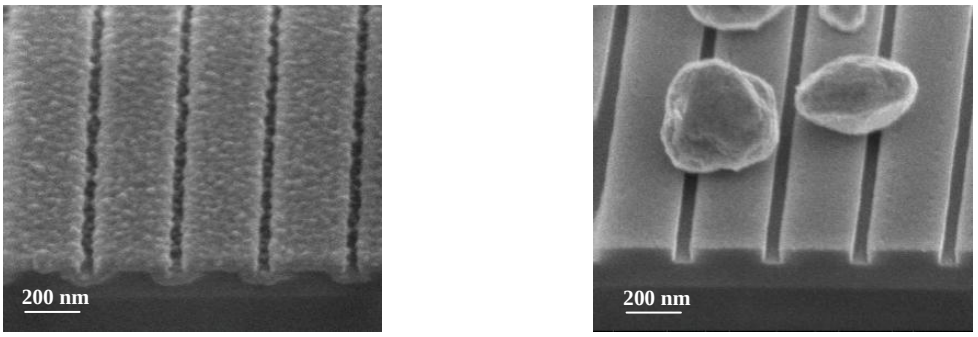

(a) (b)

Figure 1.7: Tilted SEM images of 50 nm trenches with 2 nm PVD RuTa subsequent to copper deposition showing two extreme cases, illustrating the importance of achieving a thin coalescence thickness. Copper deposition was performed at constant current density of -10 mA cm^{-2} for 1*s* from solutions of 1.8 M H_2SO_4, 1.4×10^{-3} M HCl and (a) 0.01 M $CuSO_4$ (b) 0.6 M $CuSO_4$.

After achieving the formation of a continuous thin Cu film inside the features, the next challenge is to achieve void-free fill of the small features (Figure 1.8). Note that once the Cu seed layer is formed along the sidewalls of features, feature fill commences. This can be performed with 2 steps deposition, using an alkaline Cu bath for the seed formation followed by a fill from an acidic Cu bath. More preferably, 1 step deposition can be performed using only the acidic Cu bath for both seed formation and fill. The deposition conditions for feature filling could be quite different than those, needed for the formation of the Cu seed layer. Therefore, another challenge is to find the conditions in which both the formation of the wet seed and the filling of the sub-30 nm features are possible from the same acidic Cu plating bath.

Figure 1.8: Schematic representation of in-situ wet Cu-seed formation and subsequent Cu fill of individual features.

During this process, however, it is not only necessary to achieve void-free fill in the small features but also to have a fast propagation rate of the Cu front across the large resistive substrate (the wafers are currently 300 mm in diameter and will go to 450 mm in the near future) [6,7]. Plating copper on a highly resistive wafer results in highly non-uniform current distribution, and

a formation of a Cu film front propagating along the wafer radius, from the edge of the wafer, where the electrical contact is, toward the center of the wafer [6,7]. Due to this so-called terminal effect, features closer to the electrical contact will be plated first and those close to the center last (Figure 1.9). Note that in the areas where the current density is low (at the edge of the copper front), the nucleation density would be smaller than at the edge of the wafer (where the electrical contact is), where the current density is large and Cu islands already coalesced into a continuous film. This could lead to poor filling of the sub-30 nm features in these areas [15]. Therefore, information on the deposition conditions that would allow a uniform filling across the 300 mm wafer is needed. Thus, it is necessary to determine the set of deposition parameters and the Cu bath composition that allows 'in-situ' Cu wet seed formation with an almost simultaneous (closely followed) void-free fill of the features, and constant radial velocity of the Cu front propagating from the edge of the wafer (electrical contact) to the center.

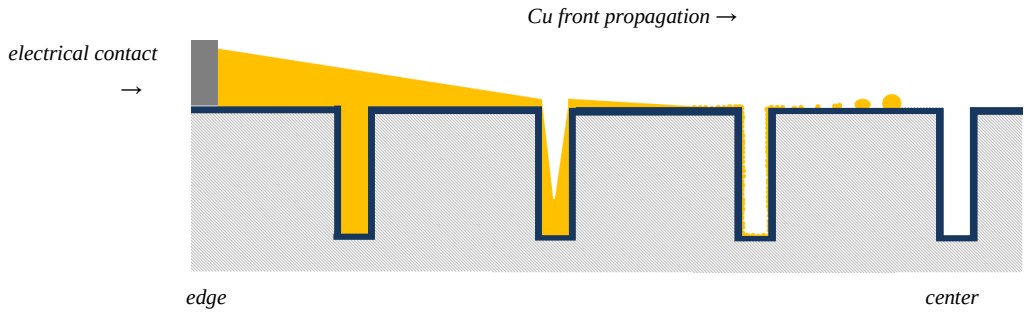

Figure 1.9: Schematic illustration of Cu front propagation with simultaneous in-situ wet seed formation, Cu fill of individual features and electrocystallization of Cu islands across a wafer.

Electrochemical nucleation and growth (electrocrystallization) of metals on top of a foreign substrate is by itself not an uncommon phenomenon. The term electrocrystallization was first coined back in the 40s by Fischer who described crystallization as a process in which mass transfer is accompanied by charge transfer [16]. The early development of the subject has been summarized by Bockris and Razumney [17] and throughout time, metal electrodeposition has been extensively studied from both the theoretical and the practical point of view [18-24]. In the case of metal electrodeposition, metal ions diffuse through a solution and are reduced on a substrate (an electrode). Generally, as in any other physical system, a minimum of additional energy is required to initiate the nucleation of metal atoms on the electrode surface. In electrodeposition, this extra energy is provided by applying a so-called overpotential, η, which

equals the difference between the electrode potential (U) and equilibrium electrode potential, U_{eq}, hence $\eta = U - U_{eq}$. The nucleation will then start when the overpotential, η, surpasses the overpotential for nucleation, η_{Nucl} i.e. when the system is out of its equilibrium. As η is the driving force for nucleation, many studies analyze the electronucleation phenomenon from an electrochemical point of view. Electrochemical techniques, such as cyclic voltammetry (CV), chronoamperometry (CA) and galvanostatic measurements (GS) are commonly used to study the process of electrochemical nucleation and growth [18-24]. From these techniques, most reports can be found on chronoamperometry as there are several available models that can be used to interpret and analyze the data [18-22]. In a typical chronoamperometry experiment, a potential is applied and the corresponding current transient is monitored. The analysis of current-time curves, recorded at different potentials, can provide information on the nucleation rate, the growth mechanism and the island density [18-22]. In contrast, the galvanostatic technique is less used as the overpotential continuously changes in order to sustain constant deposition current and thus, the analysis of the data is more difficult than in the case of chronoamperometry [23,24]. The most important issue to overcome in case of nucleation under galvanostatic conditions is to find a theoretical expression for the overpotential as a function of time [23,24]. However, the electrodeposition for industrial applications is mostly carried out at constant deposition current, i.e. under galvanostatic control. The development of galvanostatic nucleation and growth theories would provide fundamental information to better control these processes and therefore, would be very beneficial from industrial point of view.

Even though copper electrodeposition has a long history, many challenges still exist in developing a process which allows the filling of small features with copper and particularly on a wafer scale. One of the main challenges is to control the island density, N_p, and the geometry of the copper nuclei (i.e. towards pseudo-2D islands). In this perspective, the complexity of the bath chemistry, together with the incomplete understanding of the mechanism of electrochemical nucleation and growth, makes the theoretical prediction of N_p and island shape difficult. Indeed, many studies show island or nucleus densities as a function of applied potential but the relationship with overpotential is often ignored or considered irrelevant [18,19]. The use of overpotential is extremely important because it allows one to compare between different substrates, different chemistries and different deposition parameters. In this work, the overpotnetial was correlated to the N_p for different substrates, different chemistries and different

deposition current densities. This correlation shows that the overpotential can be manipulated by changing the bath chemistry or deposition parameters for a given substrate and allows better control the N_p.

1.4 Objectives of the thesis

The nucleation and growth of copper on different substrates was investigated by means of electrochemical techniques. In order to gain insight to these processes, several parameters were investigated and are reported in the experimental Chapters.

The main objectives of this study were:

- To investigate the effect of bath composition on the nucleation and growth of copper on RuTa substrate during galvanostatic deposition (constant current).
- To investigate the effect of deposition parameters on the nucleation and growth of copper on RuTa substrate during galvanostatic deposition.
- To correlate between electrochemical parameters such as overpotential to physical parameters such as N_p, island shape and coalescence thickness.
- To investigate the conditions that would allow the filling of 20 nm features by DP.

1.5 Outline of the thesis

Chapter 2 provides detailed description of the experimental work and discusses briefly the analysis techniques that are relevant for this thesis. In the other Chapters, a first part (Chapters 3, 4, 5 & 6) describes the nucleation and growth of Cu on blanket RuTa wafers under different conditions, whereas part 2 of the study, (Chapter 7) describes the filling of 20 nm features. For each Chapter, a detailed introduction section, related to the specific topic under investigation, is provided.

Chapter 3 is dedicated to studying the effects of the inorganic components in the plating bath on N_p and island shape. As the inorganic components are the basic ingredients of the plating bath, this Chapter provides an introduction to the basic bath chemistry which has a significant

effect on the N_p and island shape. In this Chapter, the effect of each component in the plating bath is investigated separately to show the exact effect on the nucleation and growth mechanism.

Chapter 4 is dedicated to studying the effects of the cupric ions and the current density on N_p and island shape. In this Chapter galvanostatic transients are used to correlate between electrochemical parameters such as overpotential and physical parameters such as nucleation density N_p and coalescence thickness. It is shown that an exponential relationship exists between the island density, N_p, and the actual deposition overpotential in the additive-free $CuSO_4$ solutions, irrespective of the Cu^{2+} concentration and current density.

In Chapter 5, the effect of different polyether molecules on N_p and island shape is studied. For this, the same method as in Chapter 4 is used to interpret the galvanostatic transients. It is shown that the N_p dependency on the overpotential is also valid for the addition of polyether suppressors in the bath for the RuTa substrate.

Chapter 6 deals with the effect of the nature of the substrate on N_p and island shape. For the different substrates under investigation, an exponential dependency of N_p on overpotential is found.

Chapter 7 is dedicated to filling experiments. In this Chapter we use the overall understanding gained in part 1 (optimized solution and conditions) to form an in-situ Cu seed layer and to fill 20 nm features.

Finally, summary and perspectives are given.

The Appendix provides some details of the theoretical calculations used in Chapters 4, 5 & 6.

[1] J. S. Kilby, Invention of the integrated circuit, IEEE Transaction Electron. Devices 23, (1976) 648.
[2] Tapan K. Gupta, Copper Interconnect Technology, New York, Springer Science+Business Media, LLC (2009).
[3] Y. Shacham-Diamand, T. Osaka, M. Datta, T. Ohba, Editors, Advanced Nanoscale ULSI Interconnects:Fundamentals and Applications, New York, Springer Science+Business Media, LLC 2009.
[4] E. Edelstein, J. Heidenreich, R. Goldblatt, W. Cote, C. Uzoh, N. Lustig, Roper, P. McDevitt,T. Motsiff, W.; A. Simon, J. Dukovic, R. Wachnik, H. Rathore, R. Schulz, L. Su, Luce, S.; and Slattery, J.: Full copper wiring in a sub-0.25 um CMOS ULSI technology. IEDM Tech. Dig. (1997) 773.
[5] P. C. Andricacos, Copper on-chip interconnections. The Electrochem. Soc. Interface 8, (1999) 32.
[6] S. Armini, P. M. Vereecken, Impact of "Terminal Effect" on Cu Plating: Theory and Experimental Evidence, ECS Transactions 25 (2010) 185.
[7] S. Armini , Z. Tokei, H. Volders, Z.El-Mekki, A. Radisic, G. Beyer, W. Ruythooren, P. M. Vereecken, Impact of ''terminal effect" on Cu electrochemical deposition: Filling capability for different metallization options, Microelectronic Engineering 88 (2011) 754.
[8] G. Oskam, P. M. Vereecken, and P. C. Searson, Electrochemical Deposition of Copper on n-Si/TiN, Journal of the Electrochemical Society 146 (1999) 1436.
[9] T. P. Moffat, M. Walker, P. J. Chen,J. E. Bonevich, W. F. Egelhoff, L. Richter, C. Witt, T. Aaltonen, M. Ritala, M. Leskel and D. Josella, Electrodeposition of Cu on Ru barrier layers for damascene processing, Journal of the Electrochemical Society 153(1) (2006) C37.
[10] O. Chyan, T.N. Arunagiri and T. Ponnuswamy, Electrodeposition of Copper Thin Film on Ruthenium A Potential Diffusion Barrier for Cu Interconnects, Journal of the Electrochemical Society 150 (2003) C347.
[11] H. Volders, L. Carbonell, N. Heylen, K. Kellens, C. Zhao, K. Marrant, G. Faelens, T. Conard, B. Parmentier, J. Steenbergen, M. Van de Peer, C.J. Wilson, E. Sleeckx, G.P. Beyer, Z. Tokei, V. Gravey, K. Shah, A. Cockburn, Barrier and seed repair performance of thin RuTa films for Cu interconnects, Microelectronics Engineering, 88 (5) (2011) 690.
[12] N. Jourdan, L. Carbonell, N. Heylen, J. Swerts, S. Armini, A. Maestre Caro, S. Demuynck, K. Croes, G. Beyer, Z. Tökei, S. Van Elshocht, and E. Vancoille, Evaluation of metallization options for advanced Cu interconnects application, ECS Transactions 34(1) (2011) 515.
[13] J. A. Venables, G. D. T. Spiller and M. Hanbucken, Nucleation and growth of thin films, Reports on Progress in Physics 47(4) (1984) 399.
[14] L. Guo, and P. C. Searson, On the influence of the nucleation overpotential on island growth in electrodeposition. Electrochimica Acta, 55(13) (2010) 4086.
[15] A. Radisic, M. Nagar, K. Strubbe, S. Armini, Z. El-Mekki, H. Volders, W. Ruythooren and P. M. Vereecken, Copper Plating on Resistive Substrates, Diffusion Barrier and Alternative Seed Layers, ECS Transactions, 25 (27) (2010) 175.
[16] H. Fischer, Elektrokristallisation von Metallen, Z. Elektrochem, 49 (1943) 342.
[17] J.O.M. Bockris and G.A. Razumney, Fundamental aspects of electrocrystallization, New York, Plenum Press (1967) pp. 36.

[18] A. Radisic, F.M. Ross and P.C. Searson, In situ study of the growth kinetics of individual island electrodeposition of copper,Journal of Physical Chemistry 110 (2006) 7862.
[19] A. Milchev, B.R. Scharifker and G. Hills, A potentiostatic study of the electrochemical nucleation of silver on vitreous carbon, Journal of Electroanalytical Chemistry 132 (1982) 277.
[20] B.R. Scharifker and J. Mostany, Three-dimensional nucleation with diffusion controlled growth: Part I. Number density of active sites and nucleation rates per site, Journal of Electroanalytical Chemistry 177(1) (1984) 13.
[21] A. Milchev, T. Zapryanova, Nucleation and growth of copper under combined charge transfer and diffusion limitations, Electrochimica Acta 51 (2006) 2926.
[22] G. Gunawardena, G. Hills, I. Montenegro and B.R. Scharifker, Electrochemical nucleation: Part I. General considerations, Journal of Electroanalytical Chemistry 138 (1982) 225.
[23] D. Kashchiev, Kineticks of the initial stage of electrolytic deposition of metals III. Galvanostatic conditions, thin solid films, 29 (1975) 193.
[24] A. Milchev, M.I. Montenegro, A gavanostatic study of electrochemical nucleation, Journal of Electroanal. Chem. 333 (1992) 93.

CHAPTER 2: SUBSTRATES, EXPERIMENTAL DETAILS AND ANALYSIS TECHNIQUES.

In this thesis, the electrochemical nucleation and growth of copper on Ru-based substrates for the damascene process was investigated. For this purpose, several substrates were used as working electrodes for various electrochemical measurements. The blanket wafers were mainly used to investigate the nucleation and growth of copper under different conditions i.e. to count the resulted N_p subsequent each experiment. The patterned wafer was used for filling experiments of 20 nm features.

2.1 Substrates

Description of the fabrication procedure of the substrates used during the course of this work is given below.

2.1.1 Blanket wafers

- RuTa

RuTa alloy (90 *at.%* Ru and 10 *at.%* Ta) was fabricated using Physical Vapor Deposition (PVD) with EnCoRe II PVD Ta(N)^{TM} chamber from Applied Material. The thickness of the RuTa films was 2 nm with a sheet resistance of 200 Ω Sq^{-1}. To achieve layer thickness non-uniformities below 5% on 300 mm wafers a sequence of deposition and re-sputtering was applied. The RuTa was deposited on top of 600 nm SiO_2, fabricated by Chemical Vapor Deposition (CVD).

- Copper (Cu)

100 and 1200 nm copper films on top of 15 nm Ta/TaN layer were fabricated using PVD with Endura^{TM} chamber from Applied Material. The sheet resistance was 20 and 0.14 Ω Sq^{-1} for the 100 and 1200 nm Cu films, respectively. The Cu/Ta/TaN layers were deposited on top of 600 nm SiO_2, fabricated by Chemical Vapor Deposition (CVD).

- Platinum (Pt)

5 nm Pt film on top of 15 nm Ti layer were fabricated using Physical Vapor Deposition (PVD) with Nimbus chamber from NEXX systems. The sheet resistance of the 5 nm Pt film was 43 Ω Sq^{-1}. The Pt/Ti layers were deposited on top of 300 nm SiO_2, fabricated by Chemical Vapor Deposition (CVD).

2.1.2 Patterned SD-20

The patterned single damascene (SD-20) wafers contained arrays of 20 nm wide trenches with 60 nm spacing in a single SD structure fabricated by Plasma Enhanced CVD (PE-CVD) silicon dioxide (Figure 2.1). Ru/RuTiN barrier layer was deposited on top of the patterned SD-20 wafers. The RuTiN multi-layers were composed of a 1.3 nm closed Ru film on top of a 2.2 nm RuTiN film (79 at.% Ru 21at.%TiN). The Ru/RuTiN layers were fabricated by plasma enhanced Atomic Layer Deposition (PE-ALD) with Colorado™ chamber from Applied Material. The sheet resistance of the top Ru surface was 200 Ω Sq^{-1}.

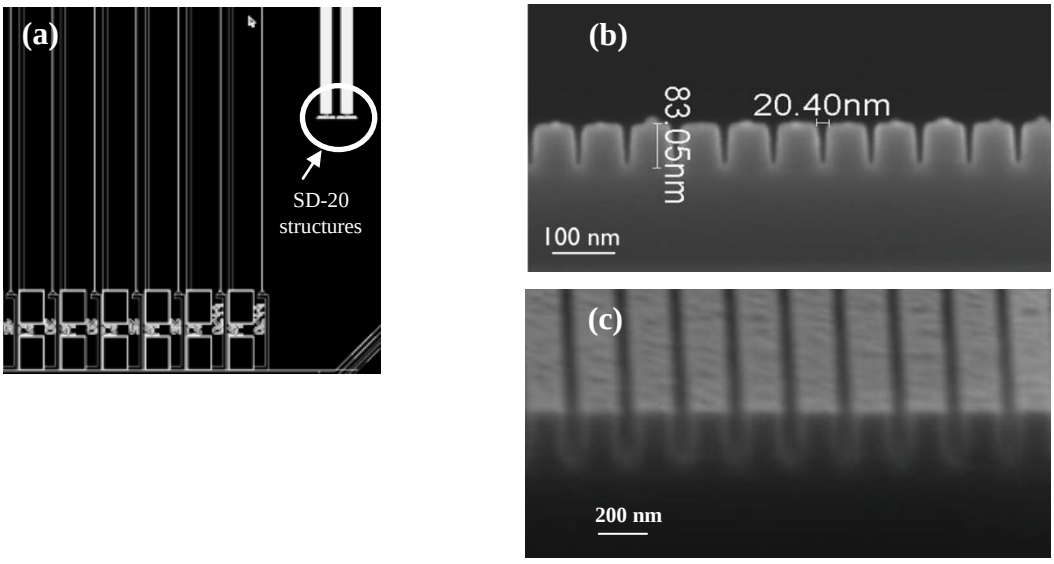

Figure 2.1: Schematic view of (a) the SD-20 structures layout (c) cross-sectional and (d) tilted SEM images showing the 20 nm width trenches with the 60 nm space lines.

2.2 Solution preparation and chemicals

Different solution compositions were used through this thesis in order to investigate the effect of the bath composition on the nucleation and growth of copper on RuTa. Description of the chemicals used during the course of this work is given in Table 2.1. The composition of each solution used for a specific deposition experiment is specified in the experimental paragraph of each Chapter.

Chemical name	*Molecular weight/ g mol^{-1}*	*Molecular formula*	*vendor*
Copper sulfate pentahydrate	249.70 (pentahydrate)	$CuSO_4 \cdot 5H_2O$	> 98%, Alfa Aesar
Sulfuric acid	98.079	H_2SO_4	96% Assay, Baker
Hydrochloric acid	36.46	HCl	37% Assay, Baker
Polyethylene glycol (PEG)	200	$H(OCH_2CH_2)_nOH$	Sigma Aldrich
PEG	400	$H(OCH_2CH_2)_nOH$	Sigma Aldrich
PEG	1000	$H(OCH_2CH_2)_nOH$	Sigma Aldrich
PEG	4000	$H(OCH_2CH_2)_nOH$	Sigma Aldrich
PEG	8000	$H(OCH_2CH_2)_nOH$	Sigma Aldrich
PEG	20000	$H(OCH_2CH_2)_nOH$	Sigma Aldrich
Polyoxyethylene methyl ether (Methyl PEG)	1000	$CH_3(OCH_2CH_2)_nOH$	Sigma Aldrich
Polypropylene glycol (PPG)	725	$(C_3H_8O_2)_n$	Sigma Aldrich
Polyoxyethylene cetyl ether (Cetyl PEG)	1124	$HO(CH_2CH_2O)_{20}C_{16}H_{33}$	Sigma Aldrich
Pluronic 10R5, a triblock copolymer (block copolymer 10R5)	2000	$(C_3H_6O.C_2H_4O)_n$	BASF
Bis-(3-sulphopropyl)-disulphide (SPS)	354.37	$C_6H_{12}Na_2O_6S_4$	Raschig GmbH
Via-form commercial additives (suppressor, accelerator and leveler)	N/A	N/A	Enthone

Table 2.1: Description of the chemicals used during the course of this work.

2.3 Electrochemical techniques

The electrochemical techniques used in the scope of this work were performed in order to characterize the electrochemical reactions involved during copper deposition on different substrates. The experimental conditions for the different electrochemical techniques described below are specified in the experimental paragraph of each Chapter.

2.3.1 Current-potential curves

The current-potential curves were used mainly to determine the potential range at which copper deposition occurs and whether charge-transfer or diffusion from the bulk is the rate determining process during the potential scan. Depending on the scan rate, different processes can be detected [1]. For example, when a very slow scan rate is applied, the current-potential curves can be used to estimate the steady state nucleation overpotential, η_{Nucl}. At very fast scan rates, the current-potential curves can be used to follow the kinetics of slow processes such as the underpotential deposition (UPD) process [1,2]. In addition, the effects of surface pretreatment, addition of suppressor etc. on the copper deposition reaction can be detected in the current-potential curves.

The current-potential curves are obtained by scanning the potential of the working electrode at a certain scan rate between two set potential limits. During the potential scan, the current passing through the working electrode is recorded as shown in Figure 2.2. Note that Figure 2.2 shows only the cathodic currents resulting from a negative potential scan for a system with no agitation. Initially, the current increases due to non-Faradaic processes such as the charging of the double-layer [1]. These non-Faradaic currents do not result in electrochemical reactions on the working electrode surface. Once the electrical double-layer is formed Faradaic processes can proceed via charge transfer across the electrical double layer [1]. In case of metal deposition on noble substrates, currents can be detected more positive than the copper equilibrium potential, $U_{(Cu^{2+}/Cu),eq}$. These currents are attributed to the underpotential deposition (UPD) of copper on the noble substrate surface, as well as to the partial reduction of Cu^{2+} to Cu^{+}. The Cu UPD results in the formation of a thin deposit, which can be between a sub-monolayer and a small number of monolayers, depending on the surface conditions. After $U_{(Cu^{2+}/Cu),eq}$ is

reached, the cathodic current rises, copper nucleates on the WE surface and the cathodic current continues to rise as copper bulk deposition proceeds on the nucleated Cu islands. The copper bulk deposition process involves the flux of Cu^{2+} ions towards the WE surface and electron transfer. During the negative potential scan, three different regimes can be observed. The three regimes, resulting from a concentration profile at the WE surface once the potential is applied, define the surface concentration of the Cu^{2+} ions, C_s, with respect to the bulk concentration of the Cu^{2+} ions, C_b [1]. When $C_s=C_b$, the WE potential is under kinetic control (marked as (1) in Figure 2.2). This regime corresponds to very low current densities where the kinetics of the electrochemical reaction is small and mass transport can easily maintain the surface concentrations equal to the bulk concentration. Thus, in this case, the electron transfer is the limiting step. When $C_s<C_b$, the WE potential is under mixed kinetic-mass transport control (marked as (2) in Figure 2.2). In this regime the current at the WE continues to rise as the electrode becomes more reducing and more Cu^{2+} ions at the electrode surface are reduced. Note that diffusion of Cu^{2+} ions from the bulk does not limit the current yet. When $C_s=0$, the WE potential is under mass-transport control (marked as (3) in Figure 2.2). In this regime all Cu^{2+} ions at the electrode surface are already reduced and the current becomes limited by the diffusion rate of Cu^{2+} ions from the bulk solution to the electrode surface. Consequently, the current stops rising and starts to decrease. A Further negative shift of the potential results in an additional increase in the current due to additional reduction reactions (hydrogen evolution in case of acidic $CuSO_4$ solution).

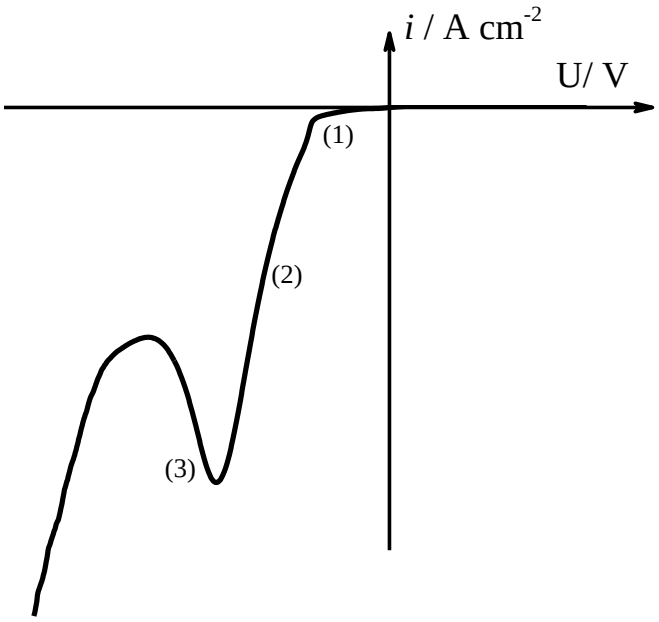

Figure 2.2: Typical current-potential response for copper deposition with no agitation.

2.3.2 Chronopotentiometry (Galvanostatic)

The potential-time curves were used mainly to establish a relationship between the Cu island density and the overpotential, taking into account the effective surface area of the Cu islands. Depending on the applied current or solution composition, the potential-time responses also allow to determine qualitatively different reactions at the electrode surface with every change of the electrode potential (see Chapters 4 and 5). In addition, the potential-time curves allow to determine quantitatively different physical parameters such as b_{coal} or thickness at which a closed Cu film is achieved on the WE surface (see Chapter 5).

In this technique, a constant current is applied to the working electrode and the resulting potential is measured as a function of time. For a simple metal deposition reaction as described by Equation 2.1, a typical potential-time response will look like the plot in Figure 2.3. Note that Figure 2.3 shows potential-time response for a system with no diffusion limitation i.e. a sufficient amount of Cu^{2+} ions diffuse to the electrode surface and sustain the applied current.

Equation 2.1: $$M^{n+} + ne \leftrightarrow M$$

Within a few tens of milliseconds after the current is applied, the measured potential drops sharply from OCP to a minimum value and then gradually changes with time. The initial potential drop towards the minimum value resembles charging of the double layer, UPD region and partial reduction to Cu^{+}. Copper nucleates on the electrode surface just before reaching the minimum potential value. After reaching the minimum potential value the potential gradually increases with time to more positive values as copper deposition proceeds on Cu islands. The times t_1, t_2 and t_3 represent different times at which the Cu/WE surface changes gradually as copper covers the WE surface.

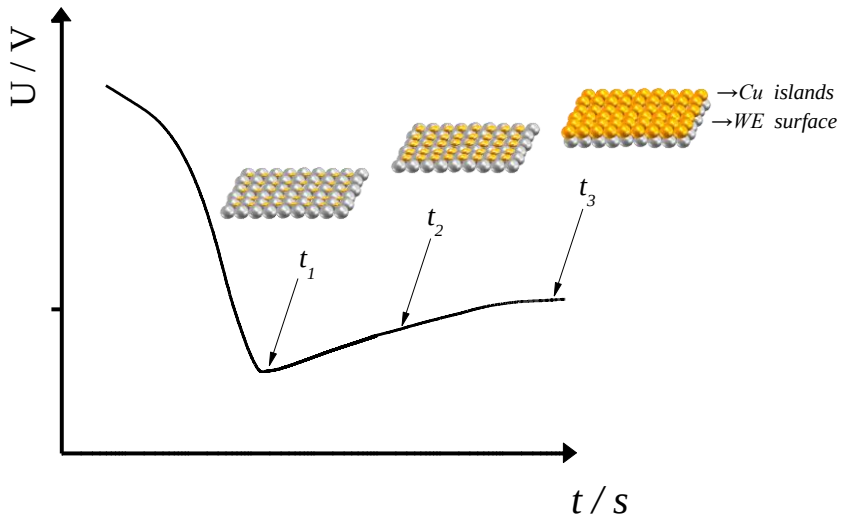

Figure 2.3: Typical potential-time response for a system with no diffusion limitation where only one potential drop is observed.

Figure 2.4 shows potential-time transient where an additional drop is observed. Since the potential is developed as a function of C_s (i.e. the surface concentration of the Cu^{2+} ions) any change in the C_s might affect the potential value. For example, for systems with no suppressor additive, the potential is driven more negative due to depletion of Cu^{2+} ions at the electrode surface (see Chapter 4). For systems with suppressor additive, the potential is driven more negative due to adsorption of the polyether suppressor on the Cu islands (see Chapter 5). Detailed description of these systems can be found in the experimental Chapters.

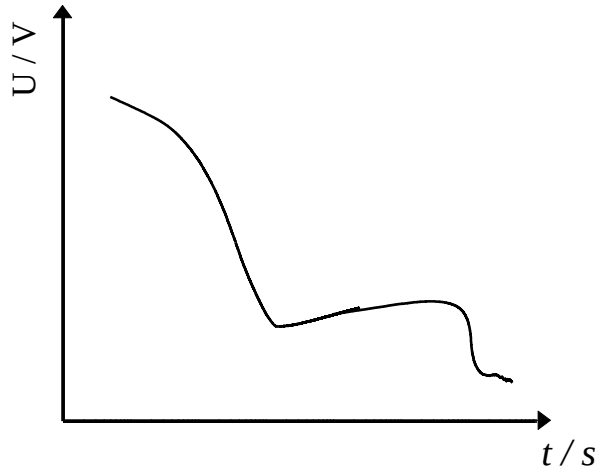

Figure 2.4: Typical potential-time response for a system under diffusion limitation or with suppressor additive where additional potential drop is observed.

2.4 Experimental set-up and equipment

The electrochemical experiments were carried out with an Autolab potentiostat PGSTAT30 (Metrohm) controlled by GPES software to control potential and current. All experiments were performed at room temperature (21° C). The experiments on blanket wafers were performed without agitation while experiments on patterned wafers (i.e. filling experiments) were performed at rotation rate of 500 rpm. For each experiment a fresh sample was used without any further pretreatment unless otherwise is mentioned. After copper deposition, samples were immediately removed from the solution, rinsed with de-ionized water and dried in nitrogen flow.

2.4.1 Stationary electrode set-up

The electrochemical measurements on the blanket wafers were performed using a Teflon three-electrode electrochemical cell clamped on the different working electrodes (WE) as shown schematically in Figure 2.5. The blanket wafers were cut in coupons of 2 cm × 2 cm. A copper foil with a punched-out hole of 5 mm in diameter was placed on top of the RuTa sample and was masked with Teflon tape, leaving a circular opening exposing area of 0.07 cm^2. The copper foil

thus provided good electrical contact to the working electrodes for the whole of the area exposed to the solution. A platinum mesh counter electrode (CE) was placed opposite to the WE. The reference electrode (RE) was a silver/silver chloride Ag/AgCl/3M KCl (BASi, RE-5B), $U_{(Ag/AgCl)}$=0.22 V vs. standard hydrogen electrode (SHE) and was connected to the cell compartment via a Luggin capillary. All potentials are reported versus Ag/AgCl electrode.

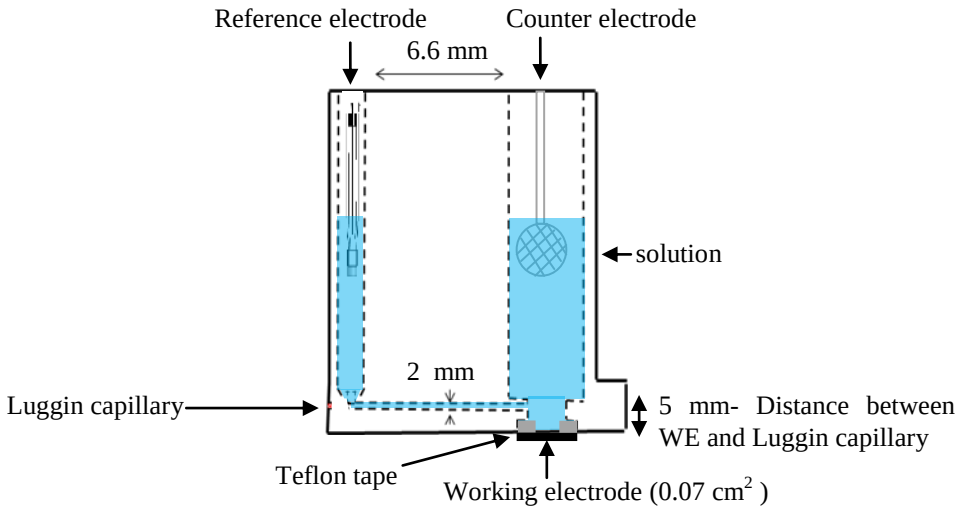

Figure 2.5: Schematic view of the stationary three-electrode electrochemical cell set-up.

2.4.2 Rotating disk electrode set-up

The electrochemical measurements on the patterned wafers were performed using a three-electrode electrochemical cell as shown schematically in Figure 2.6. The patterned wafers, containing the desired 20 nm features, were cut in coupons of 2 cm × 2 cm. The samples were mounted into a rotating (500 rpm) sample holder connected to a Metrohm (16280010) rotator. The exposed area of the WE was 1.54 cm^2. A platinum rod separated from the main compartment by a porous glass frit was used as the CE. The RE was a silver/silver chloride Ag/AgCl/3M KCl (Metrohm), $U_{(Ag/AgCl)}$=0.22 V vs. SHE and was connected to the cell compartment via a Luggin capillary.

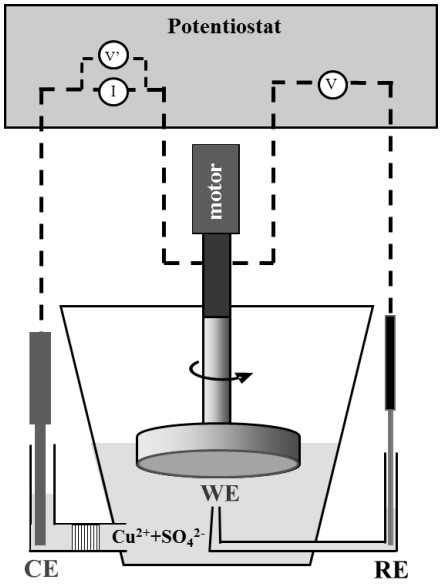

Figure 2.6: Schematic view of the rotating disk electrode set-up.

2.5 Analysis techniques

2.5.1 Scanning electron microscopy (SEM)

In this study the Cu islands were examined by Scanning Electron Microscopy (SEM Nova 200, FEI). All images were produced by secondary electrons (SE). In a typical measurement the accelerating voltage of the electron beam was 5 kV with a 3 nm spot size and working distance of ~4 mm. The SEM images were analyzed with Image *J* digital analysis software [3] in order to count the number of copper islands and determine the average diameter. For one data point an average of 3 images, taken at different spots near the center of the plated area, were analyzed.

2.5.2 Atomic force microscopy (AFM)

In this study AFM measurements were performed in order to study the topography of the deposited copper particles and the coalesced copper film subsequent to deposition under different conditions. The AFM measurements were performed with a Bruker Dimension Icon-PT atomic force microscope with Peak Force Tapping mode. The AFM images were analyzed with WSxM

digital analysis software [4] in order to determine the roughness and effective copper surface area of the coalesced copper film.

Atomic Force Microscope (AFM) is a technique used to characterize surface topography with nanometer resolution. A schematic view of the setup is presented in Figure 2.7. A cantilever with a sharp tip (probe) is used to scan the sample surface. The probe and sample are moved relative to each other and the forces between the tip and sample surface are calculated by measuring the deflection of the free end of the attached cantilever. The displacement of the cantilever is measured by a laser beam reflected from the top surface of the cantilever into a photodetector. A feedback system acts on a piezoelectric tube to tune the distance and keep constant the force between the tip and the sample. The resulting map of the tube extension represents the topography of the sample (AFM image). In tapping mode, an oscillating cantilever is used. Consequently, the tip is in contact with the surface only for a short time, thus avoiding the issue of lateral forces and drag across the surface.

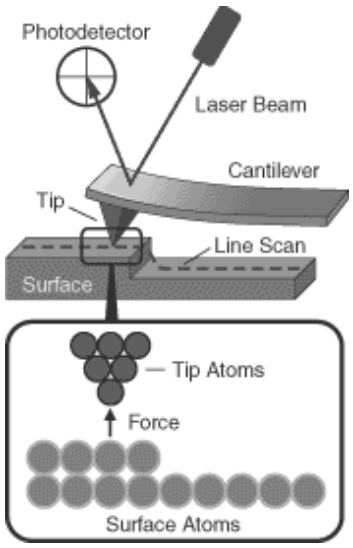

Figure 2.7: Schematic view of the AFM setup [5].

2.5.3 Time-of-Flight Secondary Ion Mass Spectrometry (TOF-SIMS)

In this study TOF-SIMS measurements were performed in order to study the thickness at which a closed Cu film was obtained on Pt. The TOF-SIMS measurements were performed with a TOF-SIMS IV from ION-TOF GmbH.

Time-of-Flight Secondary Ion Mass Spectrometry (TOF-SIMS) is a surface analytical technique that provides information on the chemical composition and distribution of chemical species present on the sample top surface (~1-2 monolayers). A schematic view of the TOF-SIMS process is presented in Figure 2.8. A pulsed beam of primary ion is used to ionize species from the sample surface. The emitted secondary ions are extracted into the TOF analyzer by applying a high voltage potential between the sample surface and the mass analyzer. The secondary ions travel through the TOF analyzer with different velocities, depending on their mass to charge ratio (m/z). For each primary ion pulse, a full mass spectrum is obtained by measuring the arrival times of the secondary ions at the detector and performing a simple time to mass conversion.

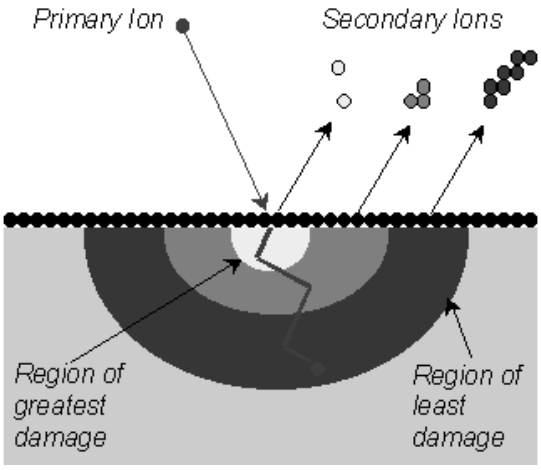

Figure 2.8: Schematic diagram of the SIMS process [6].

[1] Electrochemical Methods: Fundamentals and Applications, Allen J. Bard, Larry R. Faulkner, New-York, Wiley & Sons, INC (2002).
[2] A.I. Danilov, E.B. Molodkina, Yu.M. Polukarov, V. Climent, J. Feliu, Active centers for Cu UPD–OPD in acid sulfate solution on Pt(111) electrodes, Electrochim. Acta 46 (2001) 3137.
[3] http://rsb.info.nih.gov/ij/docs/index.html
[4] http://www.nanotec.es/products/wsxm/index.php
[5] http://www.bruker.jp/axs/nano/imgs/pdf/AN133.pdf
[6] http://www.phi.com/surface-analysis-techniques/tof-sims.html

PART 1: INVESTIGATION OF NUCLEATION AND GROWTH OF COPPER ON BLANKET RUTA WAFERS.

CHAPTER 3: THE EFFECT OF THE INORGANIC COMPONENTS IN THE CU PLATING BATH ON THE ISLAND MORPHOLOGY AND ISLAND DENSITY.

This Chapter describes experiments and results of copper deposition on a RuTa alloy from additive-free copper sulfate ($CuSO_4$) solutions with varying composition. The main focus is to investigate the effect of the concentration of the individual inorganic components on the nucleation and growth processes during galvanostatic deposition. The experimental results show that each of the inorganic components significantly affects the island morphology and island density, N_p. It is shown that the island density is the highest when Cu^{2+} and Cl^- concentration are low while H_2SO_4 concentration is high. Furthermore, it is shown that the inorganic components affect the Cu island morphology as well as the N_p. The individual effect of each component remain similar once all the components are mixed together. This study illustrates the importance of solution optimization towards faster coalescence of the Cu islands into a continuous Cu film enabling the fill of sub-30 nm features by direct plating.

3.1 Introduction

The fabrication of copper interconnects in the damascene process is performed by a electrodeposition process, during which copper is electrochemically deposited on a conductive Cu seed layer, present on top of features with high-aspect-ratio topologies [1,2]. The void-free filling of these features is accomplished by electrodeposition from solutions that contain a source of Cu^{2+} ions. The initial copper chemistry for the damascene process was originally used for printed circuit board (PCB) applications and was capable of void-free fill of sub-0.25 µm features with copper [1]. Typical plating solutions have $CuSO_4$ electrolytes, acidified with sulfuric acid (H_2SO_4). The acidified $CuSO_4$ solution also contains small amounts of Cl^- ions and organic additives (polyether molecules as suppressor, disulfide molecule as accelerator and a nitrogen compound as a leveler). Each component in the $CuSO_4$ solution has a role in the deposition process and together, with their relative diffusion coefficients and adsorption characteristics, enable the void-free filling of the trenches and vias [3].

Table 3.1 summarizes the inorganic components in a typical plating solution and the concentration range that is conventionally used for copper interconnect metallization.

Component	*Function*	*Conventional concentration*
$CuSO_4$	reactant	between 0.2 and 0.6 M
H_2SO_4	supporting electrolyte	between 0.5 and 2 M
Cl^-	promoter	between 1×10^{-3} and 2.7×10^{-3} M

Table 3.1: Overview of the Inorganic species, their function and conventional concentration in a plating solution for fabrication of copper interconnects.

The $CuSO_4$ provides the Cu^{2+} ions for the deposition process. In the early days of the damascene process, the $CuSO_4$ concentration ranged between 0.2 and 0.6 M, similar to what was used for PCB applications [1,2]. A shift to higher $CuSO_4$ concentration, in the range of 0.6 to 1 M, was made in order to avoid depletion of Cu^{2+} ions within the high aspect-ratio features [4]. However, it was also shown that low $CuSO_4$ solutions provide better deposit uniformity due to a uniform charge transfer resistance across the wafer [2,5]. Ultimately, the $CuSO_4$ concentration is dictated by the deposition parameters, such as desired deposition rate and diffusion limited current.

H_2SO_4 is added to the solution to increase its conductivity [1-5]. In general, in conductive solutions most of the current is carried within the solution and thus the potential gradient is minimized. This results in a more uniform current distribution and geometry- independent interfacial kinetics [6]. Therefore, a high H_2SO_4 concentration is preferred for applications such as the filling of very high aspect ratio (20:1) features [2]. With the scaling-down technology trends of feature sizes, thinner and resistive Cu seed layers are required for the fabrication of smaller interconnects [7]. The resistive Cu seed layer introduces the so called “terminal effect” phenomenon, i.e. a severe potential drop across the resistive substrate and consequently a non-uniform thickness distribution across the wafer [2,4,7]. The non-uniform distribution arises because the current favors passing through the solution towards the contact rather than passing through the resistive substrate. Thus, in order to minimize the resistive substrate effect, Landau *et al.* suggested to lower the solution conductivity by completely eliminating H_2SO_4 from the solution [4]. According to Landau *et al.*, the lower acidity would then offer a greener process and a less corrosive medium with respect to the copper seed and the used equipment [4].

Cl^- ions are present in the solution, typically in a narrow concentration range between 1×10^{-3} and 2.7×10^{-3} M. It has been shown that small concentrations of Cl^- ions (in the range of 10^{-5} M) are sufficient to accelerate copper deposition rate by three orders of magnitude [8-11]. Copper deposition from acidic solutions occurs through the two successive one-electron transfer reactions:

Equation 3.1: $$Cu^{2+} + e \leftrightarrow Cu^{+}$$

and

Equation 3.2: $$Cu^{+} + e \leftrightarrow Cu$$

while a small amount of Cu^+ ions is always present at the interface between the electrode and the solution due to reverse of Cu^+ disproportionation reaction:

Equation 3.3: $$Cu^{2+} + Cu \leftrightarrow 2Cu^{+}$$

The presence of Cl^- ions in the solution stabilizes the Cu^+ ions at the copper surface by forming an adsorbed $CuCl_{ads}$ complex. The cupric ion reduction in these circumstances is accelerated by the second set of electron transfer reactions [8-11]:

Equation 3.4: $$Cu^{2+} + Cl^{-}_{ads} + e \leftrightarrow CuCl_{ads}$$

followed by:

Equation 3.5: $$CuCl_{ads} + e \leftrightarrow Cu + Cl^{-}$$

Nevertheless, when polyether suppressor additive is present in the solution, the $CuCl_{ads}$ complex can also interact with the oxygen atoms in the ethylene oxide (EO) repeating unit of the polyether molecule [12]. This interaction forms a $Cu(EO)Cl_{ads}$ complex on the copper surface which strongly inhibits the copper deposition rate [13,14]. Moreover, the Cl^- ions also interact with the disulfide molecule (accelerator) and enhance its acceleration performance up to a certain

concentration [15]. Therefore, acceleration or inhibition of copper deposition occurs depending on the Cl^- ion concentration and the presence of certain organic molecules in the solution. In this Chapter, we will only discuss the effect of the inorganic components on the nucleation and growth of copper on RuTa. The detailed function of the organic additives will be discussed in the following Chapters.

In the direct plating (DP) approach, copper is electrodeposited directly on a substrate without a copper seed [24]. As such, copper electrodeposition proceeds through electrochemical nucleation and growth processes. Figure 3.1 illustrates some of the steps involved during these processes for copper deposition from acidic solutions (see Equation 3.1 and Equation 3.2). As shown schematically in Figure 3.1, these processes take place at the interface between the electrode and the solution. First, the copper ions must be transported via diffusion to the interface. Following surface adsorption, electron transfer reactions occur and Cu adatoms diffuse on the surface, nucleate and grow. The nucleation and growth mechanism of copper from various solutions onto various substrates has been extensively studied [16-22]. These studies show that the number of nuclei and the deposit morphology is affected by several parameters such as hydrodynamic conditions, pH, chemical reactions in solution and at the surface, ionic strength (*I*), adsorption, presence of cations and anions, nature of the substrate, active sites, concentration of the reactants, etc.

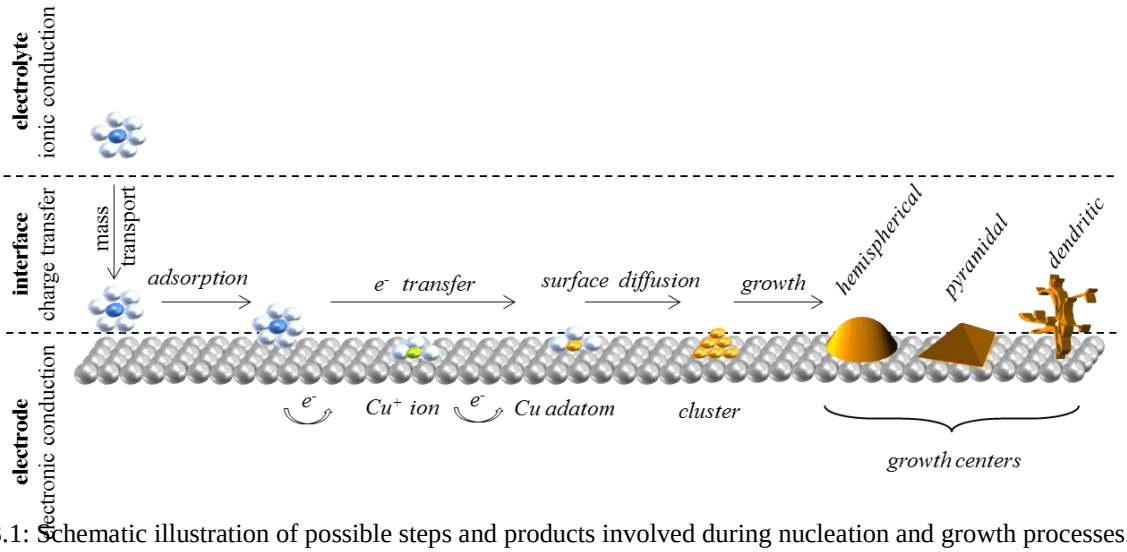

Figure 3.1: Schematic illustration of possible steps and products involved during nucleation and growth processes.

The most critical obstacle for copper metallization by DP is the requirement to form a high island density, N_p, in the initial stages of the process to assure the formation of a uniform continuous film inside the small features [24]. The coalescence thickness of this continuous film depends not only on N_p, but also on the geometry of the islands, i.e. disk shaped islands will lead to a thinner coalescence thickness than sphere shaped islands (assuming the same N_p) [24]. Thus, to make future prospects of DP technology possible, a thorough understanding of the nucleation and growth mechanism and the role of the different solution components on the process is necessary. This information should enable the formulation of advanced copper plating chemistries that suit copper metallization by DP. In this Chapter, the effect of each one of the inorganic components ($CuSO_4$, H_2SO_4 and Cl^- ions) on the nucleation and growth mechanism of Cu on the RuTa surface is shown. The Chapter is divided into two main parts: the first part deals with the effect of the concentration of $CuSO_4$, H_2SO_4 and Cl^- ions, individually. In the second part, all the components are present in the solution and the concentration of one component is varied while keeping the other parameters constant. The systematic study provides insight into which solution composition can enable high N_p, and serves as a potential candidate for the copper filling of small features in RuTa by means of DP.

3.2 Experimental details

Copper was electrodeposited on RuTa substrates. Details concerning the experimental set-up and substrate properties can be found in Chapter 2. The current-potential curves were obtained by polarizing the potential from 0.5 V to -0.5 V vs. Ag/AgCl at a rate of 0.02 V s^{-1}. The galvanostatic experiments were performed at current densities of -2.5 and -10 mA cm^{-2}. The plating solutions contained various concentrations of $CuSO_4$ (> 98%, Alfa Aesar), H_2SO_4 (96% Assay, Baker) and HCl (37% Assay, Baker). In the first part of the study (part I), the effect of concentration of individual inorganic components on the nucleation and growth of copper on RuTa is shown. The different solutions for the study in part I were tailored as follows: solution that contained only Cu^{2+} ions, with no support electrolyte (termed the base solution), base solution with the addition of various H_2SO_4 concentrations (0.018, 0.18 or 1.8 M) and base solution with the addition of various HCl concentrations (0.14×10^{-3}, 1.4×10^{-3} or 7×10^{-3} M). In the second part of the study (part II), all components were present in the solution and only one

component concentration was varied while keeping the other parameters constant. The different solutions for the study in part II were tailored as follows: 1.8 M H_2SO_4, 1.4×10^{-3} M HCl and various concentrations of $CuSO_4$ (0.05, 0.1 or 0.6M); 0.6 M $CuSO_4$, 1.4×10^{-3} M HCl and various concentrations of H_2SO_4 (0.018, 0.18 or 1.8 M) and 0.6 M $CuSO_4$, 1.8 M H_2SO_4 and various concentrations of HCl (0.14×10^{-3}, 1.4×10^{-3} or 7×10^{-3} M). The copper equilibrium potentials, $U_{(Cu^{2+}/Cu),eq}$ for the solutions in part II were determined experimentally by open-circuit potential (OCP) measurements on a Cu electrode for 60*s* without agitation. The Cu OCP changed in solutions that contained various $CuSO_4$ concentrations however, did not change in solutions that contained various H_2SO_4 or Cl^- concentrations. The OCP of the as-received PVD RuTa with an air-formed oxide film ranged between +0.57 and +0.65 vs. Ag/AgCl and did not change in all solutions under investigation (i.e. in solutions that contained various concentrations of $CuSO_4$, H_2SO_4 and Cl^-). The solution resistance (R_s) of solutions in part II was determined from the reciprocal slope of the linear part of the *I*-U relationship. For the acidified solutions (1.8 M H_2SO_4) with various $CuSO_4$ concentrations, the R_s was 39, 39 and 44 Ω for the 0.05, 0.1 and 0.6 M $CuSO_4$ solutions, respectively. For the 0.6 M $CuSO_4$ solutions with various H_2SO_4 concentrations, the R_s was 94, 74 and 44 Ω for the 0.018, 0.18 and 1.8 M H_2SO_4 solutions, respectively. For the acidified (1.8 M H_2SO_4) 0.6 M $CuSO_4$ solutions with various HCl concentrations, the R_s was 44 Ω and did not change with changing HCl concentration. The R_s values were verified with electrochemical impedance spectroscopy (EIS) measurements. The EIS measurements were conducted on a 150 nm copper film electrodeposited on the RuTa wafers (at current density of -10 mA cm^{-2} from solution that contained 0.25 M $CuSO_4$ and 1.8 M H_2SO_4). The measurements were conducted 10 mV more negative than the OCP value for the different $CuSO_4$ solutions after immersion of the samples into the different $CuSO_4$ solutions for 30*s*. The AC amplitude was 10 mV and the frequency ranged from 50 Hz to 100 kHz. EIS measurements were performed with a PGSTAT30 with frequency response analyzer (FRA2-Metrohm). Similar values of R_s to those observed from the reciprocal slope of the linear part of the *I*-U relationship were observed with the EIS measurements. For the acidified (1.8 M H_2SO_4) solutions with various $CuSO_4$ concentration, the R_s was 44, 43 and 51 Ω for the 0.05, 0.1 and 0.6 M $CuSO_4$ solutions, respectively. For the 0.6 M $CuSO_4$ solutions with various H_2SO_4 concentrations, the R_s was 96, 60 and 51 Ω for the 0.018, 0.18 and 1.8 M H_2SO_4 solutions, respectively. For the acidified (1.8 M H_2SO_4) 0.6 M $CuSO_4$ solutions with various HCl concentrations, the R_s was 51

Ω and did not change with HCl concentration. For the *IR* correction of the *i*-U curves, the R_s values obtained from the reciprocal slope in the linear part of the *I*-U relationship were used. The solution pH was measured using a 827 pH lab, from Metrohm Ltd. The solution conductivity was measured using a 712 Conductometer from Metrohm Ltd. All experiments were performed at room temperature (21° C) and without agitation. For each experiment a pristine RuTa or Cu electrode was used without any further pretreatment. After copper deposition, samples were immediately removed from the solution, rinsed with de-ionized water and dried in nitrogen flow. The copper islands were examined by Scanning Electron Microscopy (SEM Nova 200, FEI). The SEM images were analyzed with Image*J* digital analysis software [23] in order to count the number of copper islands and determine the average diameter. For one data point an average of 3 images, taken at different spots near the center of the plated area, were analyzed.

3.3 Nucleation and growth of copper during galvanostatic deposition - part I

3.3.1 The effect of Cu^{2+} ion concentration

Figure 3.2 shows top-down SEM images of Cu islands electrodeposited on RuTa from the base solutions that contained (a) 0.05 M (pH 3.5) and (b) 0.6 M (pH 3.8) $CuSO_4$ at current densities of -2.5 and -10 mA cm^{-2} for deposition charge density of 0.01 C cm^{-2}. Unlike the typical spherical or hemispherical shaped islands observed for copper deposition from acidic solutions (pH≈-0.2) [24], several crystal morphologies were observed: at -2.5 mA cm^{-2}, octahedral-shaped Cu islands were observed on the RuTa surface subsequent to deposition from the 0.6 M $CuSO_4$ base solution. With the decrease in Cu^{2+} concentration to 0.05 M, a mixture of pyramidal and octahedral-shaped Cu islands was observed on the RuTa surface. Increase in the deposition current to -10 mA cm^{-2} also led to a change in the islands morphology: for the 0.6 M $CuSO_4$ base solution, truncated octahedral-shaped islands were observed on the RuTa surface while a mixture of truncated octahedral and cubooctahedral-shaped Cu islands was observed for the 0.05 M $CuSO_4$ base solution.

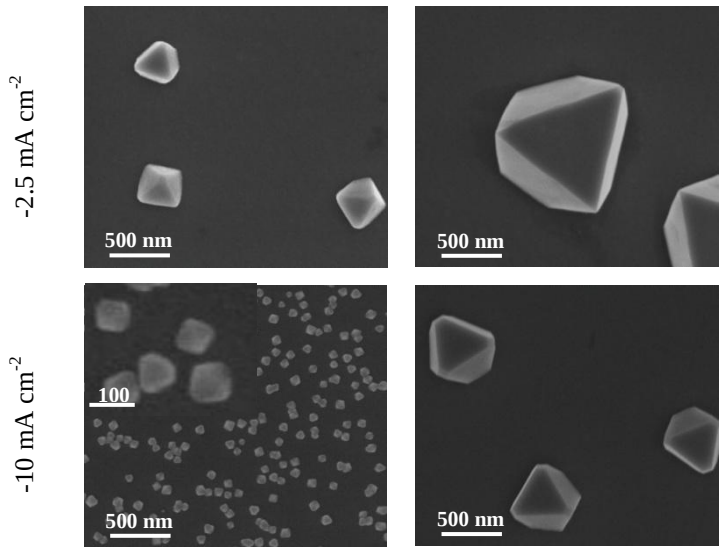

Figure 3.2: Top-down SEM images of Cu islands electrodeposited from solutions of (a) 0.05 and (b) 0.6 M $CuSO_4$ (base solution) at current densities of -2.5 and -10 mA cm^{-2} for deposition charge density of 0.01 C cm^{-2}. In the inset: cross-sectional SEM images of the truncated octahedron shaped Cu nuclei.

As schematically represented in Figure 3.1, electrocrystallization proceeds through the nucleation of stable clusters, followed by the attachment of adatoms to these clusters. As in any physical system, the adatoms attach to the clusters in a manner that uses the lowest surface energy [32]. Generally, the shape of deposits or so-called islands is determined by the limiting planes with the slower growth rate (i.e. with the lowest free energies), which are (100) and (111) planes for Cu [25,32]. Cu nuclei, deposited on foreign substrates are found to exhibit different shapes, including spheres and hemispheres [24], asymmetric triangular pyramidal shapes with four (111) facets [26], cubic shapes with six (100) facets [27,28], cuboctahedral shapes with eight (111) and six (100) facets [29] and octahedral shapes with eight (111) facets [30]. Figure 3.3 summarizes the different shapes of Cu islands depending on the relative growth rates along the [100] and [111] directions [31]. In Figure 3.3(a), the growth rate in [111] direction is faster than that in [100] direction, resulting in the exposure of (100) facets i.e. in formation of a cube. In Figure 3.3(f), the growth rate in [100] direction is faster than that in [111] direction, resulting in the exposure of (111) facets i.e. in formation of a octahedron. The octahedron and its truncated intermediate shapes observed for the 0.05 and the 0.6 M $CuSO_4$ base solutions is therefore the result of changes in the growth rates in the [111] and [100] directions [32]. The exact reason of a given shape for the Cu deposits on the RuTa surface subsequent deposition from the base

depends on various parameters, such as anion adsorption, pH, applied current etc. and is at present not fully understood. Similar morphologies were observed for copper deposition on silicon from 0.01 M $NaClO_4$ solutions with various $CuSO_4$ concentrations [32].

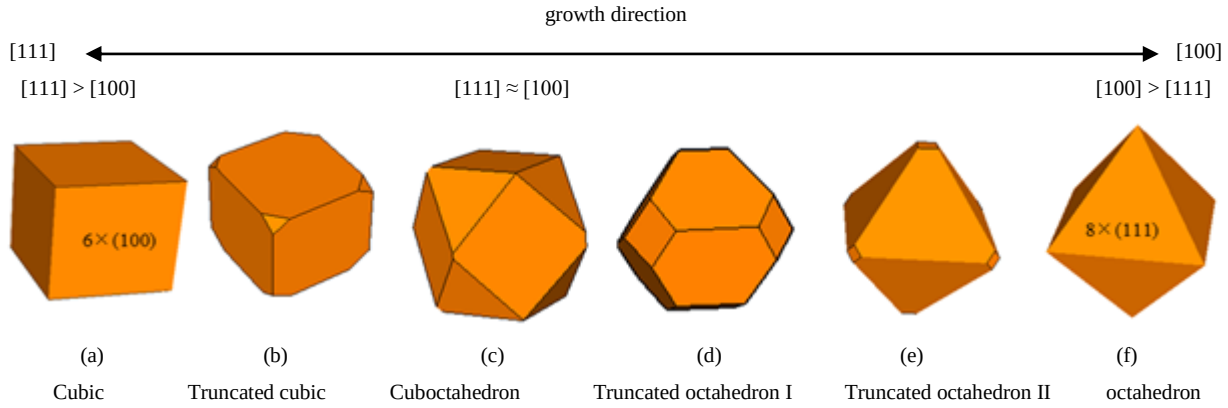

Figure 3.3: Schematic diagram of the shape evolution of Cu islands at different relative growth rates along the [100] and [111] directions.

The decrease in Cu^{2+} concentration not only altered the island morphology but led to higher island densities as well. Deposition at -2.5 mA cm^{-2} from the 0.6 M $CuSO_4$ base solution resulted in an island density, N_p, of 1.8×10^6 cm^{-2}. Decrease in the Cu^{2+} concentration to 0.05 M led to an increase in N_p to 6.3×10^7 cm^{-2}. Furthermore, increase in the current density to -10 mA cm^{-2} resulted in an increase in the N_p to 3.5×10^9 and 2.3×10^7 cm^{-2} for the 0.05 and 0.6 M base solutions, respectively. The decrease in Cu^{2+} concentration as well as the increase in the current density results in higher overpotentials for nucleation (Chapter 4). As such, higher island density, N_p, is achieved. The effect of [Cu^{2+}] ions and the current density on N_p, along with a full treatment of the galvanostatic transients will be discussed in detail in Chapter 4.

3.3.2 The effect of H_2SO_4 concentration

Figure 3.4(a) shows the island density, N_p, as a function of H_2SO_4 concentration as obtained from SEM images (not shown) for Cu deposition on RuTa from the 0.05 and 0.6 M $CuSO_4$ base solutions with various H_2SO_4 concentrations at current density of -10 mA cm^{-2} and for deposition charge density of 0.01 C cm^{-2}. As mentioned before, for the 0.6 M $CuSO_4$ base solution, truncated octahedron shaped Cu islands were observed on the RuTa surface with N_p of

2.3×10^{7} cm^{-2}. The addition of 0.018 M H_2SO_4 resulted in a sharp increase in N_p to 3.3×10^{8} cm^{-2}. Further increase in the H_2SO_4 concentration to 0.18 and 1.8 M led to a further increase in N_p to 5.8×10^{8} and 1.4×10^{9} cm^{-2}, respectively. As the deposited charge was the same in all cases (0.01 C cm^{-2}), the average size of the Cu islands decreased with increasing N_p. Similar to the 0.6 M $CuSO_4$ case, N_p increased with increasing H_2SO_4 concentration for the 0.05 M $CuSO_4$ base solution as well for all solutions investigated. Importantly, a systematic increase in the island density was observed when lowering the $CuSO_4$ concentration in the solutions with different concentrations of H_2SO_4 under investigation. A 12 fold decrease in the $CuSO_4$ concentration from 0.6 M to 0.05 M resulted in a 20 fold increase in N_p (for the acidified solutions). These observations indicate that the Cu^{2+} concentration effect on N_p remains similar at all H_2SO_4 concentrations under investigation. Figure 3.4(b-d) shows cross sectional SEM images, illustrating the island shape: the addition of H_2SO_4 not only resulted in higher N_p but led to transformation of the island morphology as well, from truncated octahedral shaped islands to hemispherical shaped islands. Figure 3.5 shows a schematic diagram of the Cu islands shape evolution from truncated octahedron to a sphere. The evolution of the Cu island shapes with rounded edges (i.e. from truncated octahedron to a sphere) may be resulted due to changes in the elastic strain energy of the Cu deposits as demonstrated by Onaka *et al*. [31].

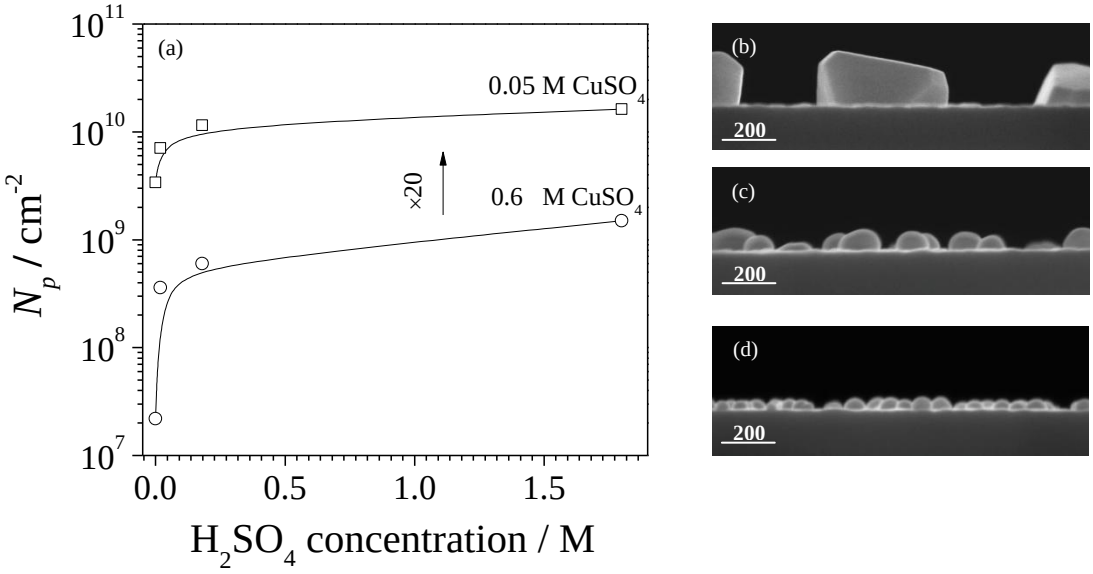

Figure 3.4: (a) Cu island density, N_p, as a function of H_2SO_4 concentration. The deposition experiments were performed in solutions of 0.05 or 0.6 M $CuSO_4$ and with the addition of 0.018, 0.18 and 1.8 M H_2SO_4 at current density of -10 mA cm^{-2} for deposition charge density of 0.01 C cm^{-2}. (b-d) cross-sectional SEM images of the Cu

islands illustrating the islands shape subsequent to deposition from the (b) 0.6 M $CuSO_4$ base solution and with the addition of (c) 0.018 and (d) 1.8 M H_2SO_4.

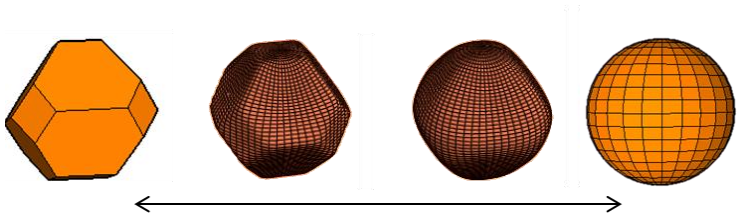

Figure 3.5: Schematic diagram of the shape evolution of Cu islands from truncated octahedron to a sphere.

To better understand the increase in N_p, we investigated the changes in the solution that were induced by the addition of H_2SO_4; with the addition of H_2SO_4, the solution pH decreased while the solution ionic strength, I, increased. Both pH and ionic strength can affect electron transfer reactions as well as nucleation and growth processes [21]. To have a fair comparison for the influence of pH, we adjusted the ionic strength with lithium sulfate (Li_2SO_4). For this purpose, 0.6 M $CuSO_4$ solutions with various concentration of Li_2SO_4 and H_2SO_4 were hence also investigated. Li_2SO_4 was chosen as a supporting electrolyte because Li^+ ions are next in size to H^+. Note that Li^+ cations are much less mobile than H^+ protons (molar ion conductivity of 38.7 $S.m^2.mol^{-1}$ vs. 349.8 $S.m^2.mol^{-1}$, respectively). The ionic strength was calculated according to :

Equation 3.6:
$$I = \frac{1}{2}\sum_{i=1}^{n} C_i z_i^2$$

where C_i is the molar concentration of the i^{th} ion present in the solution and z_i is the charge of that ion. Summation is done for all ions present in the solution. The molar concentration of the different species, [Cu^{2+}], [SO_4^{2-}], [HSO_4^-], [H^+], [$LiSO_4^-$], and [Li^+], were calculated according to their corresponding dissociation constant, K[1] at 21° C [33]. Table 3.2, summarizes the concentrations of the dissociated and associated species for H_2SO_4, $CuSO_4$ and Li_2SO_4 as calculated from Equation 3.6 along with pH and solution conductivity, σ , measured for the different solutions under investigation.

[1] $CuSO_4$ with K = 0.8817, H_2SO_4 with K_{a1} = 80.36 and K_{a2} = 0.01164 and Li_2SO_4 with K_1 = 4.536 and K_2 = 0.1128

	Solution composition	*Dissociated species*	*Concentration/ mol l^{-1}*	*Associated species*	*Concentration/ mol l^{-1}*	*I/ mol l^{-1}*	*pH*	*σ/ mS.cm^{-1}*
(1)	0.6 M $CuSO_4$	Cu^{2+}	0.409	$CuSO_4$	0.190	1.63	3.8	39
		SO_4^{2-}	0.409					
(2)	0.6 M $CuSO_4$ + 0.018 M H_2SO_4	Cu^{2+}	0.414	$CuSO_4$	0.186	1.64	1.8	39.2
		SO_4^{2-}	0.397					
		H^+	0.001	H_2SO_4	4.2×10^{-7}			
		HSO_4^-	0.035					
(3)	0.6 M $CuSO_4$ + 0.18 M H_2SO_4	Cu^{2+}	0.453	$CuSO_4$	0.147	1.66	1.1	84.5
		SO_4^{2-}	0.287					
		H^+	0.014	H_2SO_4	5.74×10^{-5}			
		HSO_4^-	0.346					
(4)	0.6 M $CuSO_4$ + 1.8 M H_2SO_4	Cu^{2+}	0.586	$CuSO_4$	0.014	3.01	-0.2	NA
		SO_4^{2-}	0.021					
		H^+	1.270	H_2SO_4	3.58×10^{-2}			
		HSO_4^-	2.330					
(5)	0.6 M $CuSO_4$ + 0.018 M H_2SO_4 + 0.162 M Li_2SO_4	Cu^{2+}	0.434	$CuSO_4$	0.166	1.72	1.9	46.9
		SO_4^{2-}	0.338					
		H^+	0.001	H_2SO_4	4.92×10^{-7}			
		HSO_4^-	0.035	Li_2SO_4	0.004			
		Li^+	0.079					
		$LiSO_4^-$	0.237					
(6)	0.6 M $CuSO_4$ + 1.8 M Li_2SO_4	Cu^{2+}	0.586	$CuSO_4$	0.102	2.75	3.8	62.6
		SO_4^{2-}	0.021					
		Li^+	1.270	Li_2SO_4	0.407			
		$LiSO_4^-$	2.330					

Table 3.2: Composition of the solutions under investigation along with concentrations of the dissociated and associated species for H_2SO_4, $CuSO_4$ and Li_2SO_4, ionic strength, *I*, (as calculated from Equation 3.6), pH and conductivity, σ.

Figure 3.6(a) shows the island density, N_p, as a function of ionic strength as obtained from the SEM images (not shown) subsequent to deposition from solutions with the varying compositions described in Table 3.2. The minor increase in ionic strength from 1.63 to 1.64, resulted in a sharp increase in N_p by a factor of ~15, from 1.6×10^7 to 3.3×10^8 cm^{-2} for solutions (1) and (2), respectively. Note, that the pH for these solutions decreased from 3.5 to 1.8. In the next part of the discussion, we divide the solutions in a group with "low pH" (solutions 3 and 4, pH 1.1 and -0.2,) and a group with "high pH" (solutions 5 and 6, pH is 1.9 and 3.8). Two trends are now shown with arrows indicating increase in the ionic strength in solutions with lower pH along line A from solution (2) to solutions (3) and (4) and increase in the ionic strength with higher pH along line B from solution (2) to solutions (5) and (6). In path A, further increase in

the ionic strength from 1.64 to 3.01 resulted in a further increase in N_p by a factor of ~4, from 3.3×10^8 to 1.4×10^9 cm^{-2} for solutions (2) and (4), respectively. Conversely, in path B, further increase in the ionic strength from 1.64 to 2.75, resulted in a decrease in N_p by a factor of ~9, from 3.3×10^8 to 4.1×10^7 cm^{-2} for solutions (2) and (6), respectively. For solutions (1) and (6), where the same pH was measured, the increase in ionic strength from 1.63 to 2.75 resulted in a minor increase in N_p by factor of ~2.5 whereas increase in the ionic strength from 1.63 to 3.01 for solution (1) and (4) resulted in a significant increase in N_p by a factor of 62. Note that solution (4) has pH of -0.2 compared with pH 3.8 for solution (6). These observations indicate that the ionic strength has a smaller effect on the nucleation process i.e. on the resulting N_p than the pH of the solution. Therefore, the elimination of H_2SO_4 suggested by Landau *et al.* or even its substitution with Li_2SO_4, would not be suitable for DP applications (i.e. for direct plating with Ru-based substrates such as RuTa investigated here). Figure 3.6(b-d) shows cross-sectional SEM images of Cu islands electrodeposited from the 0.6 M $CuSO_4$ base solution and with the addition of 1.8 M Li_2SO_4 or 1.8 M H_2SO_4 at current density of -10 mA cm^{-2} for deposition charge density of 0.01 C cm^{-2}. Deposition with the 0.6 M $CuSO_4$ base solution with the addition of 1.8 M Li_2SO_4 modified the preferential island growth and cuboctahedral-shaped islands were observed on the RuTa surface (see also Figure 3.3(c)).

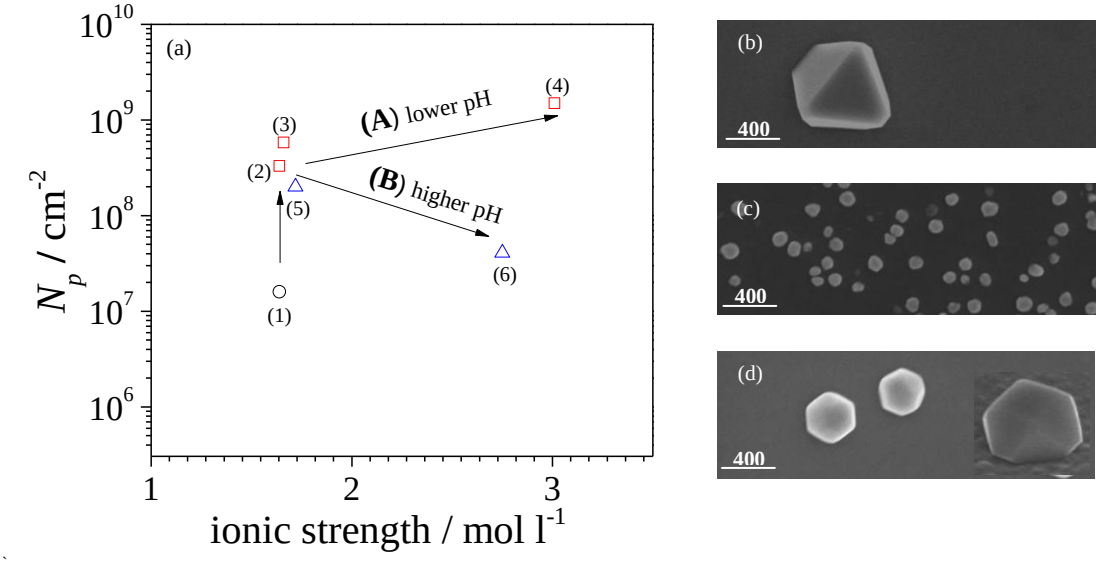

Figure 3.6: (a) Cu island density, N_p, values of Cu islands electrodeposited from solutions of (1) 0.6 M $CuSO_4$ base solution and with the addition of (2) 0.018 (3) 0.18 (4) 1.8 M H_2SO_4 (5) 0.018 M H_2SO_4 +0.162 M Li_2SO_4 M or (6) 1.8 M Li_2SO_4 at current density of -10 mA cm^{-2} for deposition charge density of 0.01 C cm^{-2}. (b-d) cross-sectional

SEM images of Cu islands electrodeposited from the (b) 0.6 M $CuSO_4$ base solution and with the addition of (c) 1.8 M H_2SO_4 or (d) 1.8 M Li_2SO_4 at current density of -10 mA cm^{-2} for deposition charge density of 0.01 C cm^{-2}. The inset of Figure 3.6(d) illustrates the cuboctahedral-shaped Cu islands.

As mentioned above, the island morphology also plays a significant role (as well as the N_p) in achieving a thin coalesced Cu film inside the small features. Figure 3.7 shows a schematic presentation of different island shapes at coalescence, illustrating the contact area with the substrate. It can be seen that island shapes like octahedrons, cuboctahedrons and spheres result in low contact area with the substrate. This, in turn, may result in poor adhesion between the coalesced Cu film and the substrate. Therefore, the shape of the islands not only determines the coalescence thickness but also the resulting adhesion strength between the coalesced Cu film and the substrate. It hence follows that, the hemispherical Cu islands observed subsequent to deposition with acidified $CuSO_4$ solutions are beneficial for DP of copper on Ru-based seed substrate.

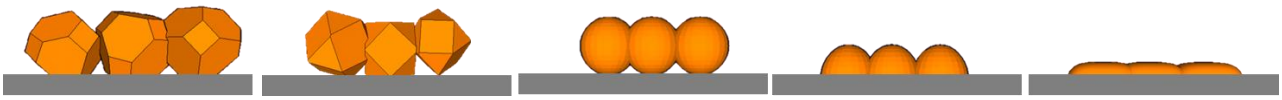

Figure 3.7: Schematic presentation of different island shapes (a) truncated octahedron (b) cuboctahedron (c) spheres (d) hemispheres and (e) ellipse at coalescence, illustrating the contact area of the coalesced Cu film with the substrate.

3.3.3 The effect of Cl^- ion concentration

Figure 3.8 shows the island density, N_p, as a function of Cl^- concentration as obtained from SEM images (not shown) for Cu deposition on RuTa from the 0.05 and 0.6 M $CuSO_4$ base solutions with different Cl^- concentrations at current density of -10 mA cm^{-2} for deposition charge density of 0.01 C cm^{-2}. In contrast to the addition of H_2SO_4 (see Figure 3.4(a) in §3.3.2), the addition of 0.14×10^{-3} M HCl to the 0.6 M $CuSO_4$ solution, resulted in a decrease in N_p from 1.6 x 10^7 to 8.7×10^6 cm^{-2}. Further increase in the Cl^- concentration to 1.4×10^{-3} and 7×10^{-3} M led to further decrease in N_p to 5.5×10^6 and 4.4×10^6 cm^{-2}, respectively. Also in the 0.05 M $CuSO_4$ solution, N_p decreased with increase in Cl^- ion concentration for all solutions under investigation. Importantly, as in §3.1.1., a systematic decrease in the island density was observed when the

$CuSO_4$ concentration in solution decreased: a 12 fold decrease in the $CuSO_4$ concentration from 0.6 M to 0.05 M, resulted in a 13 fold increase in N_p. These observations indicate that the Cu^{2+} concentration effect on N_p remains similar at all Cl^- concentration under investigation. Figure 3.8(b and c) shows tilted and cross sectional SEM images, illustrating the island shape for the Cl^- containing solutions. It can be seen that the addition of Cl^- ions did not only affect the island density but the growth mode as well: a transformation of the island morphology from truncated octahedral-shaped islands (Figure 3.4(b)) to dendritic-shaped islands was observed with the addition of Cl^- ions to the $CuSO_4$ solution (for all HCl concentrations under investigation). The morphology of Cu deposits has already been reported for copper deposition from $CuSO_4$ containing chloride solutions [34-37]. In this work, the addition of Cl^- ions was found to lead to anisotropy among the various crystallographic directions, favoring dendritic growth [34-37]. Generally, dendritic growth results from differences in growth rate of the different crystal planes. At slow rates of crystal growth, the interface between the solution and substrate remains planar, and growth occurs uniformly parallel to the surface. At faster rates of crystal growth, instabilities are more likely to occur resulting in disruption of the planar symmetry. Under these conditions, crystal growth develops along columns perpendicular to the surface [38-40]. Faster growth rates can be the result of different deposition conditions i.e. higher current density or adsorption of anions on a specific plane. Cl^- ions adsorb preferentially on the (110) planes and hence increase the growth rate in the perpendicular directions [110], consequently leading to formation of dendrites with the same preferential orientation [36]. Obviously, the dendritic growth does not suit DP applications where thin films are required.

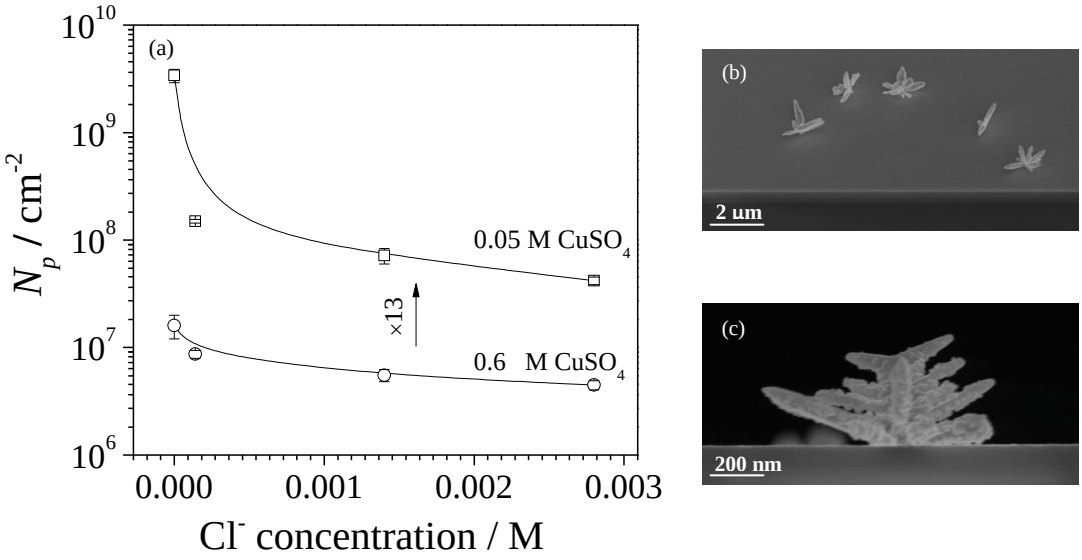

Figure 3.8: (a) Cu island density, N_p, as a function of Cl^- concentration. The deposition experiments were performed from solutions of 0.05 or 0.6 M $CuSO_4$ and with the addition of 0.14×10^{-3}, 1.4×10^{-3} or 7×10^{-3} M HCl at current density of -10 mA cm^{-2} for a deposition charge density of 0.01 C cm^{-2}. (b and c): tilted and cross-sectional SEM images of the Cu islands illustrating the islands shape subsequent to deposition from 0.6 M $CuSO_4$ base solution with 0.14×10^{-3} M HCl.

3.4 Nucleation and growth of copper during galvanostatic deposition-part II

3.4.1 The effect of Cu^{2+} ion concentration

Figure 3.9(a) shows the island density, N_p, as a function of $CuSO_4$ concentration as obtained from SEM images (not shown) for copper deposition on RuTa from solutions of 1.4×10^{-3} M HCl, 1.8 M H_2SO_4 and different $CuSO_4$ concentrations (0.05, 0.1 or 0.6 M). Higher island density was observed with the decrease in Cu^{2+} concentrations. Figure 3.9(b) shows current density, i, versus overpotential corrected for IR drop, η_{IR}, curves for copper deposition on RuTa from solutions with the different Cu^{2+} concentrations as in Figure 3.9(a). The overpotential was determined with respect to the Cu OCP in the different solutions (Table 3.3) and corrected for IR_s drop with R_s= 39, 39 and 44 Ω for the 0.05, 0.1 and 0.6 M $CuSO_4$ solutions, respectively:

Equation 3.7:
$$\eta_{IR} = U - U_{(Cu^{2+}/Cu),eq} - IR_s$$

The equilibrium potentials were determined experimentally from OCP measurements on a Cu electrode and are summarized in Table 3.3. The decrease in Cu^{2+} concentration resulted in a gradual polarization of the current-potential curve, exhibiting higher nucleation overpotentials. Importantly, the negative shift in overpotential with decrease in Cu^{2+} concentration followed a similar trend as N_p. i.e. both a higher overpotential and N_p were observed with a decrease in Cu^{2+} concentration. The inset of Figure 3.9(a) shows cross-sectional SEM images of Cu islands electrodeposited on RuTa at -10 mA cm^{-2} for charge density of 0.01 C cm^{-2} from the solutions under investigation. In the acidified solution the decrease in the Cu^{2+} concentration from 0.6 M to 0.1 and 0.05 M $CuSO_4$ resulted in transformation of the island morphology from spherical-shaped islands to hemispherical-shaped islands, respectively.

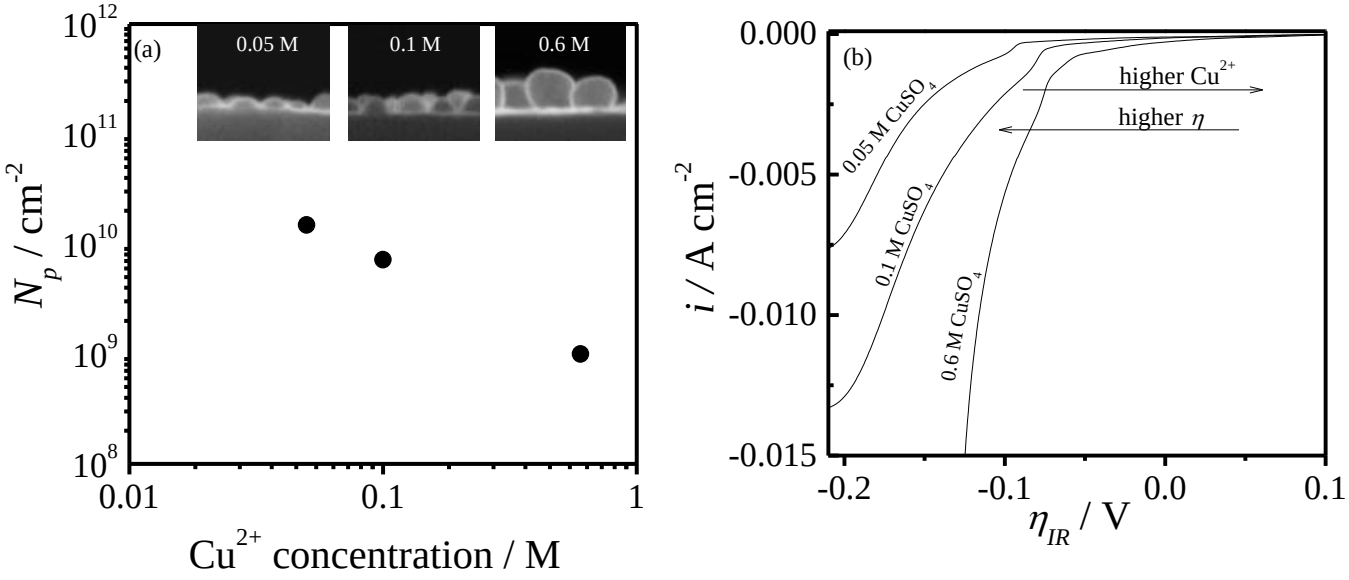

Figure 3.9: (a) N_p as a function of Cu^{2+} concentration for copper deposition on RuTa at current density of -10 mA cm^{-2} and a charge density of 0.01 C cm^{-2}. The deposition experiments were performed from solutions of 1.4×10^{-3} M HCl, 1.8 M H_2SO_4 and different $CuSO_4$ concentrations (0.05, 0.1 or 0.6 M $CuSO_4$). In the inset: cross-sectional SEM images of the Cu islands as a function of Cu^{2+} concentration for the solutions under investigation. (b) Current density- overpotential curves for copper deposition on RuTa from the solutions under investigation at a polarization rate of 0.02 V s^{-1}. The overpotential was determined with respect to the Cu OCP in the different solutions (Table 3.3) and corrected for IR_s drop with R_s= 39, 39 and 44 Ω for the 0.05, 0.1 or 0.6 M $CuSO_4$ solutions, respectively.

Solution composition	*Cu (OCP) (V vs. Ag/AgCl)*	*Nernst potential (V vs. Ag/AgCl)*
0.05 M $CuSO_4$ +1.4×10^{-3} M HCl + 1.8 M H_2SO_4	0.072	0.078
0.1 M $CuSO_4$ + 1.4×10^{-3} M HCl + 1.8 M H_2SO_4	0.080	0.087
0.6 M $CuSO_4$ +1.4×10^{-3} M HCl + 1.8 M H_2SO_4	0.100	0.110

Table 3.3: Open-circuit potential measured on a fresh copper surface for solutions that contained 1.8 M H_2SO_4, 1.4×10^{-3} M HCl and 0.05, 0.1 or 0.6 M $CuSO_4$. For comparison, also the calculated Nernst potential is given assuming activity of free Cu^{2+} equal to $CuSO_4$ concentration.

3.4.2 The effect of H_2SO_4 concentration

Figure 3.10(a) shows the island density, N_p, as a function of H_2SO_4 concentration as obtained from SEM images (not shown) for copper deposition on RuTa from solutions of 0.6 M $CuSO_4$, 1.4×10^{-3} M HCl and different H_2SO_4 concentration (0.018, 0.18 or 1.8 M). The effect of H_2SO_4 concentration remained similar as observed for the chloride free solution (see § 3.3.2) i.e. a higher island density was observed with the increase in H_2SO_4 concentration. Figure 3.10(b) shows current density, i, versus overpotential corrected for IR_s drop, η_{IR}, curves for copper deposition on RuTa from the same solutions as in Figure 3.10(a). The overpotential was determined with respect to the Cu OCP (0.10 V) for the 0.6 M $CuSO_4$ solution as shown in Table 3.3 and corrected for IR_s drop with R_s= 94, 74 and 44 Ω for the 0.018, 0.18 and 1.8 M H_2SO_4 solutions, respectively. The increase in H_2SO_4 concentration resulted in a gradual shift of the current-overpotential curve, exhibiting higher nucleation overpotential for the highest H_2SO_4 concentrations. The negative shift in overpotential with increasing H_2SO_4 concentration is similar to the trend seen for N_p: a higher overpotential and N_p are observed with the increase in H_2SO_4 concentration. The inset of Figure 3.10(a) shows cross-sectional SEM images of Cu islands, electrodeposited on RuTa at -10 mA cm^{-2} for charge density of 0.01 C cm^{-2} from the solutions under investigation. Deposition from the 0.018 M H_2SO_4 solution resulted in finger-shaped islands with rounded tips, whereas dendrites were seen in the presence of HCl when no H_2SO_4 is present (see Figure 3.8 in §3.3.3). The increase in H_2SO_4 concentration to 0.18 resulted in a more rounded island shape and spherical islands were observed for the 1.8 M H_2SO_4 solution (see inserts in Figure 3.10(a)).

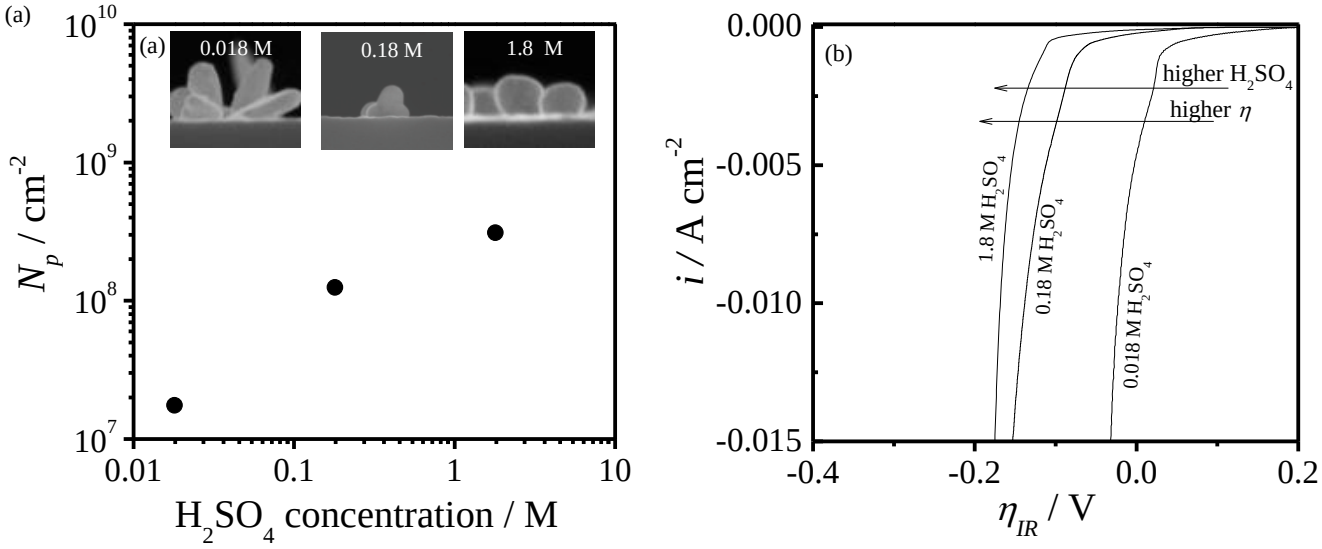

Figure 3.10: (a) N_p as a function of H_2SO_4 concentration for copper deposition on RuTa at current density of -10 mA cm^{-2} and charge density of 0.01 C cm^{-2}. The deposition experiments were performed from solutions of 0.6 M $CuSO_4$, 1.4×10^{-3} M HCl and different H_2SO_4 concentrations (0.018, 0.18 or 1.8 M). In the inset: cross-sectional SEM images of the Cu islands as a function of H_2SO_4 concentration for the solutions under investigation. (b) Current density-overpotential curves for copper deposition on RuTa from solution under investigation at a polarization rate of 0.02 V s^{-1}. The overpotential was determined with respect to the Cu OCP (0.1 V vs. Ag/AgCl) for the 0.6 M $CuSO_4$ solution as shown in Table 3.3 and corrected for IR_s drop with R_s= 94, 74 and 44 Ω for the 0.018, 0.18 and 1.8 M H_2SO_4 solutions, respectively.

3.4.3 The effect of Cl^- concentration

Figure 3.11(a) shows the island density, N_p, as a function of HCl concentration as obtained from SEM images (not shown) for copper deposition on RuTa from solutions of 0.6 M $CuSO_4$, 1.8 M H_2SO_4 and different HCl concentrations (0.14×10^{-3}, 1.4×10^{-3} or 7×10^{-3} M). The effect of HCl concentration for the acidified 0.6 M $CuSO_4$ solution was similar to the effect observed in the H_2SO_4 free solutions (see §3.3.3) i.e. an increase in Cl^- concentration led to a decrease in island density. Figure 3.11(b) shows current density, i, versus overpotential corrected for IR_s drop, η_{IR}, curves for copper deposition on RuTa from the same solutions as in Figure 3.11(a). The overpotential was determined with respect to the Cu OCP (0.1 V vs. Ag/AgCl) for the 0.6 M $CuSO_4$ solution as shown in Table 3.3 and corrected for IR_s drop with R_s = 44 Ω. From the figure it follows that the increase in Cl^- concentration resulted in a gradual depolarization of the current-overpotential curve, exhibiting smaller nucleation overpotential. Note that for concentrations

higher than 10×10^{-3} M HCl, an opposite effect might be observed as indicated by Saho *et al.* For copper deposition on silicon from acidified $CuSO_4$ solutions containing various Cl^- concentrations [36]. The positive shift in overpotential with the increase in Cl^- concentration is similar to the trend seen for N_p. i.e. smaller overpotential and lower N_p were observed with the increase in Cl^- concentration. In the inset of Figure 3.11(a) cross-sectional SEM images of Cu islands are shown, electrodeposited on RuTa at -10 mA cm^{-2} for a charge density of 0.01 C cm^{-2} from the solutions under investigation. The increase in the Cl^- concentration from 0.14×10^{-3} M to 1.4×10^{-3} M promoted growth in a direction perpendicular to the surface, resulting in transformation of the island shape from hemispherical to spherical. Further increase in the Cl^- concentration to 7×10^{-3} M disturbed the spherical growth and variation of shapes were observed. Saho *et al.* reported a dendritic growth for copper deposition on silicon from solution of 0.01 M $CuSO_4$, 0.5 M H_2SO_4 and 14×10^{-3} M HCl [36]. Thus, at higher Cl^- concentrations the spherical growth can be completely disturbed.

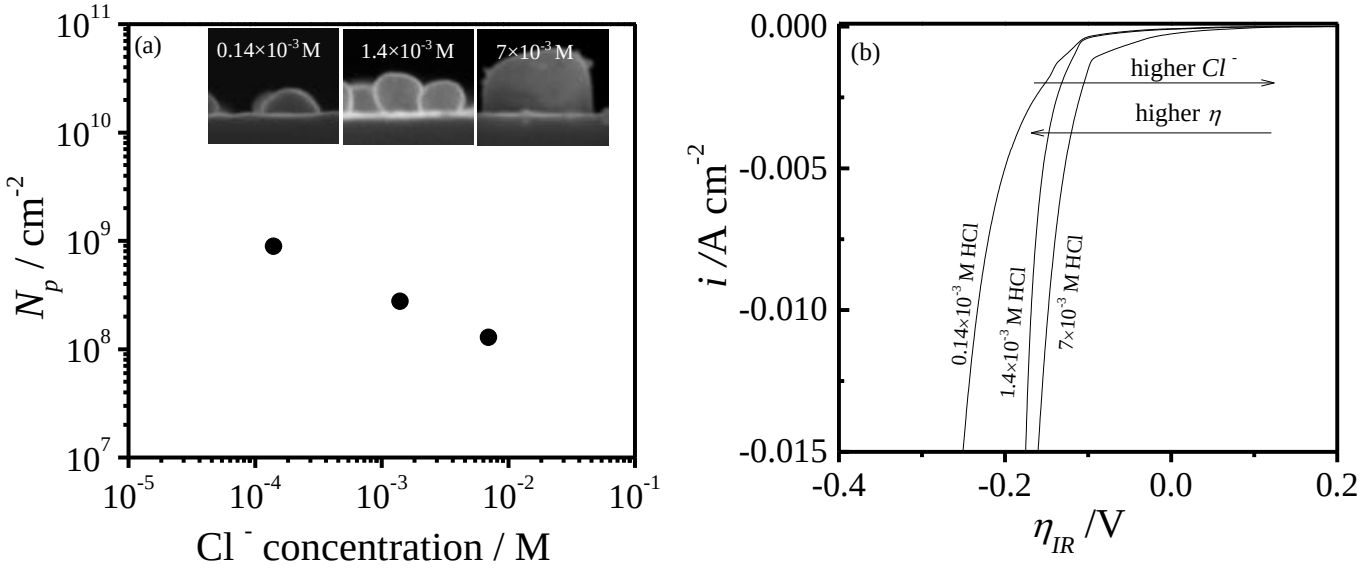

Figure 3.11: (a) N_p as a function of Cl^- concentration for copper deposition on RuTa at current density of -10 mA cm^{-2} and charge density of 0.01 C cm^{-2}. The deposition experiment were performed from solutions of 0.6 M $CuSO_4$, 1.8 M H_2SO_4 and different HCl concentration (0.14×10^{-3}, 1.4×10^{-3} or 7×10^{-3} M). In the inset: cross-sectional SEM images of the Cu islands as a function of HCl concentration, elecrodeposited from the solutions under investigation. (b) Current density-overpotential curves for copper deposition on RuTa from the solutions under investigation at a polarization rate of 0.02 V s^{-1}. The overpotential was determined with respect to the Cu OCP (0.1 V vs. Ag/AgCl) for the 0.6 M $CuSO_4$ solution as shown in Table 3.3 and corrected for IR_s drop with $R_s = 44\ \Omega$.

3.5 Summary

The effect of the inorganic components, H_2SO_4, $CuSO_4$ and Cl^- ions on the nucleation and growth of copper on RuTa was studied. The experimental results show that the island morphology and the island density are determined by the concentration ratio of Cu^{2+}/ Cl^- /H_2SO_4. When only $CuSO_4$ is present in solution, a range of island morphologies is obtained depending on the Cu^{2+} concentration. Adding H_2SO_4 promoted spherical growth whereas Cl^- ions promote growth in directions perpendicular to the RuTa surface. The effect of the individual components remained similar when they were all present in the solution. For the islands density N_p, it followed that lowering the $CuSO_4$ and/or HCl concentration leads to an increase in the N_p, whereas for sulphuric acid the opposite effect was observed: high H_2SO_4 concentration leads to increase in the N_p. Further, it was found that the solution pH is the one that has strong effect on the island density rather than the ionic strength. In addition, it was shown that when a higher N_p was observed for a specific change in the solution composition, also increase in the overpotential for nucleation was measured, a relationship can be made between the overpotential for nucleation and N_p. Combination of all results leads to the conclusion that acidified solutions with a low $CuSO_4$ concentration and with low Cl^- content are favorable to achieve faster coalescence of the Cu islands into a continuous thin Cu film. These solutions would hence be beneficial to use for the deposition of copper into small features by DP approach.

[1] J. Reid, S. Mayer, E. Broadbent, E. Klawuhn and K. Ashtiani, Factors influencing damascene feature fill using copper PVD and electroplating. Solid State Technology, 43(7) (2000) 86.
[2] J. Reid, Copper electrodeposition: principles and recent progress, Japanese Journal of Applied Physics 40 (2001) 2650.
[3] P. C. Andricacos, C. Uzoh, , J.O. Dukovic, J. Horkans and H. Deligianni, Damascene copper electroplating for chip interconnections, IBM Journal of Research and Development, 42(5) (1998) 567.
[4] U. Landau, Copper metallization of semiconductors interconnects-Issues and prospects. In Proceedings–Electrochemical Society, 26 (2000) 231.
[5] K.M. Takahashi, Electroplating copper onto resistive barrier films, Journal of The Electrochemical Society, 147(4) (2000) 1414.
[6] E.K. Broadbent, E.J. McInerney, L.A. Gochberg, and R.L. Jackson, Experimental and analytical study of seed layer resistance for copper damascene electroplating, Journal of Vacuum Science & Technology B: Microelectronics and Nanometer Structures, 17(6) (1999) 2584.

[7] S. Armini and P. M. Vereecken, Impact of Terminal Effect on Cu Plating: Theory and Experimental Evidence, ECS Transactions, 25(27) (2010) 185.
[8] Z. Nagy, J.P. Blaudeau, N.C. Hung, L.A. Curtiss and D. J. Zurawski, Chloride ion catalysis of the copper deposition reaction, Journal of The Electrochemical Society, 142(6) (1995) L87-L89.
[9] W. Shao, G. Pattanaik and G. Zangari, Influence of chloride anions on the mechanism of copper electrodeposition from acidic sulfate electrolytes, Journal of The Electrochemical Society, 154(4) (2007) D201.
[10] Y.L. Kao, K.C. Li, G.C. Tu and C.A. Huang, Microstructural study of the effect of chloride ion on electroplating of copper in cupric sulfate-sulfuric acid bath, Journal of The Electrochemical Society, 152(9) (2005) C605.
[11] W.P. Dow, H.S. Huang, M.Y. Yen and H.H. Chen, Roles of chloride ion in microvia filling by copper electrodeposition ii. studies using epr and galvanostatic measurements, Journal of The Electrochemical Society, 152(2) (2005) C77.
[12] Z. V. Feng, X. Li and A. A. Gewirth, Inhibition Due to the Interaction of Polyethylene Glycol, Chloride, and Copper in Plating Baths: A Surface-Enhanced Raman Study,The Journal of Physical chemistry B, 107 (2003) 9415.
[13] J.P. Healy, D. Pletcher and M. Goodenough, The chemistry of the additives in an acid copper electroplating bath: Part I. Polyethylene glycol and chloride ion, Journal of Electroanalytical Chemistry, 338(1) (1992) 155.
[14] J.J. Kelly and A.C. West, Copper deposition in the presence of polyethylene glycol I. Quartz crystal microbalance study, Journal of The Electrochemical Society, 145(10)(1998) 3472.
[15] M. Kang, M.E. Gross and A.A. Gewirth, Atomic force microscopy examination of Cu electrodeposition in trenches, Journal of The Electrochemical Society, 150(5) (2003) C292.
[16] Y.D. Gamburg and G. Zangari, Theory and practice of metal electrodeposition, Springer (2011), Chapter 6, Morphology of the Growing Metal Surface, p. 123-141.
[17] D. M. Soares, S. Wasle, K.G. Weil and K. Doblhofer, Copper ion reduction catalyzed by chloride ions, Journal of Electroanalytical Chemistry, 532(1) (2002) 353.
[18] L. Guo, S. Zhang and P. Searson, Growth kinetics of disk-shaped copper islands in electrochemical deposition, Physical Review E, 79(5) (2009) 051601.
[19] G. Oskam, P.M. Vereecken, P.C. Searson, Electrochemical deposition of copper on n–Si/TiN, Journal of the Electrochemical Society 146 (1999) 1436.
[20] T.P. Moffat, M. Walker, P.J. Chen, J.E. Bonevich, W.F. Egelhoff, L. Richter, C. Witt, T.Aaltonen, M. Ritala, M. Leskel, D. Josella, Electrodeposition of Cu on Ru barrier layers for damascene processing, Journal of the Electrochemical Society 153 (2006) C37.
[21] D. Grujicic, B. Pesic, Electrodeposition of copper: the nucleation mechanisms, Electrochimica Acta 47 (2002) 2901.
[22] N. Jourdan, L. Carbonell, N. Heylen, J. Swerts, S. Armini, A. Maestre Caro, S. Demuynck, K. Croes, G. Beyer, Z. Tökei, S. Van Elshocht, E. Vancoille, Evaluation of metallization options for advanced Cu interconnects application, ECS Transactions 34 (2011) 515.
[23] http://rsb.info.nih.gov/ij/docs/index.html
[24] M. Nagar, A. Radisic, K. Strubbe and P.M. Vereecken, The effect of cupric ion concentration on the nucleation and growth of copper on RuTa seeded substrates, Electrochimica Acta, 92 (2013) 474.

[25] C.R. Henry, Morphology of supported nanoparticles, Progress in surface science, 80(3) (2005) 92.
[26] W.Y. Ko, W.H. Chen, S.D. Tzeng, S. Gwo and K.J. Lin, Synthesis of pyramidal copper nanoparticles on gold substrate, Chemistry of materials,18(26) (2006) 6097.
[27] L. Gouand C.J. Murphy, Solution-phase synthesis of Cu2O nanocubes, Nano Letters, 3(2) (2003) 231.
[28] D.K. Sarkar, X.J. Zhou, A. Tannous, M. Louie and K.T. Leung, Growth of self-assembled copper nanostructure on conducting polymer by electrodeposition, Solid state communications, 125(7) (2003) 365.
[29] I. Lisiecki, Size, shape, and structural control of metallic nanocrystals, The Journal of Physical Chemistry B, 109(25) (2005) 12231.
[30] S.C. Tang, X.K. Meng and S.Vongehr, An additive-free electrochemical route to rapid synthesis of large-area copper nano-octahedra on gold film substrates, Electrochemistry Communications, 11(4) (2009) 867.
[31] S. Onaka, T. Fujii and M.Kato, Elastic strain energy due to misfit strains in a polyhedral precipitate composed of low-index planes, Acta materialia, 55(2) (2007) 669.
[32] A. Radi, D. Pradhan, Y. Sohn and K.T. Leung, Nanoscale Shape and Size Control of Cubic, Cuboctahedral, and Octahedral Cu/Cu2O Core Shell Nanoparticles on Si [100] by One-Step, Templateless, Capping-Agent-Free Electrodeposition, ACS nano, 4(3) (2010) 1553.
[33] E.L. Shock and H.C. Helgeson, Calculation of the thermodynamic and transport properties of aqueous species at high pressures and temperatures: Correlation algorithms for ionic species and equation of state predictions to 5 kb and 1000 C, Geochimica et Cosmochimica Acta, 52(8) (1988) 2009.
[34] D. Barkey, F. Oberholtzer and Q. Wu, Kinetic Anisotropy and dendritic growth in electrochemical deposition, Physical review letters, 75(16) (1995) 2980.
[35] F. Oberholtzer, D. Barkey and Q. Wu, Kinetic selection of morphology and growth velocity in electrochemical deposition. Physical Review E, 57(6) (1998) 6955.
[36] W. Shao and G. Zangari, Dendritic growth and morphology selection in copper electrodeposition from acidic sulfate solutions containing chlorides, The Journal of Physical Chemistry C, 113(23) (2009) 10097.
[37] N.D. Nikolić, K.I. Popov, L.J. Pavlović and M.G. Pavlović, Morphologies of copper deposits obtained by the electrodeposition at high overpotentials, Surface and Coatings Technology, 201(3) (2006) 560.
[38] J.S. Langer, Instabilities and pattern formation in crystal growth, Reviews of Modern Physics, 52(1) (1980) 1.
[39] Y. Sawada, A. Dougherty and J.P. Gollub, Dendritic and fractal patterns in electrolytic metal deposits, Physical review letters, 56(12) (1986) 1260.
[40] J. A. Dirksen and T.A. Ring, Fundamentals of crystallization: kinetic effects on particle size distributions and morphology, Chemical Engineering Science, 46(10) (1991) 2389.

CHAPTER 4: THE EFFECT OF CUPRIC ION CONCENTRATION ON THE NUCLEATION AND GROWTH OF COPPER ON RUTA SEEDED SUBSTRATES.

This Chapter describes experiments and results of copper deposition on a RuTa alloy from acid copper sulfate solutions without additives. The main focus is on the effect of cupric ion concentration, [Cu^{2+}], and deposition current density on the nucleation and growth processes during galvanostatic deposition. Based on the experimental results, we propose a method to interpret the galvanostatic transients and correlate the island density, N_p, with the copper deposition overpotential. It is shown that an exponential relationship exists between the island density and the actual deposition overpotential irrespective of Cu^{2+} concentration and applied current density. From this relationship it follows that N_p values can be estimated for a given substrate, based solely on the copper deposition overpotential as determined from the galvanostatic transients.

4.1 Introduction

Many challenges exist in developing a process which will allow the filling of small features with copper by direct plating. One of the main challenges is to control the island density, N_p, and the geometry of the copper nuclei (i.e. towards pseudo-2D islands). In this aspect, the complexity of the bath chemistry, together with the incomplete understanding of the mechanism of electrochemical nucleation and growth of copper on foreign substrates, makes the theoretical prediction of N_p difficult. Indeed, many studies show the variation of island or nucleus densities during copper deposition as a function of the applied potential, but the relationship with overpotential is often ignored or irrelevant [1]. Furthermore, most of the published studies discuss potentiostatic rather than galvanostatic deposition [1-5]. When comparing solutions with different [Cu^{2+}] concentration, the copper equilibrium potentials shift, and therefore, one should compare overpotentials instead of potentials. In this work, galvanostatic transients are used to correlate N_p to the overpotential subsequent to copper deposition from solutions that contain different [Cu^{2+}] concentrations. In addition, the use of overpotentials allows a fair comparison

between different substrates as well as a variety of changing parameters such as different current density, presence of additives etc. Further, as copper deposition in the industrial environment is mostly carried out under galvanostatic control, the interpretations of the galvanostatic transients can be very beneficial.

4.2 Experimental details

Copper was electrodeposited on a RuTa alloy from acid copper sulfate solutions without additives. Details concerning the experimental set-up and substrate properties can be found in Chapter 2. The current-potential curves were obtained by polarizing the potential negatively from 0.5 V to -0.5 V vs. Ag/AgCl and positively from -0.5 V to 0.5 V vs. Ag/AgCl at a rate of 0.02 V s^{-1}. The galvanostatic experiments were performed at current densities between -1 and -200 mA cm^{-2}. The plating solutions contained 1.8 M H_2SO_4, 1.4×10^{-3} M HCl and 0.01, 0.05, 0.1 or 0.6 M $CuSO_4 \cdot 5H_2O$. The copper equilibrium potentials, $U_{(Cu^{2+}/Cu),eq}$ for solutions with different cupric ion concentration were determined experimentally by open-circuit potential (OCP) measurements on a 100 nm PVD copper seed on 15 nm Ta/TaN for 60*s* without agitation. The solution resistance (R_s) was determined from the slope reciprocal in the linear part of *I*-U relationship. The R_s was 38, 39, 39 and 44 Ω for the 0.01, 0.05, 0.1 or 0.6 M $CuSO_4$ solutions, respectively. The R_s values were verified with electrochemical impedance spectroscopy (EIS) measurements. The EIS measurements were conducted on a 150 nm copper film electrodeposited on the RuTa wafers (at current density of -10 mA cm^{-2} from a solution that contained 0.25 M $CuSO_4$ and 1.8 M H_2SO_4). For the different $CuSO_4$ solutions, the measurements were performed 10 mV more negative than the OCP value) and after immersion of the samples into the different $CuSO_4$ solutions for 30*s*. The AC amplitude was 10 mV and the frequency ranged from 100 Hz to 50 kHz. For these measurements, a PGSTAT30 with frequency response analyzer (FRA2-Metrohm) was used. The values of R_s were 43, 44, 43 and 51 Ω for the 0.01, 0.05, 0.1 or 0.6 M $CuSO_4$solutions, respectively. For the *IR* correction of the *i*-U curves, the R_s values obtained from the slope reciprocal in the linear part of *I*-U relationship were used. The increase in $CuSO_4$ concentration leads to a decrease in the concentration of protons at a given concentration of sulfuric acid as the equilibrium position for H_2SO_4 dissociation shifts to the left. Since protons are the main contributors to the solution conductivity (they have 5-10 times higher mobility

compared with other ions present in solution), the solution resistivity increased slightly with the increase in $CuSO_4$ concentration [6]. All experiments were performed at room temperature (21° C) without agitation of the solution. For each experiment a fresh RuTa sample was used without any further pretreatment. After copper deposition, samples were immediately removed from the solution, rinsed with de-ionized water and dried in nitrogen flow. The copper islands were examined using Scanning Electron Microscopy (SEM Nova 200, FEI). The SEM images were analyzed with Image*J* digital analysis software [7] in order to count the number of copper islands and determine the average diameter. For one data point, 3 images taken at different spots near the center of the plated area were analyzed.

4.3 Current-potential characteristics

Figure 4.1 shows the current-potential curves at RuTa in the acid solution in the absence and the presence of 0.01M $CuSO_4$. In the presence of Cu^{2+} ions, a small cathodic current wave (prewave of -0.02 mA cm^{-2}) appeared before the copper equilibrium potential, $U_{(Cu^{2+}/Cu),eq,}$ of 0.05 V vs. Ag/AgCl, determined from OCP measurements on a fresh copper surface (see Table 4.1). Since such currents were not observed in the absence of Cu^{2+} ions, the prewave can be attributed to the underpotential deposition (UPD) of copper on RuTa, as well as to the partial reduction of Cu^{2+} to Cu^{+}. Indeed, copper UPD and cuprous ion formation at noble metals such as platinum, gold and ruthenium [8,9] are well-known. The onset of copper deposition on RuTa appeared at -0.06 V, i.e. 110 mV more negative than the Nernst equilibrium potential $U_{(Cu^{2+}/Cu),eq.}$ The difference between the onset potential for deposition on foreign substrates and the Nernst equilibrium potential is commonly known as the nucleation overpotential [10,11]. At potentials more negative than -0,06 V, the cathodic current increased sharply with potential and reached a maximum value at -0.15 V. The occurrence of a peak is characteristic for a diffusion limited copper electrodeposition reaction. At -0.25 V the cathodic current increased again due to hydrogen evolution. On the reverse scan, the cathodic current gradually decreased and became zero at 0.001 V. Upon further polarization towards positive potentials, an anodic stripping peak was observed with a maximum at 0.14 V. The charge under the stripping peak was 0.027 C cm^{-2}, equivalent to about 10 nm of deposited copper.

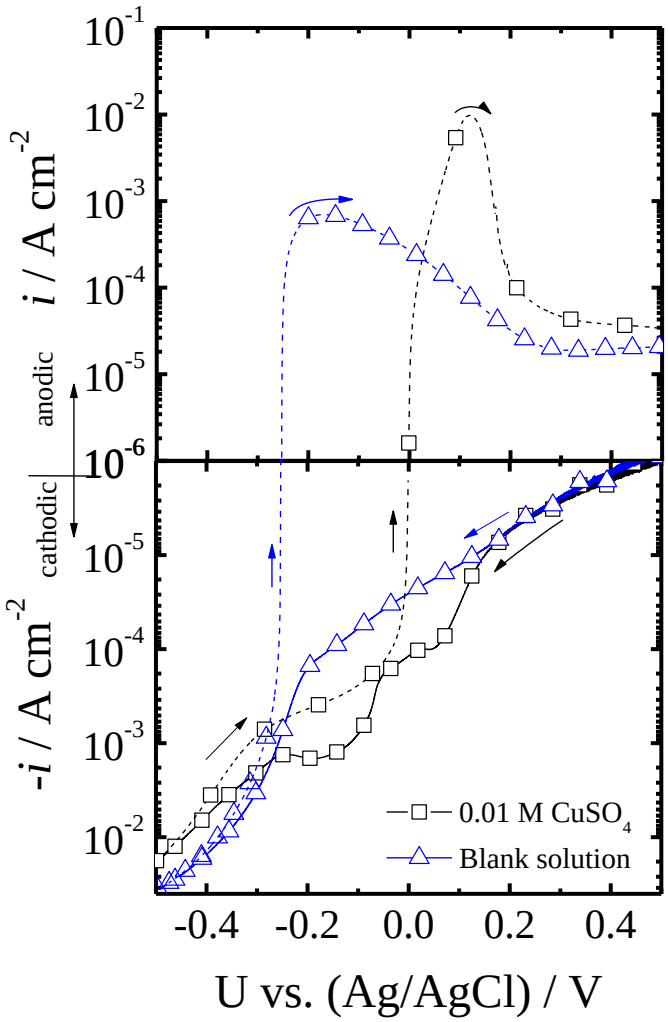

Figure 4.1: Semi-logarithmic plots of current density, *i*, versus potential, U vs. (Ag/AgCl), at RuTa in solutions of 1.8 M H_2SO_4, 1.4 $\times 10^{-3}$ M HCl in the absence (blank solution) and in the presence of 0.01M $CuSO_4$ at a polarization rate of 0.02 V s^{-1}. Solid lines indicate the forward scan from 0.5 V towards more negative potentials and the dashed lines indicate the reverse scan from -0.5 V towards more positive potentials.

Figure 4.2 shows current-potential measurements carried out in the solutions with the Cu^{2+} concentrations. In solutions with different cupric ion concentrations, the copper equilibrium potentials differ, and therefore, one should compare the overpotentials, η, in the different solutions instead of potentials. The η values were determined with respect to the copper equilibrium potential, $U_{(Cu^{2+}/Cu),eq}$ for the solutions with different $CuSO_4$ concentration as summarized in Table 4.1:

Equation 4.1:
$$\eta = U - U_{(Cu^{2+}/Cu),eq}$$

For all solutions, the UPD/(Cu^{2+}/Cu^{+}) region is now clearly positioned positive of zero overpotential. An increase in Cu^{2+} concentration resulted in a gradual shift of the onset of copper deposition to smaller overpotentials (i.e. smaller nucleation overpotential). On the reverse scan, the potential of zero current diverged somewhat from $U_{(Cu^{2+}/Cu),eq}$ especially for the solutions with the lowest Cu^{2+} concentration as at this point in the potentiodynamic measurement the actual surface concentration of Cu^{2+} is lower than bulk concentration due to cupric ion depletion (see also Table 4.1).

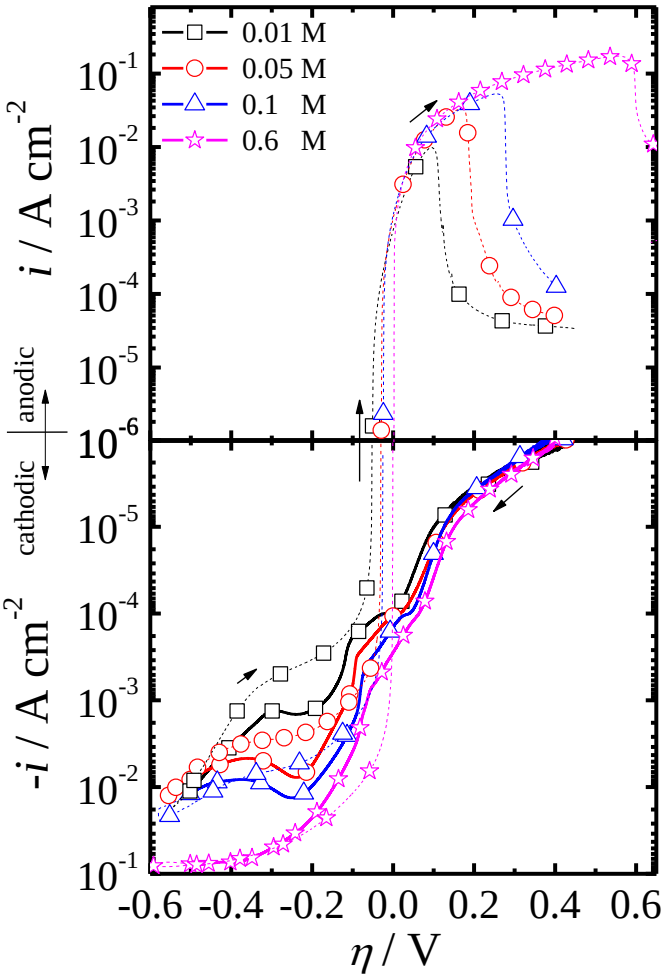

Figure 4.2: Semi-logarithmic plots of current density, *i,* versus overpotential, *η,* at RuTa in solutions of 1.8 M H_2SO_4 1.4 $\times 10^{-3}$ M HCl and 0.01, 0.05, 0.1 or 0.6 M $CuSO_4$ at a polarization rate of 0.02 V s^{-1}. solid lines indicate the negative polarization scans and the dashed lines indicate the positive polarization scans. The equilibrium potential for copper was determined by open-circuit potential measurements on a 100 nm PVD Cu seed on 15 nm Ta/TaN barrier for each solution.

	Nominal $CuSO_4$ concentration/ M			
	0.01	**0.05**	**0.1**	**0.6**
Cu (OCP) (V vs. Ag/AgCl)	0.050	0.072	0.080	0.100
Nernst potential (V vs. Ag/AgCl)	0.058	0.078	0.087	0.110
Zero current potential (V vs. Ag/AgCl)	0.001	0.042	0.067	0.099

Table 4.1: Open-circuit potentials, measured on a fresh copper surface (100 nm PVD Cu seed on 15 nm Ta/TaN barrier) for solutions of 1.8 M H_2SO_4, 1.4 $\times 10^{-3}$ M HCl and 0.01, 0.05, 0.1 or 0.6 M $CuSO_4$. For comparison, the calculated Nernst potential is given assuming activity of free Cu^{2+} equal to $CuSO_4$ concentration and the zero current potential as obtained from the reverse scan of current-potential curves on Cu/RuTa surface in Figure 4.2.

4.4 Galvanostatic deposition

4.4.1 The effect of the current density on the nucleation density, N_p

Figure 4.3 shows the overpotential, η, as a function of time during the galvanostatic deposition of copper on RuTa at different current densities from the 0.6 M $CuSO_4$ solution. The η values for copper deposition were determined with respect to the copper OCP for the 0.6 M $CuSO_4$ solution (see Table 4.1). The inset in Figure 4.3 shows the η transient for a current density of -200 mA cm^{-2} with the different features of interest indicated. For current densities $-50 \leq i \leq -200$ mA cm^{-2}, η dropped from OCP to a value in a first potential plateau (P_1) within a few tens of milliseconds after applying the current. The potential remained there for some time and then an additional drop to a second plateau (P_2) was observed. The resident time in plateau P_1 increased with decreasing current density. For current densities between -1 and -10 mA cm^{-2}, no such second potential drop was observed, not even after 3600*s* of deposition. The initial drop in η is designated as P_0 in the inset of Figure 4.3 (inset). The initial potential drop, P_0, towards plateau P_1 resides at positive η and corresponds to charging of the double layer, partial reduction to Cu^+, formation of 2D islands and UPD region. Note that when RuTa is pre-polarized in the 0.6 M $CuSO_4$ solution in the UPD potential range (0.5 V to 0.13 V vs. Ag/AgCl), the OCP changed to 0.16 V vs. Ag/AgCl, indicating a Faradaic component in P_0. Only when η becomes negative, nucleation and growth of 3D islands on RuTa can proceed [12]. Note that 2D nucleation and growth preceding formation of 3D islands is not uncommon, especially not for systems with underpotential deposition (Stranski-Krastanov mode) [8,9]. At the start of plateau P_1, nucleation

is already completed and P_1 corresponds to the growth of the copper nuclei (i.e. reduction of Cu^{2+} on copper). Due to a continuous cupric ion depletion at the high current densities in the stagnant solution, Cu^{2+} surface concentration becomes zero at longer deposition times (i.e. copper deposition becomes completely diffusion controlled). When this is the case, hydrogen evolution starts as the system needs to compensate for the deficiency in the current. Consequently, the potential is driven towards more negative values and levels off at a plateau P_2 which corresponds to hydrogen evolution reaction (with a partial current density for hydrogen evolution close to the applied current density minus the steady-state diffusion-limited copper deposition current density due to natural convection). From Figure 4.3, it can be seen that η for copper deposition becomes more negative and that the time to reach P_2 decreased as the current density increased. As full depletion of cupric ions takes longer at lower current densities, the potential drop occurs at longer times. It should be emphasized that there were no additives present in the plating bath. Thus, the potential drop to P_2 seen in the η-time response corresponds to the onset of hydrogen evolution rather than to reactions associated with the presence of additives (as will be discussed in Chapter 5) [13].

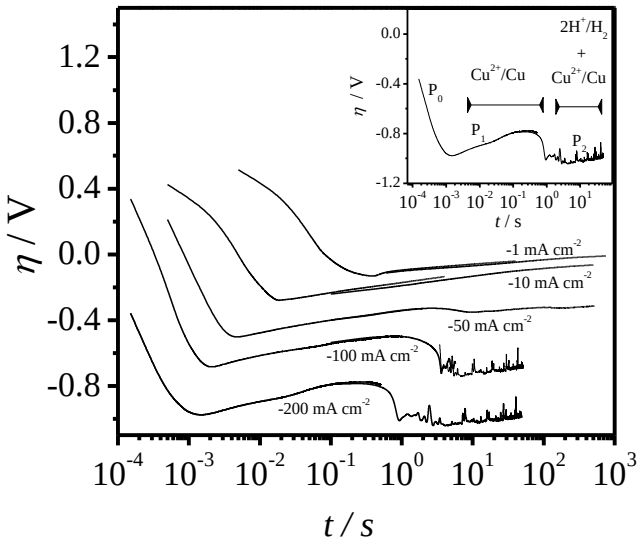

Figure 4.3: η vs. time curves at RuTa in solutions of 0.6 M $CuSO_4$, 1.8 M H_2SO_4 and 1.4×10^{-3} M HCl at current densities of -1,-10,-100 and -200 mA cm^{-2}. The overpotenial is given with respect to the equilibrium potential for copper (Table 4.1). In the inset: η-time transient for a current density of -200 mA cm^{-2} with the different features of interest indicated: P_0 for charging of the double layer, partial reduction to Cu^+, formation of 2D islands and UPD region, P_1 for copper deposition overpotential and P_2 for additional hydrogen evolution reaction.

Figure 4.4 shows linear voltammograms for copper deposition on RuTa and Cu electrodes from the 0.6 M $CuSO_4$ solution as the one shown in Figure 4.2. The values of η in plateau P_1, obtained from the galvanostatic responses in Figure 4.3, are added to the figure and are marked as circles. Note that the value for η gradually shifts to more positive values when the effective copper surface area increases as the copper islands grow (Figure 4.3). Therefore, unlike copper deposition on copper, the overpotential in case of nucleation and growth processes on RuTa should be considered after taking into account the effective copper surface area of the deposited copper particles. As such, one should compare η values for the same effective copper surface area. In Figure 4.4 the η values, corresponding to an effective copper surface area, A_{Cu}, of 0.19 (or total effective electrode area of A_{eff} =1.09 and 1.14 for hemispherical and spherical islands respectively[2]) and at steady state, A_{CuSs} i.e. when the overpotential remains constant in time. The overpotential value for A_{CuSs} was determined after 300*s* for all current densities whereas the overpotential value for A_{Cu} was determined according to the calculated time required for A_{Cu} =0.19. The dimensionless A_{Cu} is calculated from the experimentally found island density, N_p (cm^{-2}) and the effective copper deposition charge according to (for detail, see Appendix):

Equation 4.2:
$$A_{P\ (Cu)} = \frac{6\pi}{x}\left(\frac{q_{Cu}}{KN_p}\right)^{2/3}$$

where q_{Cu} ($C\ cm^{-2}$) is the partial charge density associated with copper deposition and $K\ (C \cdot cm^{-3})$ is the material constant, depending on the geometry of the islands and the material properties [18]:

Equation 4.3:
$$K = \left(\frac{\pi n F \rho}{xMw}\right)$$

where $\rho = 8.94$ g $cm^{-3}$for copper assuming a dense deposit, Mw = 63.54 g mol^{-1} is the molar mass of copper and x is a dimensionless factor indicating the shape of the island: x = 6 for

[2] A_{Cu} is 0.19 in all cases while A_{eff} is different for hemispherical and spherical islands. For the island shape determination see Appendix.

spherical and x = 12 for hemispherical nuclei (see also Appendix). A good correlation between the overpotential seen in the galvanostatic transients for A_{Cu}=0.19 and A_{CuSs} and the voltammograms for RuTa and Cu was found for the current densities under investigation. This observation confirms that, indeed, the correct overpotential value to consider while making comparison of different galvanostatic transients should be determined for the same effective copper surface area. In addition, the change of the overpotential value observed at A_{Cu}=0.19 to the one observed at A_{CuSs} confirms the transition of the electrode surface from Cu/RuTa to Cu (in our case, with a similar effective copper surface area as at a planar Cu electrode).

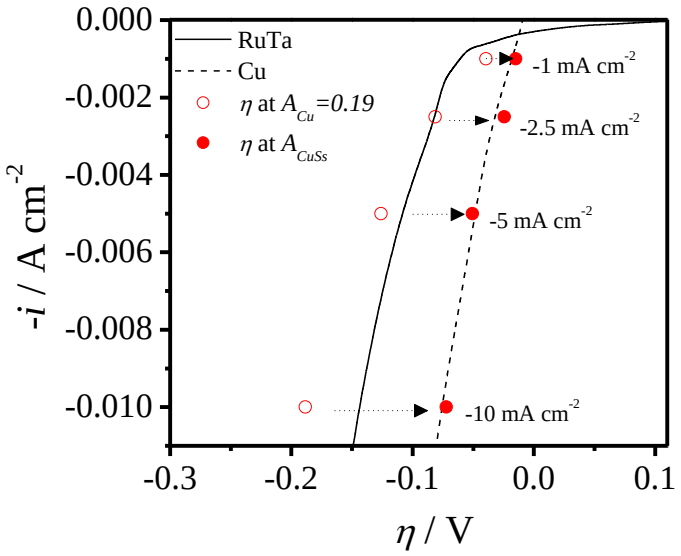

Figure 4.4: linear -*i*- η overpotential curves for copper deposition on RuTa (solid line) and on copper (dashed line). The η values in plateau P_1 for A_{Cu}=0.19 (○) and A_{CuSs} (●) as obtained from the galvanostatic responses in Figure 4.3 are also added and are marked as circles.

Figure 4.5 shows top-down SEM images of copper islands, electrodeposited on RuTa at current densities between -1 and -50 mA cm^{-2} from the 0.6 M $CuSO_4$ solution. At -1 mA cm^{-2}, relatively large, rod-like and sphere-like copper islands were formed. Increasing the deposition current to -5, -10 and -50 mA cm^{-2} led to a significant increase in the number of islands and the formation of smaller hemispherical copper islands. For the same charge, the size of the nuclei will indeed be smaller for a higher number of islands per unit of area (indicated as island density, N_p). At -1 mA cm^{-2} the island density, N_p, was 1.0×10^7 cm^{-2}. An increase in deposition current to -5, -10 and -50 mA cm^{-2} led to an increase in N_p to 1.5×10^8, 1.0×10^9 and 7.2×10^9 cm^{-2},

respectively. As an increase in current density is equivalent with an increase in overpotential, the increase in N_p shows that more nucleation sites are activated at higher current densities [14-16].

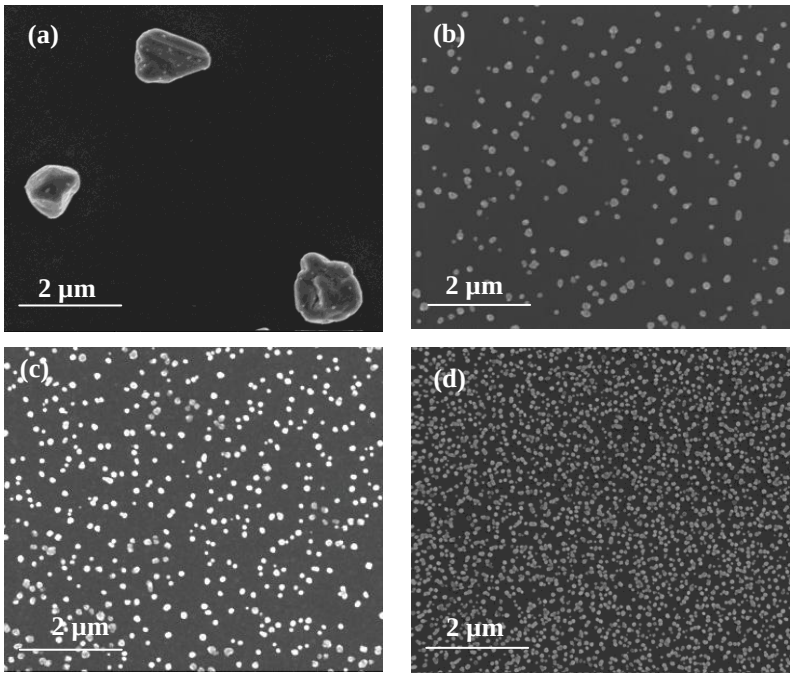

Figure 4.5: Top-down SEM images of Cu islands deposited from solution of 0.6 M $CuSO_4$ 1.8 M H_2SO_4 and 1.4×10^{-3} M HCl at current density of (a) -1 (b) -5 (c) -10 and (d) -50 mA cm^{-2} for deposition charge density of 0.04 C cm^{-2}.

Figure 4.6 shows the island density, N_p, as a function of the applied current density as obtained from SEM images such as those shown in Figure 4.5, for current densities between -1 and -200 mA cm^{-2}. A steep increase in N_p was observed with increasing i for current densities between -1 and -10 mA cm^{-2}. At -50 mA cm^{-2} the island density leveled off and no significant further increase in N_p was found for -100 and -200 mA cm^{-2}. Examination of the i-η curve (see Figure 4.2) shows that the measured shift in overpotential at higher cathodic current densities ($|i|$>10 mA cm^{-2}) is dominated by *IR* drop (e.g. the measured linear I-U behavior shows up as a clear deviation of exponential i-η relationship for 0.6 M in the semilogarithmic plot of Figure 4.2). In the true exponential i-η_{IR} relationship, the actual overpotential does not longer change much with current density, higher than -50 mA cm^{-2}. Hence, the increase of the N_p with increasing current has an apparent limit due to the exponential relationship between current density and overpotential at higher current densities. Table 4.2 shows the values of the

overpotential for copper deposition in plateau P_1 for A_{Cu} = 0.19 with and without correction for IR_s (R_s = 44 Ω) and with η_{IR} calculated as:

Equation 4.4:
$$\eta_{IR} = U - U_{(Cu^{2+}/Cu),eq} - IR_s$$

It follows that, indeed, η_{IR} changed by only ~ 10 mV when increasing the current density from -50 to -200 mA cm^{-2}. As the N_p is determined by the overpotential, no significant change in the island density is hence observed between -50 and -200 mA cm^{-2}. From these observations it follows that an increase in the current density alone is not sufficient to obtain the N_p which is needed for direct plating applications. Therefore, other parameters that affect the overpotential should be explored in order to achieve higher N_p for thinner coalesced copper films.

	Current density / mA cm^{-2}						
	-1	**-2.5**	**-5**	**-10**	**-50**	**-100**	**-200**
η in plateau P_1 (V vs. Ag/AgCl)	-0.039	-0.081	-0.120	-0.189	-0.410	-0.580	-0.880
η_{IR} in plateau P_1 (V vs. Ag/AgCl)	-0.036	-0.074	-0.110	-0.188	-0.266	-0.278	-0.276

Table 4.2: Overpotential values with and without IR_s correction (R_s = 44 Ω) for copper deposition on RuTa as obtained from the potential-time responses during galvanostatic deposition from solution of 1.8 M H_2SO_4, 1.4×10^{-3} M HCl and 0.6 M $CuSO_4$, at different current densities (-1, -5, -10, -50, -100 and -200 mA cm^{-2}). The values correspond to copper deposition potential (in plateau P_1) for A_{Cu}=0.19 (assuming spherical islands for current densities between -1 to -10 mA cm^{-2} and hemispherical islands for current densities between -50 to -200 mA cm^{-2}).

In the inset of Figure 4.6, the island density, N_p, is plotted as a function of the overpotential corrected for *IR* drop, η_{IR}, with respect to the overpotential for nucleation, η_{IRNucl}. The overpotential for nucleation, η_{IRNucl}, was found to be around -0.025 V. Note that the value of -0.025 V refers to the steady state overpotential nucleation as obtained from current-potential scan on the as-received RuTa electrode at a polarization rate of 0.001 V s^{-1}. The η_{IR} values for copper deposition were obtained from the galvanostatic responses in Figure 4.3. The η_{IR} values were determined with respect to the copper OCP (Table 4.1) and corrected for IR_s drop with R_s= 44 Ω for the 0.6 M $CuSO_4$ solution (see Equation 4.4). For direct comparison, η_{IR} values for the same effective copper area of A_{Cu} = 0.19 were considered. An exponential relationship exists between the island density, N_p, and the overpotential, $-(\eta_{IR}-\eta_{IRNucl})$. The dependency is given by:

Equation 4.5:
$$N_p(\eta) = N_{\eta,Nucl} \exp\left(-\frac{\alpha F}{RT}\left(\eta_{IR} - \eta_{IR\,Nucl}\right)\right)$$

where the pre-exponential factor, $N_{\eta,Nucl}$ describes the island density at η_{IRNucl} i.e. when $\eta_{IR}=\eta_{IRNucl}$ (with η_{IRNucl} = - 0.025 V) and the exponential component, $\frac{\alpha F}{RT}$ relates to the electrode kinetics (in resemblance to Butler-Volmer relationship). As the overpotential for nucleation, η_{IRNucl} varies for different substrates, $N_{\eta,Nucl}$ is expected to change accordingly. For example, an appropriate pretreatment can significantly increase the island density for the same plating conditions (see Chapter 6). Such a difference in island density is built-in into $N_{\eta,Nucl}$. For copper deposition on RuTa from the 0.6 M $CuSO_4$ solution at different current densities (Figure 4.6 inset) the experimentally found N_p -(η_{IR}-η_{IRNucl}) dependency is :

Equation 4.6:
$$N_p(\eta) = 1\times10^7 \exp\left(-32\left(\eta_{IR} - \eta_{IR\,Nucl}\right)\right)$$

with $N_{\eta,Nucl}$ equal to 1×10^7 and an exponential factor equal to -32, which would imply α = 0.8 according to Equation 4.5).

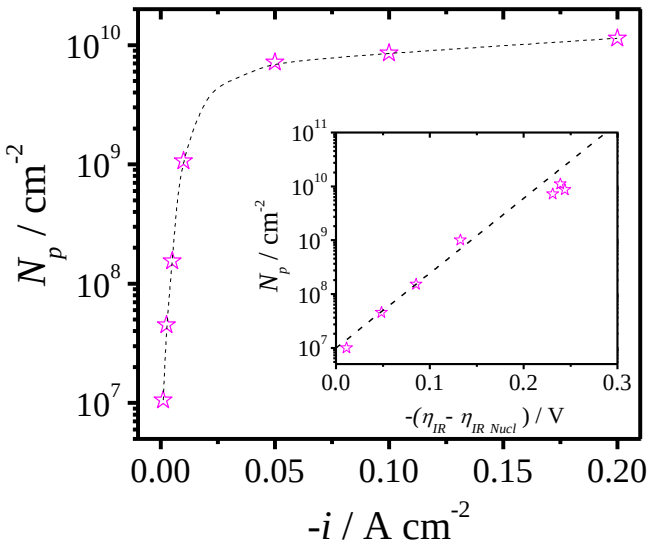

Figure 4.6: Copper island density, N_p, as a function of the applied current density, -*i*. In the inset, N_p values as a function of the corresponding overpotential corrected for *IR* drop, $\eta_{IR,}$ (R=44 Ω) found in P_1 plateau for A_{Cu}=0.19 (assuming spherical islands for current densities between -1 to -10 mA cm^{-2} and hemispherical islands for current

densities between -50 to -200 mA cm^{-2}). The deposition experiments were performed in a solution of 1.8 M H_2SO_4 1.4×10^{-3} M HCl and 0.6 M $CuSO_4$, at different current densities (-1, -2.5, -5, -10, -50, -100 and -200 mA cm^{-2}) and for a deposition charge density of 0.04 C cm^{-2}.

4.4.2 The effect of Cu^{2+} concentration on the nucleation density, N_p

Figure 4.7 shows the overpotential corrected for *IR* drop, η_{IR}, as a function of time during galvanostatic deposition of Cu at -10 mA cm^{-2} on RuTa from solutions with $CuSO_4$ concentrations between 0.01 and 0.6 M. The η_{IR} values for copper deposition were determined with respect to the copper OCP (Table 4.1) and corrected for IR_s drop (see Equation 4.4) with R_s = 38, 39, 39 and 44 Ω for the 0.01, 0.05, 0.1 and 0.6 M $CuSO_4$ solutions, respectively. The inset of Figure 4.7 shows the η_{IR} transient for the 0.1 M solution only, with the different features of interest indicated as in the inset of Figure 4.3. Table 4.3 quantifies these features for the different curves of Figure 4.7. The OCP of RuTa ranged between +0.57 and +0.65 vs. Ag/AgCl and did not change significantly with the Cu^{2+} concentration. Similar to what was observed for the 0.6 M solutions at high current densities (Figure 4.3), it can be seen for the 0.01, 0.05 and 0.1 M solutions, that η_{IR} dropped from OCP to a first potential plateau, P_1, within a few tens of milliseconds after applying the current. The potential remained there for some time and then an additional drop to a second plateau, P_2, was observed. The resident time in plateau P_1 increased with increasing $CuSO_4$ concentration. For the 0.6 M $CuSO_4$ solution, no such second potential drop was observed, not even after 3600*s* of deposition. From Table 4.3, it can be seen that the η_{IR} for copper deposition increased (became more negative) while the time to reach P_2 decreased as Cu^{2+} concentration decreased. As it takes a longer time for full depletion of cupric ions in the solutions with higher Cu^{2+} concentrations, the potential drop occurs at longer times.

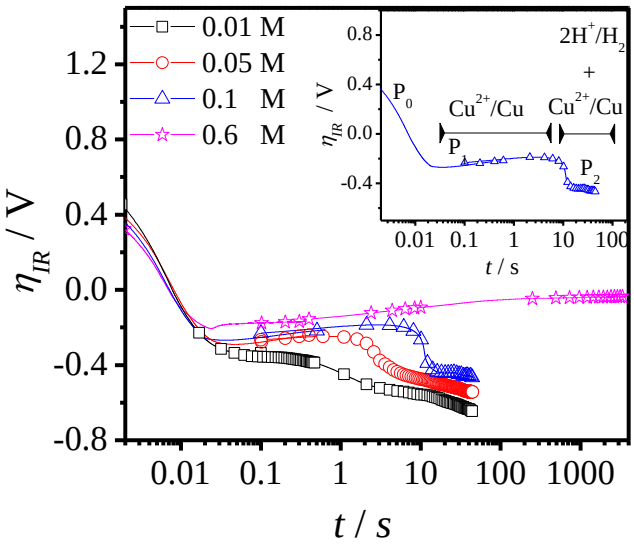

Figure 4.7: η_{IR}-time curves for RuTa in solutions of 1.8 M H_2SO_4, 1.4×10^{-3} M HCl and 0.01, 0.05, 0.1 or 0.6 M $CuSO_4$ at current density of -10 mA cm^{-2}. The η_{IR} is given with respect to the equilibrium potential for copper and corrected for IR drop (Table 4.1). In the inset: η_{IR}-time transient for the 0.1 M $CuSO_4$ solution only with the different features of interest indicated: P_0 for charging of the double layer, partial reduction to Cu^+, formation of 2D islands and UPD region, P_1 for copper deposition overpotential and P_2 for additional hydrogen evolution reaction.

	Nominal $CuSO_4$ concentration / M			
	0.01	**0.05**	**0.1**	**0.6**
RuTa OCP (V vs. Ag/AgCl)	0.65	0.60	0.63	0.59
η_{IR} in plateau P_1 (V vs. Ag/AgCl)	-0.33	-0.25	-0.22	-0.18
η_{IR} in plateau P_2 (V vs. Ag/AgCl)	-0.65	-0.55	-0.48	was not observed
Time corresponding to the start of hydrogen evolution/ s	0.1	2.1	8.5	was not observed

Table 4.3: Open-circuit potential for RuTa before copper deposition, η_{IR} for copper deposition (plateau P_1) for A_{Cu} = 0.19, η_{IR} for copper deposition plus hydrogen evolution (plateau P_2) and time to reach plateau P_2 obtained at current density of -10 mA cm^{-2} on RuTa from solutions with 1.8 M H_2SO_4, 1.4×10^{-3} M HCl and 0.01, 0.05, 0.1 or 0.6 M $CuSO_4$ (Figure 4.7).

Figure 4.8 shows the theoretical diffusion-limited current as a function of time for the solutions with the different Cu^{2+} concentrations as calculated from the Cottrell equation:

Equation 4.7:
$$i = \left(\frac{nFD^{1/2}C_b}{\pi^{1/2}t^{1/2}} \right)$$

where $n = 2$ for the number of electrons in the reaction, $F = 96485$ C mol^{-1} for Faraday's constant, C_b is the bulk concentration of Cu^{2+} -ions (1×10^{-5}, 5×10^{-5}, 1×10^{-4} and 6×10^{-4} mol cm^{-3}) and D the diffusion coefficient for Cu^{2+}. The latter is, for the different Cu^{2+} concentrations, given by the empirical relationship found by Quickenden and Jiang [17]:

Equation 4.8:
$$D = \left(7.35 - 5.3[CuSO_4]^{1/2}\right)\times10^{-6}\ cm^2 s^{-1}$$

From these equations, it follows that the current density for copper deposition reaches -10 mA cm^{-2} at 0.09, 2.2, 8.8 and 317*s* for the 0.01, 0.05, 0.1 and 0.6 M $CuSO_4$ solutions, respectively (see Table 4.4). Hence, after these times, the copper deposition reaction cannot longer supply sufficient current and the hydrogen evolution reaction commences. The partial current for copper deposition decreases with even longer times and thus the partial current of hydrogen evolution increases with time as indicated in Figure 4.8. Hence, for a galvanostatic experiment at - 10 mA cm^{-2}, the copper deposition current density will be constant and equal to the applied current density as long as it remains smaller than the diffusion limited current calculated from the Cottrell equation (see Equation 4.7). Table 4.4 shows the theoretical times and the experimental times which correspond to the start of hydrogen evolution during copper deposition in Figure 4.7. A good agreement was found between theory and experiment for solutions with low Cu^{2+} concentrations (0.01, 0.05 and 0.1 M) as deposition becomes quickly under the conditions of complete diffusion control for which the Cottrell equation holds (surface concentration C_s= 0). For the 0.6 M $CuSO_4$ solution, the agreement is poor as a significant kinetic component is still present even at longer times.

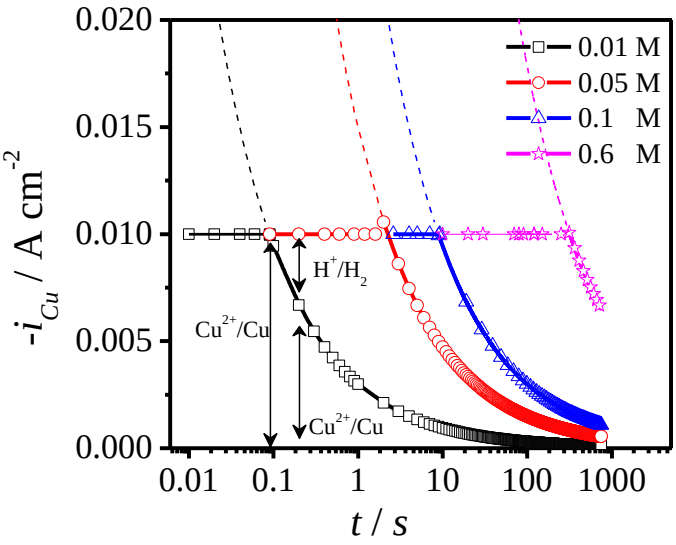

Figure 4.8: Partial copper deposition current,- i_{Cu}, for 0.01, 0.05, 0.1 and 0.6 M Cu^{2+} concentration as a function of time calculated from Cottrell equation for the case of galvanostatic deposition at -10 mA cm^{-2}.

	Time which corresponds to the start of hydrogen evolution	
$CuSO_4$ concentration/ M	Experimental time/ *s*	Theoretical time/ *s*
0.01	0.1	0.09
0.05	2.1	2.2
0.1	8.5	8.8
0.6	Was not observed after 3600*s*	317

Table 4.4: Theoretical and experimental times for the start of hydrogen evolution during galvanic deposition of Cu at -10 mA cm^{-2}. The theoretical values were calculated from the Cottrell equation and correspond to the times where the diffusion current of Cu^{2+} equals the applied current density. The experimental values correspond to the onset of plateau P_2 in Figure 4.7.

Figure 4.9 shows the island density, N_p, for copper electrodeposited from solutions with different Cu^{2+} concentrations as a function of the applied current density. As for the 0.6 M $CuSO_4$ case (Figure 4.6), N_p increased with deposition current for $|i| \leq$ 10 mA cm^{-2} in all solutions investigated, confirming the general tendency of N_p to increase with increasing driving force for deposition. Importantly, a systematic increase in the island density was observed when lowering the $CuSO_4$ concentration in solution. A 60 fold decrease in the $CuSO_4$ concentration from 0.6 M to 0.01 M, resulted in a 300 fold increase in N_p for all current densities under investigation. It should be noted that for the 0.01 M $CuSO_4$ solution at current density of -10 mA

cm^{-2}, the islands were already coalesced for the charge of 0.01 C cm^{-2} passed (equivalent thickness of 1.9 nm considering the partial deposition current at this low Cu^{2+} concentration).

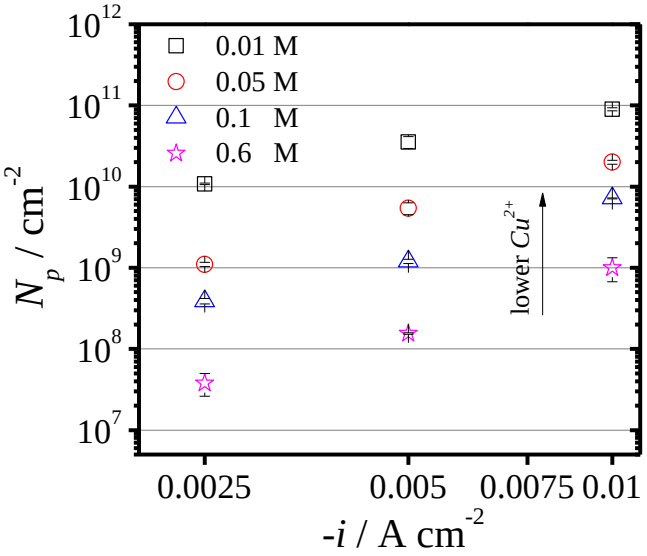

Figure 4.9 : Copper island density, N_p, as a function of the applied current density, i. The deposition experiments were performed from solutions of 1.8 M H_2SO_4, 1.4×10^{-3} M HCl and 0.01, 0.05, 0.1 or 0.6 M $CuSO_4$ and at different current densities (-2.5, -5 and -10 mA cm^{-2}).

In Figure 4.10 the island density, N_p, is plotted as a function of -(η_{IR}-η_{IRNucl}) for the different $CuSO_4$ concentrations at current densities between -2.5 and -10 mA cm^{-2}. The η_{IR} values were extracted from the galvanostatic measurements such as those shown in Figure 4.7. To have fair comparison with the 0.6 M $CuSO_4$ solution at current densities between -1 to -200 mA cm^{-2} (Figure 4.6 inset), we selected η_{IR} values that correspond to the same effective surface area of the copper islands i.e. A_{Cu} = 0.19. The island density, N_p, now follows the same exponential relationship with -(η_{IR}-η_{IRNucl}) irrespective of Cu^{2+} concentration and current density (see Equation 4.6).

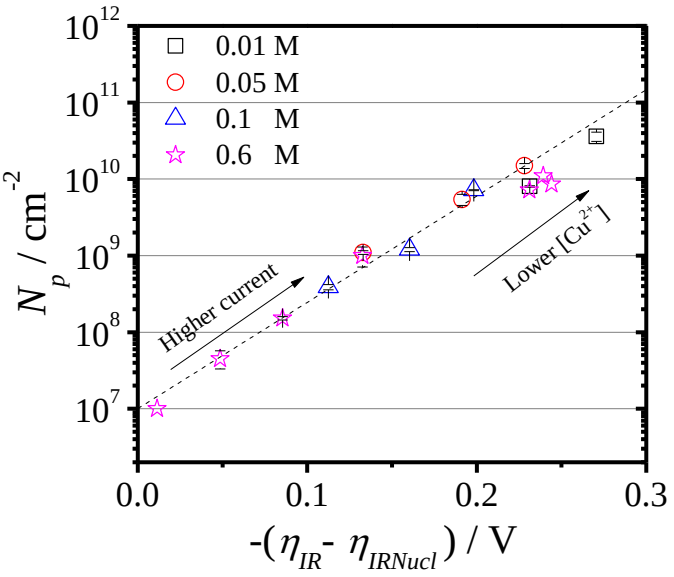

Figure 4.10: Copper island density, N_p, as a function of the corresponding η_{IR}. The η_{IR} was determined with respect to copper OCP and corrected for *IR* drop. η_{IR} was taken in P_1 plateau for A_{Cu}= 0.19 (assuming hemispherical islands for the 0.01, 0.05 and 0.1 M $CuSO_4$ solutions for all current densities and spherical islands for the 0.6 M solution for current densities between -1 to -10 mA cm^{-2} and hemispherical islands for current densities between -50 to -200 mA cm^{-2}). The deposition experiments were performed from solutions of 1.8 M H_2SO_4, 1.4×10^{-3} M HCl and 0.01, 0.05, 0.1 or 0.6 M $CuSO_4$ and at different current densities (-2.5 to -10 mA cm^{-2} for the 0.01, 0.05 and 0.1 M $CuSO_4$ solutions and -1 to -200 mA cm^{-2} for the 0.6 M $CuSO_4$ solution). The N_p dependency on -(η_{IR}- η_{IRNucl}) is given according to the: $N_p(\eta) = 1\times10^7 \exp\left[-32(\eta_{IR} - \eta_{IR\,Nucl})\right]$.

4.4.3 The effect of Cu^{2+} concentration on the growth of the copper islands

Figure 4.11 shows top-down SEM images of copper islands deposited at a current density of -10 mA cm^{-2} for different deposition times and different $CuSO_4$ concentrations. As discussed above, with lower Cu^{2+} concentration higher N_p is obtained. Consequently, island coalescence was achieved faster in the solutions with lower Cu^{2+} concentration as well: the islands were already coalesced into a continuous copper film after 10*s* for the 0.05 M $CuSO_4$ solution whereas for the 0.1 and 0.6M $CuSO_4$ solutions, the islands did not coalesce within this time region. Note that for 10 mM solution, coalescence was already obtained after 1s (see above). It is important to note that no change in N_p was observed from 1 to 10 s in all cases. Hence, the nucleation occurs rapidly in the early stages of the galvanostatic deposition to form a sufficient number of nuclei to sustain the applied current density. Once the nucleation is completed, the current is sustained by

the growing copper islands as Cu^{2+} reduction (i.e. deposition) is more favorable on copper (i.e. growth) than on a foreign substrate such as RuTa (i.e. nucleation). Thus, no significant change in N_p is observed over time.

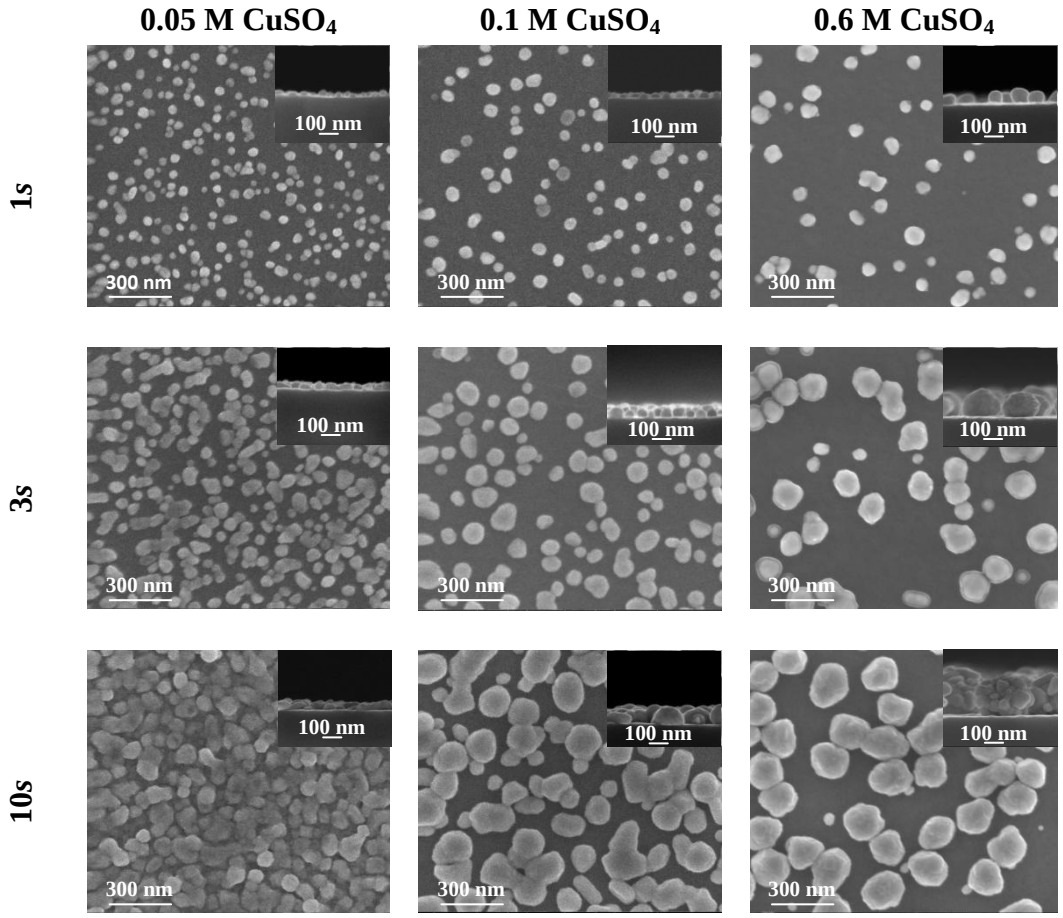

Figure 4.11: Top-down SEM images of Cu islands galvanostatically deposited at -10 mA cm^{-2} from solutions of 1.8 M H_2SO_4, 1.4×10^{-3} M HCl and 0.05, 0.1 or 0.6 M $CuSO_4$ with for different deposition times, showing the growth of the copper islands. In the inset: cross sectional SEM images of Cu islands.

Figure 4.12 shows the dependence of the island diameter with deposition time for different Cu^{2+} concentrations. From the simulated current–time responses shown in Figure 4.6, the transferred charge can be calculated by integrating the area under the curve for partial copper deposition current. From the charge for copper deposition, the diameter of a single island can be calculated if the island density, N_p is known [18]:

Equation 4.9:

$$d = \left(\frac{q_{Cu}}{KN_p} \right)^{1/3}$$

where d *(cm)* is the island diameter, q_{Cu} (C cm^{-2}) is the partial charge density for copper deposition and K (C·cm^{-3}), the material constant (see Equation 4.3). A very good correlation between the experiment and theory was found when assuming hemispherical islands for the 0.05 and 0.1 M solutions and spherical islands for the 0.6 M $CuSO_4$ solutions (see Figure 4.11).

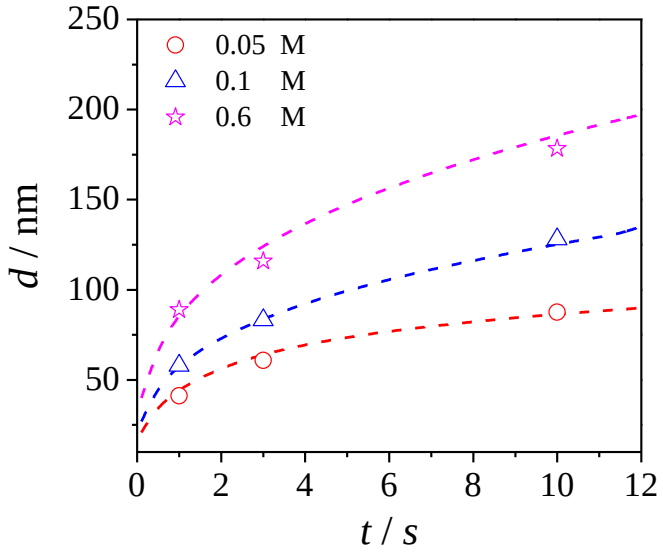

Figure 4.12: Variation of the average island diameter, *d*, with deposition time, *t*, for copper deposition at -10 mA cm^{-2} from solutions of 1.8 M H_2SO_4 1.4×10^{-3} M HCl and (○) 0.05 (△) 0.1 or (☆) 0.6 M $CuSO_4$ as obtained from digital image analysis of the SEM images (Figure 4.11). For comparison, the theoretical trend according to Equation 4.9 is shown (dashed lines).

4.4.4 The effect of Cu^{2+} concentration on the propagation of the copper front on the resistive RuTa surface

Figure 4.13 shows digital images of the RuTa surface subsequent to copper deposition at -10 mA cm^{-2}, demonstrating the effect of Cu^{2+} concentration on the propagation of the copper front on the RuTa surface. The experiments were performed on 4×4 cm^2 RuTa coupons to demonstrate the so-called terminal effect which exists across the resistive RuTa surface [19]. As

discussed in previous paragraphs, with lower Cu^{2+} concentration higher N_p and faster island coalescence is obtained. Consequently, faster propagation of the copper front on the resistive RuTa substrate was achieved from lower Cu^{2+} concentration as well: the RuTa surface was entirely covered with copper after 20*s* for the 0.01 M $CuSO_4$ solution whereas for the 0.1 and 0.6 M $CuSO_4$ solutions, the copper front did not reach the center of the 4×4 cm^2 RuTa coupons within this time region. Figure 4.14 shows tilted SEM images, showing the Cu islands at different locations across the 4×4 cm^2 RuTa coupons for the 0.01 and 0.6 M $CuSO_4$ solutions as obtained from digital images such as those shown in Figure 4.13. Coarse morphology and islands with an average diameter of about ~ 450 nm were observed on the surface for the 0.6 M $CuSO_4$ solution at the edge of the 4×4 cm^2 RuTa coupon. At the middle and the center of the 4×4 cm^2 RuTa coupon, no islands were observed as the severe potential drop across the resistive substrate, the so-called terminal effect, did not provide sufficient overpotential for nucleation. The Cu film non-uniformity across the 4×4 cm^2 RuTa coupon was less severe for the 0.01 M solution as copper deposits were observed across the entire 4×4 cm^2 RuTa coupon: at the edge, the islands already coalesced into a continuous copper film. At the middle and the center of the 4×4 cm^2 RuTa coupon, high N_p was observed however the islands did not coalesce within this region. Further investigation should be performed to elaborate the so-called terminal effect for different Cu^{2+} concentrations.

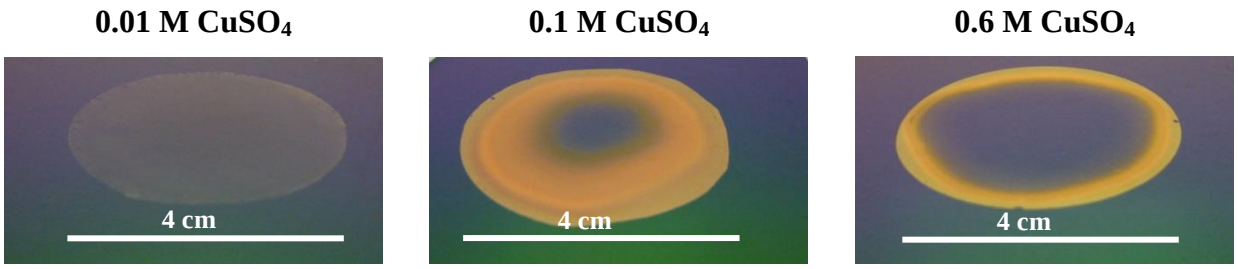

Figure 4.13: Digital images of RuTa surface subsequent to copper deposition, illustrating the effect of Cu^{2+} concentration on the propagation of the copper film on the resistive RuTa surface. The experiments were performed on 4×4 cm^2 RuTa coupons at -10 mA cm^{-2} for 20*s* from solutions of 1.8 M H_2SO_4, 1.4×10^{-3} M HCl and 0.01, 0.1 or 0.6 M $CuSO_4$ with.

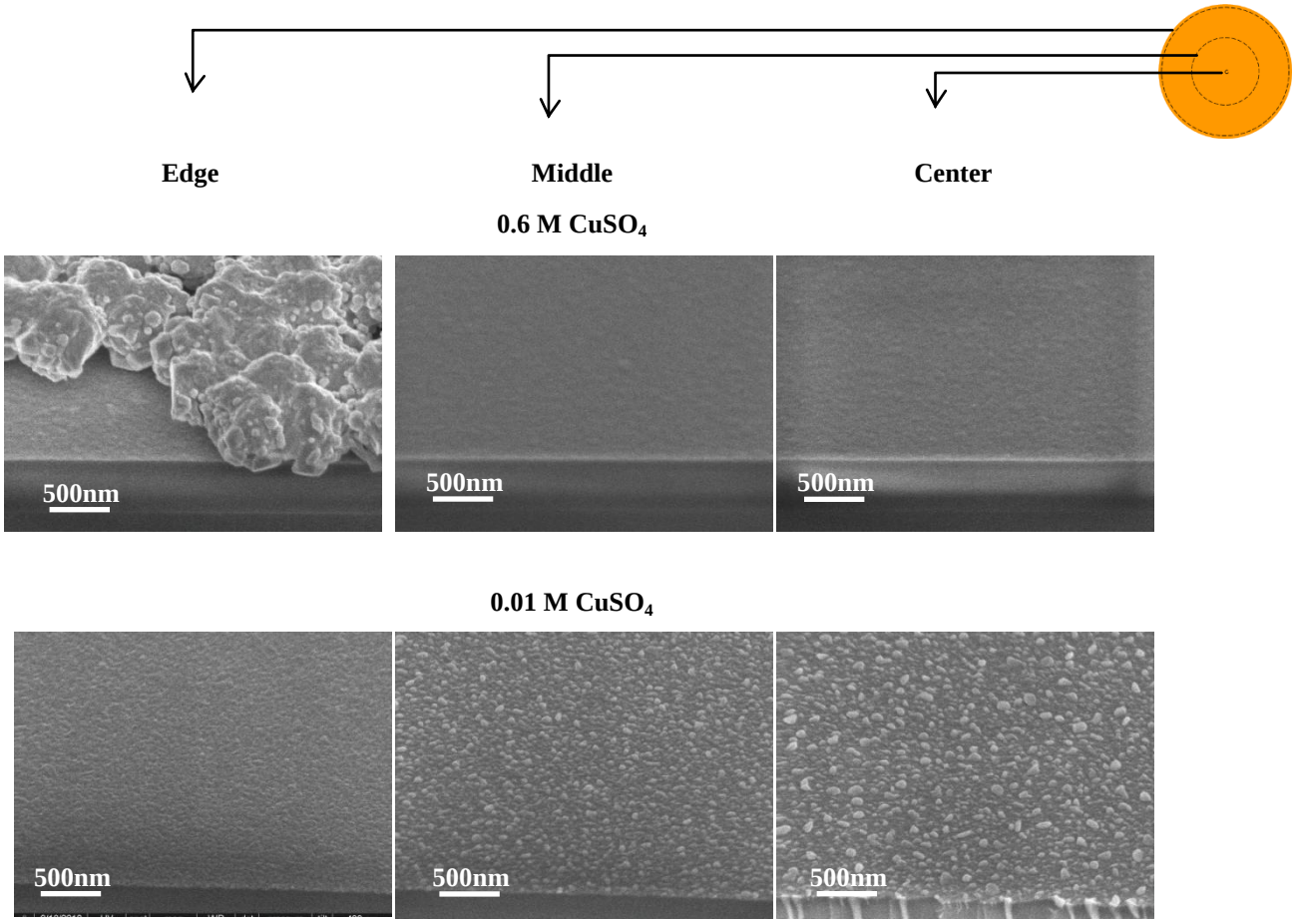

Figure 4.14: Tilted SEM images showing Cu islands at different locations across the 4×4 cm^2 RuTa coupons for the 0.01 and 0.6 M $CuSO_4$ solutions as obtained from digital images such as those shown in Figure 4.13, illustrating the Cu film non-uniformity across the 4×4 cm^2 RuTa coupons resulting from the so-called terminal effect for different [Cu^{2+}] concentration. The experiments were performed on 4×4 cm^2 RuTa coupons at -10 mA cm^{-2} for 20*s* from solutions of 1.8 M H_2SO_4, 1.4×10^{-3} M HCl and 0.01 or 0.6 M $CuSO_4$.

4.5 Summary

The effect of cupric ion concentration, [Cu^{2+}], and deposition current density on the nucleation and growth processes during galvanostatic deposition of copper on a RuTa alloy was studied. It was found that the overpotential increases with higher current density and lower Cu^{2+} concentration in the plating bath. As the copper island density, N_p, is determined by the copper deposition overpotential, higher N_p was observed with low Cu^{2+} concentration and high current density. Analysis of the galvanostatic transients for different current densities and Cu^{2+} concentrations shows an exponential relationship between the island density, N_p, and -(η_{IR}-

η_{IRNucl}) irrespective of Cu^{2+} concentration and current density. Once this correlation is established, N_p values can be estimated for the 2 nm RuTa substrate based solely on the copper deposition overpotential during the galvanostatic deposition. From an industrial point of view, this study reveals that plating baths containing decreased Cu^{2+} concentrations yield thinner coalescence thickness and faster propagation of the copper front on the resistive RuTa surface (resulted from higher island density, N_p). Thus, low Cu^{2+} concentrations baths may be more suitable for fabricating the copper in the sub-30 nm narrow lines. The results obtained so far indicate that further investigation is needed into the tailoring of advanced bath compositions, to take full advantage of the decreased Cu^{2+} concentration characteristics.

[1] A. Radisic, F.M. Ross and P.C. Searson, In situ study of the growth kinetics of individual island electrodeposition of copper, Journal of Physical Chemistry 110 (2006) 7862.

[2] A. Milchev, B.R. Scharifker and G. Hills, A potentiostatic study of the electrochemical nucleation of silver on vitreous carbon, Journal of Electroanalytical Chemistry 132 (1982) 277.

[3] B.R. Scharifker and J. Mostany, Three-dimensional nucleation with diffusion controlled growth: Part I. Number density of active sites and nucleation rates per site, Journal of Electroanalytical Chemistry 177 (1984) 13.

[4] A. Milchev, T. Zapryanova, Nucleation and growth of copper under combined charge transfer and diffusion limitations: Part I, Electrochimica Acta 51 (2006) 2926.

[5] G. Gunawardena, G. Hills, I. Montenegro and B.R. Scharifker, Electrochemical nucleation: Part I. General considerations, Journal of Electroanalytical Chemistry 138 (1982) 225.

[6] J.M. Casas, F. Alvarez, L. Cifuentes, Aqueous speciation of sulfuric acid–cupric sulfate solutions, Chemical Engineering Science 55 (2000) 6223.

[7] http://rsb.info.nih.gov/ij/docs/index.html

[8] Yong-Da Chiu, Wei-Ping Dow1, Yung-Fang Liu, Yuh-Lang Lee, Shueh-Lin Yau, Su-Mei Huang, Copper Underpotential Deposition on Gold in the Presence of Polyethylene Glycol and Chloride, International Journal of Electrochemical Science 6 (2011) 3416.

[9] P.M Vereecken, R.A. Binstead, H. Deligianni,, P.C. Andricacos, The chemistry of additives in damascene copper plating, IBM Journal of Research and Development 49 (2005) 3.

[10] B.R. Scharifker and G. Hills, Theoretical and experimental studies of multiple nucleation, Electrochimica Acta 28 (1983) 879.

[11] B.R. Scharifker, in Electrochemistry in Transition, O.J. Murphy, S. Srinivasan, and B.E. Conway, Editors, p. 499, Plenum Press, New York (1992).

[12] A. Milchev, M.I. Montenegro, A galvanostatic study of electrochemical nucleation, Journal of Electroanalytical Chemistry 333 (1) (1992) 93.

[13] A. Radisic, M. Nagar, K. Strubbe, S. Armini, Z. El-Mekki, H. Volders, W. Ruythooren, and P.M. Vereecken, Copper plating on resistive substrates, diffusion barrier and alternative seed layers ECS Transactions 25 (27) (2010) 175.

[14] M. Peykova, E. Michailova, D. Stoychev and A. Milchev, Galvanostatic studies of the nucleation and growth kinetics of copper in the presence of surfactants, Electrochimica Acta 40 (1995) 2595.

[15] D. Grujicic, B. Pesic, Electrodeposition of copper: the nucleation mechanisms, Electrochimica Acta 47 (2002) 2901.
[16] A. Radisic, P.M. Vereecken, P.C. Searson and F.M. Ross, The morphology and nucleation kinetics of copper islands during electrodeposition, Surface Science 600 (2006) 1817.
[17] T.I. Quickenden and X. Jiang, The diffusion coefficient of copper sulphate in aqueous solution, Electrochimica Acta 29 (6) (1984) 693.
[18] A. Romo-Negreira, O. Richard, S. De Gendt, K. Maex, M. Heyns and P.M. Vereecken, Selective growth of carbon nanotubes on silicon from electrodeposited nickel catalyst, Science of Advanced Materials 1 (2009) 86.
[19] S. Armini, P.M. Vereecken, Impact of terminal effect on Cu plating: theory and experimental evidence, ECS Transactions 25 (2010) 185.

CHAPTER 5: THE EFFECT OF POLYETHER SUPPRESSORS ON THE NUCLEATION AND GROWTH OF COPPER ON RUTA SEEDED SUBSTRATE FOR DIRECT COPPER PLATING.

This Chapter describes experiments and results of copper deposition on a RuTa alloy from acid copper sulfate solutions with various polyether suppressors. The main focus is on the influence of the inhibition strength and the deposition current on the nucleation and growth of copper during galvanostatic deposition. The experimental results show that differences in the polyether molecular structure (such as molecular weight (Mw), functional groups, end groups etc.) result in different inhibition behavior, which in turn affects the island density, N_p of electrodeposited copper Analysis of the galvanostatic transients show that an exponential relationship exists between the island density, N_p, and the actual deposition overpotential.The same exponential dependence between the copper island density and overpotential was found as in the additive-free $CuSO_4$ solutions. This relationship provides a universal equation for N_p on RuTa surface and the island density can be estimated from the actual overpotential for copper deposition seen during galvanostatic measurements, irrespective to the Cu^{2+} concentration, suppressor type and current density.

5.1 Introduction

The damascene process for fabrication of copper interconnects requires void-free deposition into submicron features with high-aspect-ratio structures [1-2]. The bottom-up filling of these features is accomplished by using organic additives, termed suppressor, leveler and accelerator. The suppressor promotes the bottom-up filling by suppressing Cu deposition on surfaces outside the features and thus assisting in having copper deposition at the bottom of the features [1-2]. The inhibition mechanism of the polyether suppressors with respect to copper deposition on copper has been studied frequently [1-13]: studies of copper deposition on copper in the presence of polyethylene glycol (PEG) and chloride (Cl^-) ions have demonstrated that the combination of these two additives inhibits the copper deposition current and lead to an increase of the overpotential (polarization) required for Cu^{2+} reduction. Kelly and West used a Quartz

Crystal Microbalance (QCM) to investigate charge and mass changes during copper deposition in the presence of PEG and Cl^- ions. They showed that in the presence of Cl^- ions, a monolayer of PEG molecules bundled into 'spheres' is formed on the Cu surface [3]. Surface Enhanced Raman Spectroscopy (SERS) has shown that adsorbed Cl^- ions coordinate with Cu^+ ions, which in turn bond to oxygen atoms of PEG in the ethylene oxide (EO) repeating unit [4]. This indicates that PEG has several attachment points to the Cu surface, although not all are attached at the same time. The degree of inhibition of a given suppressor, depends on the relative concentration of the suppressor and Cl^- ions [5-9] as well as on the applied potential [10], and the suppressor molecular weight and structure [11-13].

As the dimensions of interconnect architectures decrease and alternative paths such as direct plating are needed [18], a more thorough understanding on the behavior of the polyether suppressors in chloride solutions and the inhibition mechanism with respect to copper deposition on resistive substrates is needed. Studies of copper deposition on resistive substrates in the presence of PEG and chloride ions have shown that these two additives play an important role in direct plating. Ellipsometric studies have demonstrated that the PEG/Cl^- complex adsorbs on copper rather than on an oxidized Ru surface [14]. This so-called differential inhibition affects the nucleation and growth of copper on the resistive substrate; Radisic *et al.* showed that the addition of the PEG affects the island shape and leads to higher N_p and consequently to a smaller coalescence thickness [2, 15-17]. It was also shown that the polyether suppressor plays an important role in the propagation of the continuous copper film across the resistive substrate [18,19]. Figure 5.1 demonstrates the effect of the suppressor when depositing copper on a resistive substrate; in Figure 5.1(a-c), copper deposition was performed in the absence of suppressor. The low N_p resulted in slow propagation of the copper front on the resistive RuTa substrate and spherical islands were observed on the RuTa surface. With the addition of PEG (Mw 4000) to the plating solution it can be seen in Figure 5.1(d-f) that now hemispherical islands were observed on the RuTa surface and a significant increase in the N_p which led to faster propagation rate of the Cu front compared to the PEG-free solution. It follows hence that the use of polyether molecules which exhibit fast adsorption and strong suppression would be beneficial for direct copper plating.

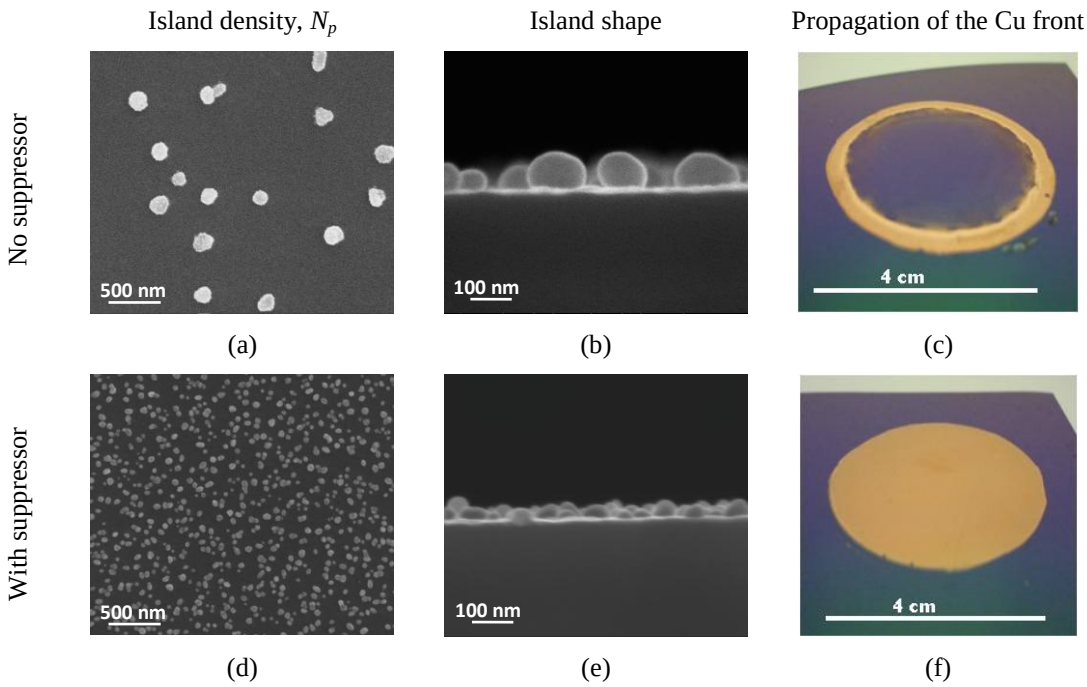

Figure 5.1: RuTa surface subsequent to Cu deposition at current density of -5 mA cm^{-2} from solutions of 0.6 M $CuSO_4$, 1.8 M H_2SO_4 and 1.4×10^{-3} M HCl (a-c) without suppressor and (d-f) with 300 ppm PEG (Mw 4000). Top view SEM (a and d) and cross section (b and e) SEM images subsequent to 2*s* of Cu deposition. (c and f): optical microscope images for 50*s* of Cu deposition illustrating the propagation of the Cu front on the resistive RuTa surface.

Although the suppression effect of PEG has been extensively studied with respect to copper on copper deposition [5-19], its effect on copper deposition on resistive substrates is not yet completely understood. In this Chapter, The nucleation and growth of copper islands on RuTa alloy from acidic 0.6 M $CuSO_4$ solutions that contain different polyether suppressors with different molecular weight and structure is studied. the investigation focused on the effect of suppression strength and deposition current on the island density during galvanostatic deposition. The electrochemistry of RuTa and Cu electrodes in the $CuSO_4$ solutions with different polyether suppressors in the presence of Cl^- ions was studied using cyclic voltammetry and potentiometry. The unique signature in the potential-time responses for different polyether suppressor molecules was used to characterize their inhibition capabilities [15,20]. The general tendency of this unique signature can be seen in Figure 5.2. The difference in the steady state overpotential ($\Delta\eta_{Sup}$) for Cu deposition with and without suppressor can be used as a measure for the inhibition strength (polarization). Δt reflects the time to achieve fully suppressed and closed copper surface on the

resistive electrode. Therefore, the potential-time transient is a valuable tool for investigating the inhibition capabilities of various polyether suppressors. Indeed, we now need to look for a polyether suppressor that is able to provide the largest $\Delta\eta_{Sup}$ and the smallest Δt.

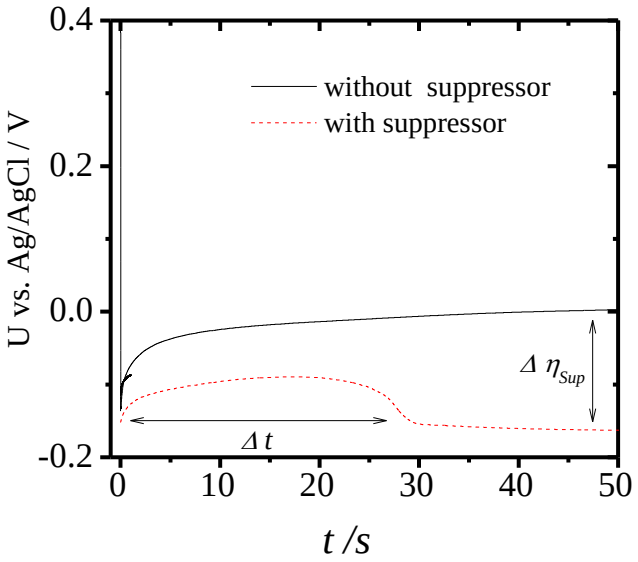

Figure 5.2: Typical Potential-time responses, seen during Cu deposition on a resistive substrate from a $CuSO_4$ acid solution in the absence (solid line) and the presence of suppressor (dashed line).

5.2 Experimental

Copper was electrodeposited on Cu and RuTa electrodes from $CuSO_4$ acid solutions with different polyether suppressors using constant current densities. Details concerning the experimental set-up and substrate properties can be found in Chapter 2. The current-potential curves on RuTa were obtained by polarizing the potential at a rate of 0.02 V s^{-1} from 0.5 V to -0.5 V vs. Ag/AgCl. The current-potential curves on Cu were recorded from the open circuit potential (OCP) to -0.5 V vs. Ag/AgCl at a rate of 0.02 V s^{-1}. The galvanostatic experiments were performed at current densities between -2.5 mA cm^{-2} and -10 mA cm^{-2}. The plating solutions contained 0.6 M $CuSO_4 \cdot 5H_2O$ (> 98%, Alfa Aesar), 1.8 M H_2SO_4 (96% Assay, Baker), 1.4×10^{-3} M HCl (37% Assay, Baker) in the absence (denoted as the base solution) and the presence of different suppressors. Note that the currents used are far below the diffusion limited current (-100 mA cm^{-2}) for the 0.6 M $CuSO_4$ solution for the time periods under investigation

(see Chapter 4). The suppressors' concentration was 300 ppm in all cases so that in all solutions approximately the same concentration of polymer repeating units was obtained. All polyether suppressors in form of homopolymer were purchased from Sigma-Aldrich. In this work we used; polyethylene glycol (PEG) with different Mw: 200, 400, 1000, 4000, 8000 and 20,000 g mol^{-1}, polypropylene glycol (PPG) with Mw 725 g mol^{-1}, polyoxyethylene methyl ether (Methyl PEG) with Mw 1000 g mol^{-1} and polyoxyethylene cetyl ether (Cetyl PEG) with Mw 1124 g mol^{-1}. Block copolymer of PEG and PPG, known by the trade name Pluronic 10R5 was purchased from BASF. The block copolymer (denoted as block copolymer 10R5) consists repeating units of a propylene oxide (PO) block in-between two ethylene oxide (EO) blocks (EO-PO-EO) with Mw 2000 g mol^{-1}. Specification by proton nuclear magnetic resonance (NMR) indicates EO:PO ratio of 1.38:1 which indicates 50 wt. % EO and 50 wt.% PO units [21]. Table 5.1 summarizes the suppressors under investigation along with their chemical structure and number of ether groups per molecule. Note that the number of ether groups serve as possible attachment points to the copper surface. The number of ether groups is calculated by subtracting the end groups Mw from the polyether Mw and then dividing the sum by the repeating unit Mw with 44 g mol^{-1} for ethylene oxide (EO) and 58 g mol^{-1} for propylene oxide (PO). The copper equilibrium potentials, $U_{(Cu^{2+}/Cu),eq}$ in the base solution in the absence and the presence of the different suppressors were determined experimentally by open-circuit potential (OCP) measurements on the Cu electrode for 300*s* without agitation. It should be noted that the OCP value for the Cu electrode in the base solution was stable during the whole measurement time (300*s*) while the OCP value for the Cu electrode in the different polyether containing solutions was stable only for the first 10*s* and then gradually leveled off to a value close to the OCP value measured in the base solution (0.1 V). As the initial potential reflects the fast adsorption of the polyether molecules on the Cu electrode (0.4*s*) [11], we refer to the potential value seen for the first 10*s* as the Cu OCP value in the different polyether containing solutions. The solution resistance (R_s) was determined at 44 Ω from the slope reciprocal in the linear part of *I*-U relationship and 51 Ω from electrochemical impedance spectroscopy (EIS) For the *IR* correction of the *i*-U curves, the R_s value of 44 Ω obtained from the slope reciprocal in the linear part of *I*-U relationship was used. The presence of suppressor had no effect on the conductivity of the plating bath, and ohmic correction was the same as in base solution case [12]. All experiments were performed at room temperature (21° C) without agitation. For each experiment a pristine RuTa or Cu sample was used without any

further pretreatment. After copper deposition, samples were immediately removed from the solution, rinsed with de-ionized water and dried in nitrogen flow. The copper islands were examined by Scanning Electron Microscopy (SEM Nova 200, FEI). The SEM images were analyzed with Image*J* digital analysis software [22] in order to count the number of copper islands and determine the average diameter. For one data point an average of 3 images, taken at different spots near the center of the plated area, were analyzed. Atomic Force Microscope (AFM) measurements were performed with a Bruker Dimension Icon-PT atomic force microscope with Peak Force Tapping mode. The AFM images were analyzed with WSxM digital analysis software [23] in order to determine the roughness and effective copper area of the coalesced copper film.

Suppressor	***Mw/ g mol^{-1}***	***Number of ether groups per molecule***	***Chemical structure***
PEG	200	4.1	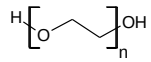
PEG	400	8.6	
PEG	1000	22.3	
PEG	4000	90.5	
PEG	8000	181.4	
PEG	20000	454.1	
Methyl PEG	1000	22.0	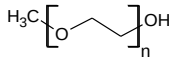
Mixture of 50% PPG 50% PEG	725 1000	(22.3+12.2) =34.5	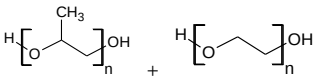
Block copolymer 10R5	2000	39.7	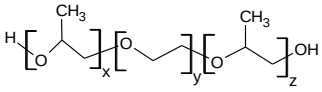
PPG	725	12.2	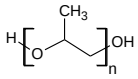
Cetyl PEG	1124	20.0	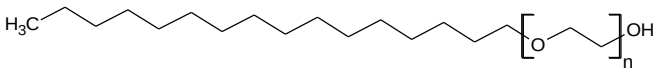

Table 5.1: Polyether suppressors under investigation along with number of ether groups per molecule and their chemical structure.

5.3 Current-potential characteristics:

Figure 5.3 shows current-potential curves for copper deposition on Cu and RuTa electrodes in the base solution and the presence of 300 ppm PEG (Mw 4000). For the Cu electrode in the base solution, the onset copper deposition potential appeared immediately from copper equilibrium potential $U_{(Cu^{2+}/Cu),eq}$ (0.1 V measured for the base solution) followed by a steep increase in cathodic current density from 0.1 V towards more negative potentials. The addition of 300 ppm PEG strongly suppressed the deposition current resulting in a polarization of the current-potential curve of about -240 mV compared to the base solution. For the RuTa electrode, a small cathodic current wave appeared before the copper equilibrium potential for the base solution and in the presence of PEG (Figure 5.3 inset). The prewave can be attributed to the underpotential deposition (UPD) of copper on RuTa, as well as to the partial reduction of Cu^{2+} to Cu^{+}, typically seen for noble metals such as platinum, gold and ruthenium [6]. The onset of bulk copper deposition on RuTa in the base solution appeared at 0.04 V, i.e. 60 mV more negative than the copper equilibrium potential (note: for polarization rate of 0.02 V s^{-1}). The difference between the (steady-state) onset potential for deposition on foreign substrates and the Nernst equilibrium potential is commonly known as the nucleation overpotential, η_{Nucl} [24]. The addition of 300 ppm PEG did not significantly affect the onset of Cu deposition on the RuTa electrode, as PEG does not interact with the RuTa surface but suppresses copper deposition on the copper nuclei [14, 25]. As the effective surface area of the copper islands is minimal at this stage, a polarization of only 40 mV is observed (compared to 240 mV observed on the Cu electrode). Subsequent to the initial rise in the current, a peak appeared at -0.2 V. This so-called suppressor peak reflects the change at the Cu/RuTa electrode: when most of the RuTa surface is covered with Cu, the deposition current decreases due to the lower effective current density at copper and the current-potential curve overlaps with the *i*-U curve for Cu deposition on Cu in the presence of suppressor [21,17]. Hence, the charge associated with the suppressor peak is a measure for the coalescence of the copper film. Higher copper island densities result in faster coalescence [18], and stronger suppression results in higher island densities as a result of inhibited growth [15, 16]. As such, the charge under the suppressor peak is also a measure for the suppression performance of the polyethylene molecule i.e. stronger suppression results in smaller charge. The charge under the suppressor peak for PEG (Mw 4000) was 0.07 C cm^{-2}, equivalent

to about 26 nm of deposited copper. In the reverse scans for the RuTa electrode (not shown), the currents became zero again at 0.10 V and 0.03 V for the base solution and in the presence of PEG, respectively. These zero-current potentials (ZCP) correspond very well to the OCP values of 0.10 V and 0.04 V on a copper electrode in the base solution and in the presence of PEG (see Table 5.1).

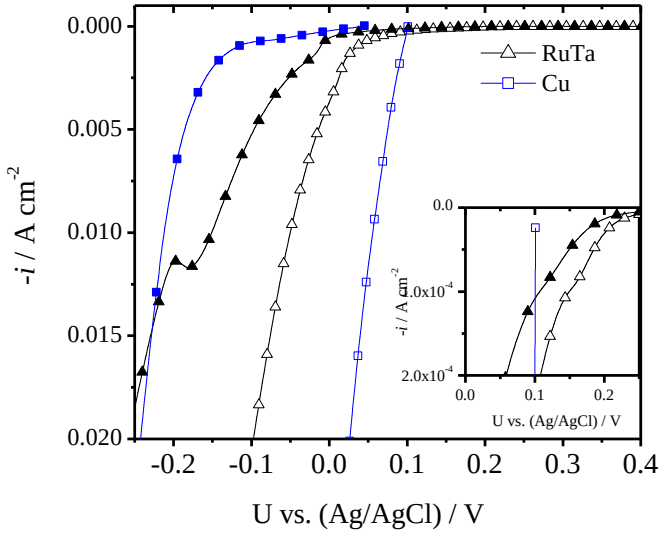

Figure 5.3: Current density, $-i$, versus potential, U, curves for (Δ) RuTa and (□) Cu electrodes in the base solution (open symbols) and with 300 ppm PEG Mw 4000 (full symbols) measured at a polarization rate of 0.02 V s^{-1}. In the inset: $-i$-U curves in potential region positive of $U_{(Cu^{2+}/Cu),eq}$ = 0.1 V, emphasizing the Cu UPD region for the RuTa electrode. Only the forward negative scans are shown for clarity.

	RuTa electrode		***Cu electrode***	
	base solution	base solution +PEG (Mw 4000)	base solution	base solution +PEG (Mw 4000)
Cu (OCP) (V vs. Ag/AgCl)	N/A	N/A	0.100	0.040
Nernst potential (V vs. Ag/AgCl)	N/A	N/A	0.110	-
ZCP (V vs. Ag/AgCl)	0.099	0.032	0.100	0.040

Table 5.2: Open-circuit potential measured on a copper electrode for the base solution and with 300 ppm PEG (Mw 4000). For comparison, also the calculated Nernst potential is given assuming activity of free Cu^{2+} equal to $CuSO_4$ concentration as well as the potential where the current becomes zero (ZCP) in the reverse scans of the current-potential curves.

Current-potential measurements were also carried out in the base solution with other suppressors. To have direct comparison, the current density was plotted as a function of overpotential corrected for *IR* drop, η_{IR}. The η_{IR} values were determined with respect to the copper equilibrium potential, $U_{(Cu^{2+}/Cu),eq}$ (0.1 V vs. Ag/AgCl) in the base solution and corrected for *IR* drop with R_s= 44 Ω:

Equation 5.1:
$$\eta_{IR} = U - U_{(Cu^{2+}/Cu),eq} - IR_s$$

Figure 5.4 shows *i*-η_{IR} curves, recorded in base solutions, containing one of the following selected group of 4 suppressors: PEG Mw 4000, PEG Mw 1000 with no end group, Methyl PEG with CH_3 as an end group and Cetyl PEG with $C_{16}H_{33}$ as an end group (for chemical structure see Table 5.1). Increase in PEG Mw from 1000 to 4000 resulted in a negative shift or polarization of the *i*-U curve. The polarization at low current densities is measured by the shift of the Cu deposition potential (*i*=-2 mA cm^{-2}) from -0.007 to -0.023 V. Furthermore, a shift to more negative potentials of both the ZCP and Cu OCP was observed as well as a smaller charge under the suppressor peak. The degree of polarization by the other polyether molecules with different molecular weight and structure can be evaluated from the shift in Cu deposition potentials at low current density (U *at i*=-2 mA cm^{-2}) summarized in Table 5.3. The effect of a single alkyl end group on PEG can be seen in Figure 5.4 when comparing suppressors with similar Mw (i.e. same number of ether group and thus possible anchor or attachment points to the copper surface through chloride bridges) but with short Methyl ($-CH_3$) and longer Cetyl ($-(CH_2)_{15}-CH_3$) end groups. From Figure 5.4 it follows that longer end groups lead to a shift of the Cu deposition potential to more negative values: from -0.007 V for PEG Mw 1000 to -0.028 V and -0.092 V for Methyl PEG and Cetyl PEG, respectively. A similar trend was observed for Cu OCP, for the ZCP and for the charge under the suppressor peak. It can be seen in Figure 5.4 that Methyl PEG with Mw 1000 exhibited similar suppression performance as PEG with Mw 4000 (i.e. similar charge under the suppressor peak, Cu deposition potential, ZCP and Cu OCP), indicating that the suppression strength can be controlled not only by the Mw but by the molecular structure of the polyethylene molecule as well [13]. All suppressors under investigation, along with the important features from the corresponding current-potential curves, are shown in Table 5.3. The suppressors are listed from the weakest to the strongest, based on the features seen in current-

potential curves (as obtained using a polarization rate of 0.02 V s^{-1}) i.e. strong suppression exhibits more negative Cu deposition potential, ZCP, Cu OCP and small charge under the suppressor peak. The effect of Mw can be seen in Table 5.3 when comparing PEG molecules with different Mw; the increase in PEG Mw from 200 to 4000 resulted in more negative Cu deposition potentials, Cu OCP and ZCP as well as a smaller charge under the suppression peak. Further increase in PEG Mw to 8000 and 20000 did not show any significant change in the current-potential features as compared to PEG Mw 4000. The effect of the functional group within the repeating unit can be seen when comparing PPG Mw 725 (with only 12.5 attachment points) with PEG Mw 400 and PEG Mw 20000 (with 9 and 454.5 attachment points, respectively); the Cu deposition potential shifted more negative from -0.007 V for the PEG Mw 400 to -0.027 V and -0.055 V for PEG Mw 20000 and PPG Mw 725, respectively. Similar trends were observed for the Cu OCP, and ZCP. The charge under the suppressor peak was 0.7, 0.077 and 0.04 C cm^{-2} (equivalent thickness of 257, 29 and 15 nm) for PEG Mw 400, PEG Mw 20000 and PPG Mw 725, respectively. Thus, the methyl group within the repeating unit of PPG exhibits stronger suppression performance compared to PEG 400 and PEG Mw 20000. A comparison is also made between solutions containing a mixture of 50/50 PEG Mw 1000 and PPG Mw 725 or a block copolymer consisting 50% EO groups. A more negative copper deposition potential, Cu OCP and ZCP was observed for the block copolymer as well as a smaller charge under the suppression peak. Thus, even though the solutions contained similar amounts of EO and PO groups, the mixture did not exhibit similar suppression performance as the block copolymer. Another comparison can be made between PPG Mw 725 and Cetyl PEG Mw 1124. Both molecules exhibit similar Cu OCP, ZCP, Cu deposition potentials and charge under the suppressor peak. This observation indicates that stronger suppression performance can be achieved by using molecules with a low Mw which can provide steric hindrance. This steric hindrance can be obtained by longer side groups (such as Cetyl PEG) or a small group in the repeating unit (such as PPG). Note that longer end group or bigger groups in the repeating unit might have a deteriorating effect on the suppression performance [13]. The suppression strength shown in Table 5.3 for copper deposition on the resistive RuTa electrode followed a similar trend to the one seen in experimental results for copper deposition on copper electrode [11,12].

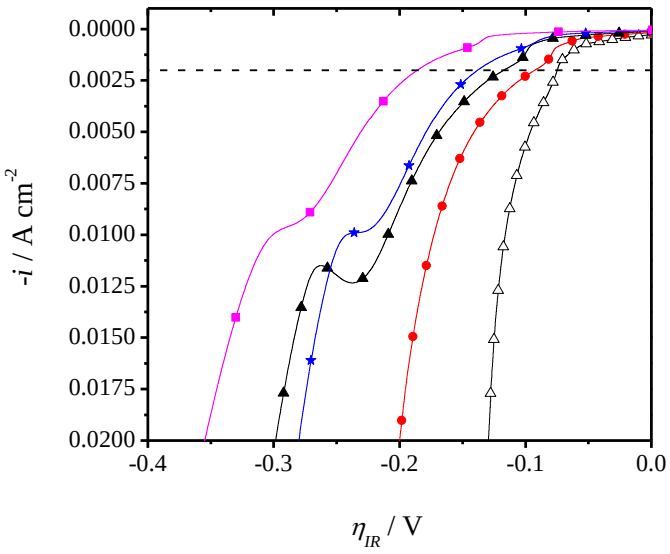

Figure 5.4: Current density, $-i$, versus overpotential, η_{IR}, curves for RuTa in the (Δ) base solution (empty symbols) and the presence (full symbols) of 300 ppm (●) PEG Mw 1000, (▲) PEG Mw 4000, (★) Methyl PEG Mw 1000 and (■) Cetyl PEG Mw 1124 at polarization rate of 0.02 V s^{-1}. η_{IR} is given with respect to the Cu OCP (0.10 V) for the base solution as shown in Table 5.2 and corrected for IR_s drop with R_s= 44 Ω. The dashed line crossing the $-i$- η_{IR} curves at -2 mA cm^{-2} indicates the point at which the polarization at low current densities was evaluated. Only the forward negative scans for negative overpotentials are shown.

Solution	***U at -2 mA cm^{-2} /V***	***ZCP /V***	***OCP Cu electrode /V***	***eq. thickness from the charge under the "suppressor peak" / nm***
base	0.018	0.099	0.100	Not observed
base + PEG Mw 200	-0.007	0.091	0.093	Not observed
base + PEG Mw 400	-0.007	0.074	0.069	257
base + PEG Mw 1000	-0.007	0.073	0.059	48
base + PEG Mw 4000	-0.023	0.032	0.040	26
base + PEG Mw 8000	-0.021	0.043	0.050	30
base + PEG Mw 20000	-0.027	0.04	0.040	29
base + Methyl PEG Mw 1000	-0.028	0.045	0.047	27
base + Mix 50% PPG Mw 725 50% PEG Mw 1000	-0.022	0.030	0.030	26
base + Block copolymer 10R5 Mw 2000	-0.054	0.018	0.015	17
base + PPG Mw 725	-0.055	0.017	0.012	15
base + Cetyl PEG Mw 1124	-0.092	0.023	0.028	17

Table 5.3: Copper deposition potential at -2 mA cm^{-2} representative for the start of steep increase in the cathodic current, ZCP in the reverse scan and equivalent thickness corresponding to the charge under the suppressor peak as obtained from the current-potential curves on RuTa at a polarization rate of 0.02 V s^{-1}. For comparison, also the OCP measured on a copper electrode during the first 10*s* of measurement is listed in the table. All measurements were performed in the base solution with 300 ppm of the different suppressors under investigation.

5.4 Galvanostatic deposition

5.4.1 Potential-time transients

Figure 5.5(a) shows the overpotential, η_{IR}, as a function of time during galvanostatic deposition of copper on RuTa from the base solution and in the presence of PEG (Mw 4000) at current density of -5 mA cm^{-2}. The η_{IR} values were determined with respect to the copper equilibrium potential, $U_{(Cu^{2+}/Cu),eq}$ (0.1 V vs. Ag/AgCl) in the base solution and corrected for *IR* drop with R_s= 44 Ω (see Equation 5.1). For the base solution, the OCP of RuTa ranged between +0.57 and +0.65 V vs. Ag/AgCl and did not change with the addition of PEG, implying that PEG does not absorb on the (air oxidized) RuTa surface [14]. At short times, a sharp drop in the overpotential is observed which corresponds to the formation of 2D islands (commonly seen for systems with under-potential deposition (Stranski-Krastanov mode) [26,27]), together with the partial reduction of Cu^{2+} to Cu^{+} at these potentials [28-30]. Only from $\eta_{IR} < 0$, copper deposition can proceed. A minimum in the overpotential is reached within a few tens of milliseconds after applying the current. This minimum represents the end of the nucleation of copper islands. As the existing copper islands on RuTa grow, the overpotential (indicated as $\eta_{IR\ Cu/RuTa}$) gradually shifts more positive with time as the effective area of the copper islands (A_{Cu}) increases with time and thus the effective current density decreases [18]. After a while, $\eta_{IR\ Cu/RuTa}$ levels off to a value (denoted as $\eta_{IR\ Cu}$) which corresponds to copper deposition on the copper covered electrode [15]. In the presence of PEG, the η_{IR} dropped from OCP to a first potential plateau (denoted as $\eta_{IR\ Cu/RuTa,\ Sup}$). The potential remained there for some time and then after a critical time (denoted as t_c) an additional drop to a second plateau (denoted as $\eta_{IR\ Cu,\ Sup}$) was observed. Similar to the base solution, $\eta_{IR\ Cu/RuTa,\ Sup}$ and $\eta_{IR\ Cu,\ Sup}$ correspond to copper deposition on existing copper islands and on a copper coated electrode, respectively. From Figure 5.5(a) it follows that, due to the inhibition of copper deposition on copper, $|\eta_{IR\ Cu/RuTa,\ Sup}| > |\eta_{IR\ Cu/RuTa}|$ and $|\eta_{IR\ Cu,\ Sup}| > |\eta_{IR\ Cu}|$, the latter showing the largest difference. Figure 5.5(b) shows the linear voltammograms as the ones shown in Figure 5.3 but plotted as a function of the overpotential (corrected for *IR* drop). The overpotential values seen in the plateaus, $\eta_{IR\ Cu,\ Sup}$ and $\eta_{IR\ Cu}$, obtained from the galvanostatic responses for current densities of -5, -7 and -10 mA cm^{-2} are plotted on Figure 5.5(b). The plateau values in the galvanostatic transients agree very well with the voltammograms for copper

electrodes in the base solution and in presence of PEG, respectively. This observation confirms that the potential drop seen in the galvanostatic transients reflects the inhibition strength (polarization) for copper deposition on a copper electrode in the absence and in the presence of suppressor: $\Delta\ \eta_{IR,\ Sup} = |\ \eta_{IR\ Cu,\ Sup} - \eta_{IR\ Cu}|$. Thus, the critical time for the second overpotential drop in the suppressor containing solution, t_c reflects the time to achieve a fully suppressed and closed copper surface on the RuTa electrode. Additional evidence of the essence of t_c in the galvanostatic transient will be discussed in detail in the following paragraphs.

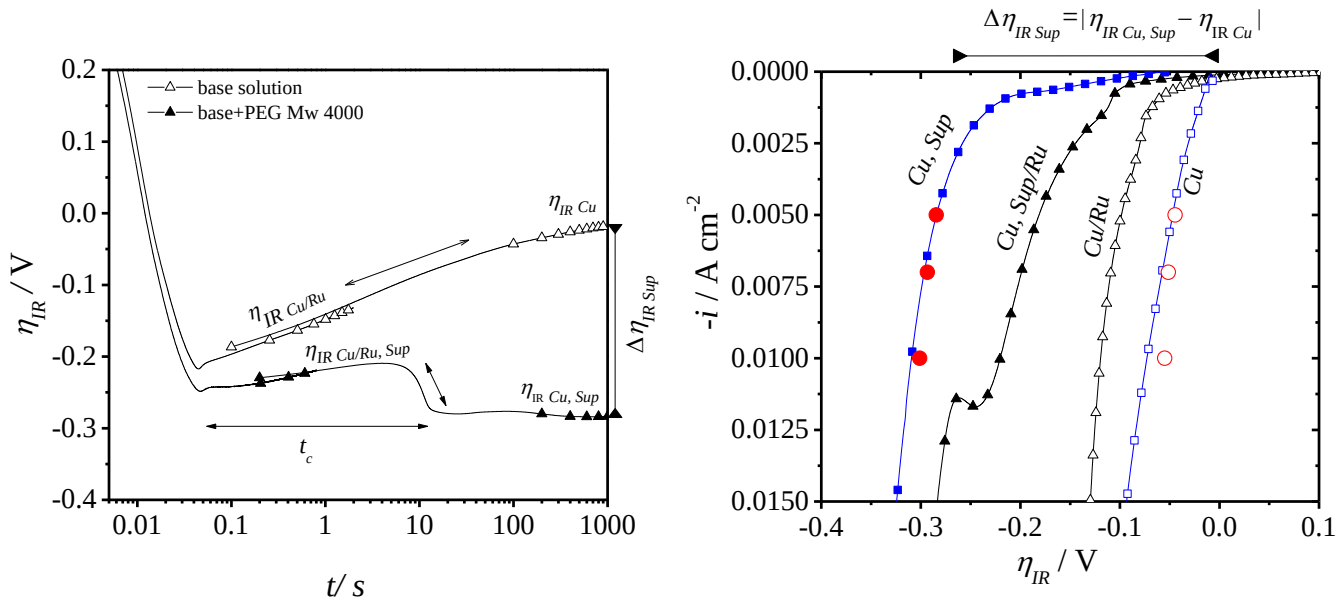

(a) (b)

Figure 5.5: (a) overpotential transients (η_{IR}-t) for RuTa in the base solution in the absence and in the presence of 300 ppm PEG (Mw 4000) at current density of -5 mA cm^{-2}. Two experiments are shown for each case; one with short sampling interval time of 0.0005*s* (0-2*s*) and one with larger sampling interval time 0.1*s* (0-1000*s*). (b) the values for $\eta_{IR\ Cu,\ Sup}$ (full circles) and $\eta_{IR\ Cu}$ (open circles) obtained from galvanostatic responses as those in Figure 5(a) for current densities of -5, -7 and -10 mA cm^{-2} are plotted in the current density (-*i*)- overpotential (η_{IR}) voltammograms for Cu (square symbols) and RuTa (triangle symbols) in the base solution in the presence (full symbols) and absence (open symbols) of PEG Mw 4000. The overpotential is given with respect to the copper equilibrium potential (0.1 V) for the base solution as shown in Table 5.2 and corrected for IR drop with R_s= 44 Ω.

5.4.2 The effect of suppressor on the nucleation and growth of copper islands

The nucleation and growth processes in the base solution are described in our previous study for the same deposition current and charge density as described herein (see Chapter 4). For the base solution, at current density of -5 mA cm^{-2} and after 2*s*, the N_p was 1.5×10^{8} cm^{-2} and spherical islands were observed on the RuTa surface (see Chapter 4). Increasing the deposition times did not lead to a measurable increase in N_p (see Chapter 4). Figure 5.6 shows top-down SEM images of Cu islands electrodeposited on RuTa from the base solution with 300 ppm PEG (Mw 4000) at current density of -5 mA cm^{-2} and after different deposition times. After 2*s* of deposition, the island density, N_p, was 1.0×10^{10} cm^{-2} and flattened shaped islands were observed on the RuTa surface (see inset). Note that in the case of hemispherical islands, the ratio between the island diameter, *d*, and its height, *h*, is 2. Thus, the so-called flattened shaped islands refer to a case where the ratio between *d* and *h* is bigger than 2. From the SEM image shown in Figure 5.6(a), a ratio of 2.5 was found. Similar to the base solution, increasing the deposition times to 5*s* and 10.8*s* did not lead to a noticeable increase in N_p. Instead, the copper islands grew in size and after 14.3*s* of deposition the whole RuTa surface was covered with Cu. These observations indicate that the nucleation is already completed in the early stages of the galvanostatic deposition where a sufficient amount of nuclei is formed to sustain the applied current density. Once the nucleation is completed, the current is sustained by the growing copper islands (see Chapter 4). Hence, the polyether suppressor affects the nucleation at shorter times resulting in an increase of N_p and more flattened shaped islands. Note that the SEM images were obtained at $\eta_{IR\ Cu/RuTa,\ Sup}$ plateau (2 and 5*s*), at the inflection point (10.8*s*) and in the beginning of $\eta_{IR\ Cu,\ Sup}$ plateau at t_c (20*s*) for the galvanostatic transient presented in Figure 5.5(a). The images confirm that the inflection point, seen in the galvanostatic transient, corresponds to the time when the copper islands coalesce, t_{coal} while t_c corresponds to the time needed to achieve a closed Cu film (100% Cu coverage). As such, the coalescence thickness, b_{coal} and the thickness of the closed Cu film can be calculated from the deposition charge densities at t_{coal} and t_c, respectively.

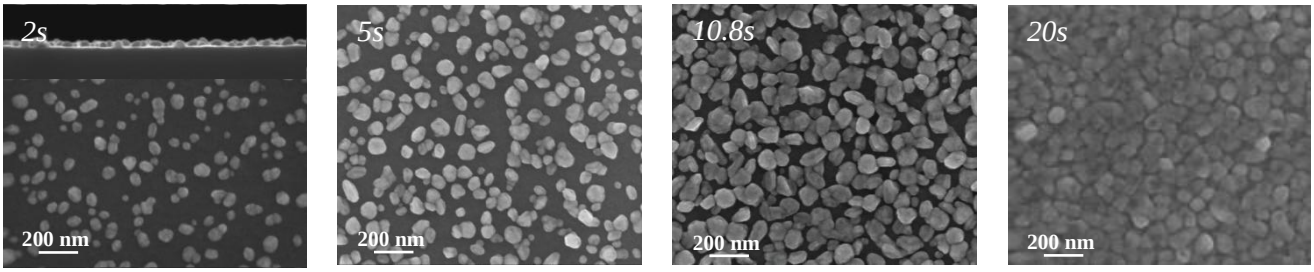

(a) (b) (c) (d)

Figure 5.6: Top-down SEM images of Cu islands deposited from the base solution with 300 ppm PEG (Mw 4000) at current density of -5 mA cm^{-2} after different deposition times (2, 5, 10.8 and 20*s*). In Figure 5.5(a) inset: cross-sectional SEM image, demonstrating the flattened island shape.

Figure 5.7 shows the copper coverage on the RuTa electrode obtained from digital image analysis of the SEM images such as those shown in Figure 5.6. The coverage is given by the sum of the projected areas of the individual islands. For the image at 10.8*s*, the islands start to coalesce (t_{coal}) and after 20*s* also the area between the particles is filled in and the whole surface is covered by copper. The copper coverage, θ_{Cu}, can also be calculated from the island density and the deposition charge as deduced in the following (for detail, see Appendix). For hemispherical-like islands, the area of the substrate covered by a single particle is given by the area of the circle projected on the surface by the particle with diameter, *d*. The total dimensionless surface coverage is then given by the product with the island density:

Equation 5.2:
$$\theta_{Cu} = \frac{\pi}{4} N_p d^2$$

The relationship between copper deposition charge density, q_{Cu} ($C.cm^{-2}$), particle diameter and island density is given by (see Appendix):

Equation 5.3:
$$q_{Cu} = K d^3 N_p \quad \text{with} \quad K = \left(\frac{\pi n F \rho}{x M w} \right)$$

where K $(C.cm^{-3})$ *is* a material constant, depending on the material properties and the geometry of the islands with $n=2$ for the number of electrons in the reaction, $F=96485$ C mol^{-1} for Faraday's constant, $\rho=8.94$ g cm^{-3} for the density of copper assuming a dense copper deposit,

Mw=63.54 g mol^{-1} is the molar mass of copper and x is a dimensionless factor indicating the shape of the island: x=6 for spherical, x=12 for hemispherical and x >12 for flattened shaped islands. As the current efficiency in the 0.6 M $CuSO_4$ solution is 100%, the passed charge, q, equals the charge, q_{Cu}, for forming the copper deposit. For galvanic deposition ($q=i\times t$) the variation of copper coverage with time is obtained after substitution of Equation 5.3 into Equation 5.2:

Equation 5.4:
$$\theta_{Cu} = \frac{\pi}{4} \cdot N_p^{1/3} \cdot \left(\frac{q_{Cu}}{K} \right)^{2/3} = \frac{\pi}{4} \cdot N_p^{1/3} \cdot \left(\frac{i}{K} \right)^{2/3} t^{2/3} \quad \text{for } q_{Cu} < q_{coal}$$

As the relationship in Equation 5.4 is based on the sum of individually growing particles, it is only valid before particle coalescence ($t < t_{coal}$). Assuming a hexagonal closed packing of the copper islands, the charge density at particle coalescence, q_{coal} is given by:

Equation 5.5:
$$q_{coal} = \frac{n\pi F\rho}{xMw\sqrt{N_p}}$$

or a copper coverage of:

Equation 5.6:
$$\theta_{Cu,coal} = \frac{\pi}{4} \quad \text{for } q_{Cu}=q_{coal}.$$

The theoretical coverage according to Equation 5.4 is plotted in Figure 5.7 for the case of N_p=1.0×10^{10} cm^{-2} as obtained from SEM analysis. A very good correlation between experiment and theory was found for x=16 indicating that the islands are close to hemispherical. The point of particle coalescence (t_{coal}=10.8s as observed from SEM) gives a coverage close to 0.8 as predicted by Equation 5.4. The island coalescence at time, t_{coal}, corresponds to the inflection point in the transient; i.e. the time between first ($\eta_{IRCu/RuTa,\ Sup}$) and second plateau ($\eta_{IRCu,\ Sup}$). Interestingly, the time t_c for drop to the second plateau in the galvanostatic transients of Figure 5.5(a) correlates well with the time at which the copper film closes (Θ_{Cu} =1).

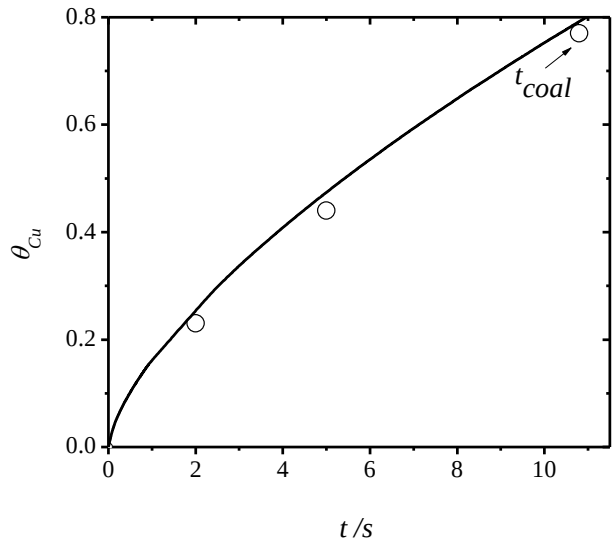

Figure 5.7: Variation of the copper coverage of the RuTa surface with deposition time, *t*, for copper deposition at -5 mA cm^{-2} from the base solution with 300 ppm PEG Mw 4000. (○) as obtained from digital image analysis of the SEM images (Figure 5.6). For comparison, the theoretical relationship according to Equation 5.4 is shown for $q_{Cu} \leq q_{coal}$ (solid line) with N_p=1.0×10^{10} cm^{-2} and x =16 for flattened shaped islands.

5.4.3 The effect of current density on copper island density

Figure 5.8(a) shows top-down SEM images of copper islands electrodeposited on RuTa at current densities of -2.5, -5, -7 and -10 mA cm^{-2} from the base solution with 300 ppm PEG (Mw 4000) for the same deposition charge density of 0.01 C cm^{-2}. At -2.5 mA cm^{-2}, sphere-like copper islands were formed with an island density, N_p, of 1.4×10^{9} cm^{-2}. Increasing the deposition current to -5 mA cm^{-2} led to an increase in N_p to 1×10^{10} cm^{-2} and the formation of flattened shaped copper islands. Further increase in the deposition current to -7 and -10 mA cm^{-2} led to a further increase in N_p to 2.8×10^{10} and 5×10^{10} cm^{-2}, respectively, and smaller islands were formed, as expected for the same deposition charge [18]. An increase in island density with increasing current density is expected since the deposition overpotential also increases (see Chapter 4). Figure 5.8(b) shows Cross-sectional SEM images of the copper deposits as observed after 1000*s* for -2.5 mA cm^{-2} and after 20, 11 and 6.6*s* (i.e. at t_c in the $\eta_{IR\ Cu\ Sup}$ plateau) for current densities of -5, -7 and -10 mA cm^{-2}, respectively. For the samples fabricated at -5, -7 and -10 mA cm^{-2} closed films were observed with a thickness of 43, 39 and 28 nm, close to the calculated equivalent thickness according to t_c of 37, 28 and 24 nm. Thus, the copper islands

have coalesced and overgrown to form a closed film. AFM measurements (not shown) confirmed root mean square (RMS) roughness values of 22.0, 17.0 and 11.8 nm for the Cu films formed at -5, -7 and -10 mA cm^{-2}, respectively. For reference, the RMS roughness value on a 100 nm PVD copper electrode was 10.4 nm. The SEM image in Figure 5.8(b) shows that at -2.5 mA cm^{-2} a rough and granular copper deposit is formed as copper islands were growing on top of each other. In this case, the RMS roughness value obtained from AFM measurements was 240.0 nm (for a layer of 920 nm in equivalent thickness). The copper deposit was not closed and part of the RuTa surface was still exposed to the solution through the porous deposit.

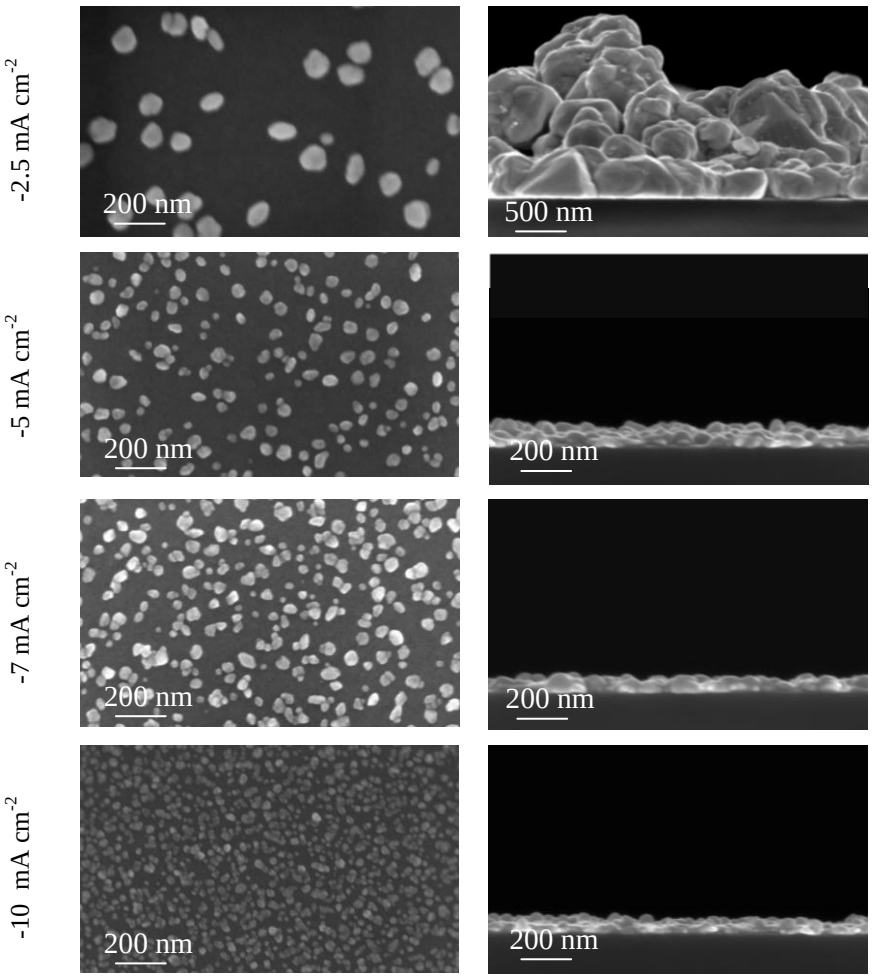

Figure 5.8: (a) Top-down SEM images of Cu islands electrodeposited from the base solution with 300 ppm PEG (Mw 4000) at -2.5, -5, -7 and -10 mA cm^{-2} for same deposition charge density of 0.01 C cm^{-2} (b) Cross-sectional SEM images of the electrode as observed after 1000*s* for -2.5 mA cm^{-2} and after 14.3, 8.3 and 5.5*s* (t_c in $\eta_{IRCu\ Sup}$ plateau) for current densities of -5, -7 and -10 mA cm^{-2} , respectively.

Figure 5.9 shows the variation of η_{IR}, with deposition time for the current densities used for the deposits in Figure 5.8. The transient for -5 mA cm^{-2} was already discussed in detail above. The transient behavior for current densities between -5 and -10 mA cm^{-2} is similar with a sudden change in the overpotential from a first plateau, $\eta_{IR\ Cu/RuTa,\ Sup}$ to a second plateau, $\eta_{IR\ Cu,\ Sup}$. The inflection points seen in the transients, t_{coal}, were observed at 10.8, 5.3 and 3.4*s* resulting in b_{coal} of 20, 14 and 12.5 nm for current densities of -5, -7 and -10 mA cm^{-2}, respectively. The time to achieve a closed Cu film, t_c, decreased from 20*s* for current density of -5 mA cm^{-2} to 11 and 6.6*s* for current densities of -7 and -10 mA cm^{-2}, respectively. For the lower current density of -2.5 mA cm^{-2}, no potential drop was reached, not even after a deposition time of 1000*s*. As shown in Figure 5.8(b), the copper deposit at -2.5 mA cm^{-2} was not closed after 1000*s* and part of the RuTa surface was still exposed to the solution through the porous deposit. As a result, no drop in overpotential is seen in this case (only $\eta_{Cu/Ru,\ Sup}$). In the inset of Figure 5.9 the critical time, t_c, as obtained from the galvanostatic transients is plotted versus the time for complete RuTa coverage by copper, t_c', as observed from the SEM analysis. A very good correlation was found between t_c' and t_c, for the current densities under investigation. As for the -5 mA cm^{-2} case, these measurements confirm that t_c corresponds to the closure of the copper film for all current densities under investigation.

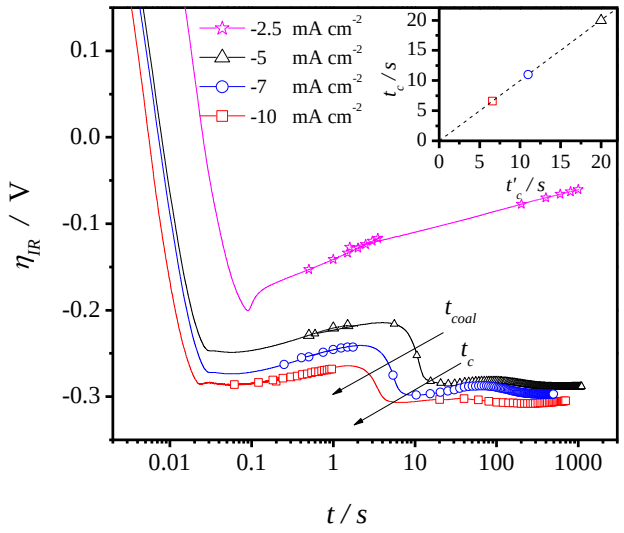

Figure 5.9: Overpotential corrected for *IR* drop, η_{IR}, as a function of time for galvanostatic Cu deposition on RuTa for the current densities used for the deposits in Figure 5.8. In the inset: time for 100% copper coverage, t_c', as

observed from the SEM analysis and critical time for the potential drop, t_c, as determined from the galvanostatic transients in Figure 5.9.

5.4.4 The effect of PEG Mw

Figure 5.10 shows top-down SEM images of copper islands electrodeposited on 2 nm RuTa from the base solution with 300 ppm (a) PEG Mw 400 (b) PEG Mw 1000 (c) PEG Mw 4000 and (d) PEG Mw 20000 at current density of -5 mA cm^{-2} for 2*s*. For the base solution (not shown), spherical copper islands were formed and N_p of 1.5×10^8 cm^{-2} was observed on the RuTa surface. The addition of PEG with Mw of 400, 1000 and 4000 led to the formation of hemispherical copper islands and to an increase in the island density to 1.5×10^9 cm^{-2}, 4.0×10^9 cm^{-2} and 9.0×10^9 cm^{-2}, respectively. Further increase in the PEG Mw to 8000 and 20000 did not show a significant change in the N_p. Our experimental results show that high Mw PEG molecules provided a better blocking layer for Cu^{2+} reduction consequently resulting in a higher N_p. The steady-state suppression characteristics depend on the coverage and the type of suppressor. In the non-steady state or transient period, also the adsorption kinetics and thus bulk diffusion of these polyether molecules needs to be considered. The adsorption of polyether suppressors happens within about 0.4*s* independent of Mw and structure [12]. Interestingly, though, Mw seems to affect the desorption times rather than their adsorption times [12]. The diffusion coefficient of PEG also decreases with increasing Mw [31], i.e. PEG molecules with higher Mw diffuse slower to the Cu surface. As kinetics of adsorption cannot explain the observed difference in particle density, it is the coverage (suppression strength) of the polyether molecules that affects the island density. Note that the number of EO groups in one polyether molecule i.e. the number of attachment points increases with Mw (Table 5.1) and thus, the probability to stick to the Cu surface is higher for polyether molecules with higher Mw. The saturation of N_p for PEG molecules with Mw above 4000 could indicate a maximal blocking of the copper electrode as indicated by Kelly *et al.* [3]. Figure 5.10(e) shows η_{IR} as a function of time during galvanostatic deposition on RuTa at current density of -5 mA cm^{-2} from the base solution with 300 ppm PEG for a selected group of PEG Mw (400, 1000, 4000 and 20000). The important features in the overpotential-time transients in base solutions with 300 ppm of the other PEG suppressors with different Mw are summarized in Table 5.4. Interestingly, the overpotential-time responses followed similar trends as that for N_p (see also Table 5.4); larger $\Delta\eta_{IR,\,Sup}$ and shorter t_{coal} and t_c

were observed with increasing PEG Mw from 400 to 4000 while no significant further change in $\Delta\eta_{IR,\ Sup}$, t_{coal} and t_c was observed for further increase in the Mw from 4000 to 20000. These observations indicate that the PEG Mw, as well as the current density (Figure 5.9) influences the transient signature i.e. the features $\Delta\eta_{IRSup}$, t_{coal} and t_c.

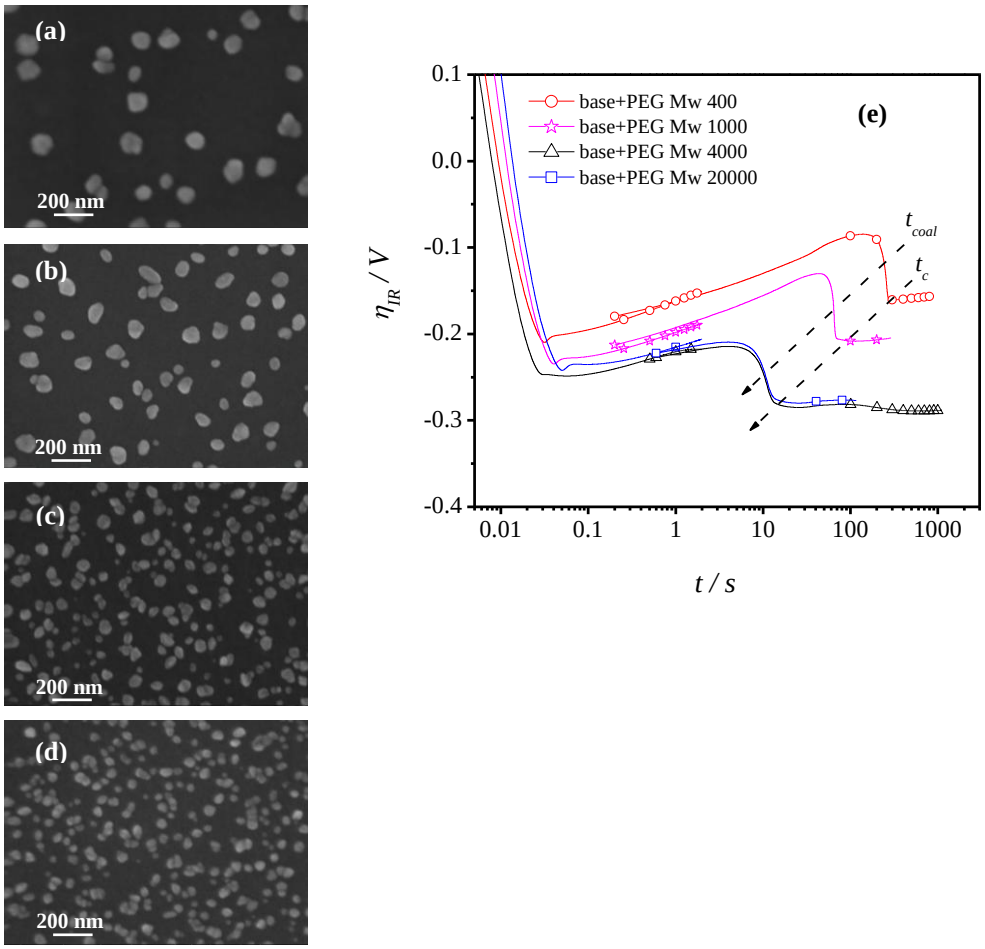

Figure 5.10: Top-down SEM images of Cu islands deposited on RuTa from the base solution with 300 ppm (a) PEG Mw 400 (b) PEG Mw 1000 (c) PEG Mw 4000 and (d) PEG Mw 20000 at current density of -5 mA cm^{-2} for 2s. (e) overpotential corrected for *IR* drop, η_{IR}, as a function of time during galvanostatic Cu deposition on RuTa from the base solution with 300 ppm PEG with the same different Mw in Figure 5.10(a-d).

Figure 5.11 shows the theoretical shape factor, *x*, as a function of PEG Mw, demonstrating the effect of PEG Mw on the island shape. The theoretical shape factor, *x* was determined from the deposition charge density q_{Cu} with N_p and island diameter, *d*, as obtained from the SEM analysis (see Figure 5.10(a-d)). The island shape factor, *x* increased from 6.2 for the base solution to 7.2, 8.8, 9.8 and 15.9 in the presence of 300 ppm PEG with Mw of 200, 400, 1000

and 4000, respectively. These observations indicate that the polyether Mw affects the island shape as well as N_p. In the inset of Figure 5.11: cross-sectional SEM images of the Cu islands electrodeposited on the RuTa surface at -5 mA cm^{-2} for 2*s* from the base solution in the presence of 300 ppm PEG with Mw of (a) 200 (b) 1000 and (c) 4000. Spherical islands were observed for deposition with PEG with Mw of 200. Increase in the Mw to 1000 and 4000 resulted in the formation of hemispherical and flattened islands on the RuTa surface, respectively.

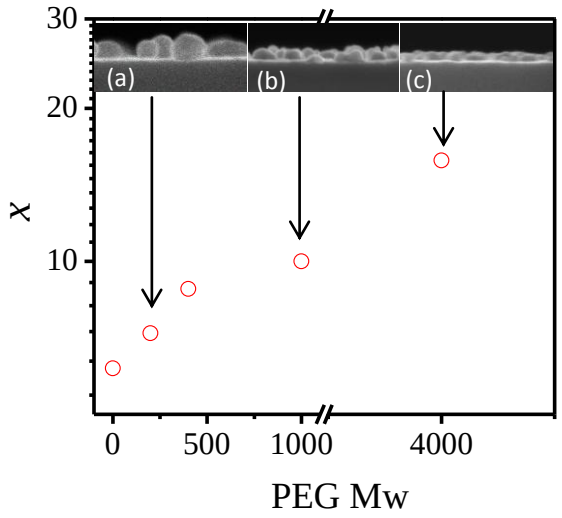

Figure 5.11: The island shape factor, *x*, as a function of PEG Mw, as obtained after deposition of 2*s* at -5 mA cm^{-2}: *x* = 6 for spherical, *x*=12 for hemispherical and *x* >12 for flattened island shapes. In the inset: cross-sectional SEM images of the Cu islands electrodeposited on the RuTa surface at -5 mA cm^{-2} for 2*s* from the base solution in the presence of 300 ppm PEG with Mw of (a) 200 (b) 1000 and (c) 4000.

5.4.5 The effect of polyether derivatives on the nucleation and growth of Cu

The effect of other polyether suppressors on the nucleation and growth of copper was also studied. Even though these polymers have similar structures (repeating units of either EO or PO), the number of attachment points to the Cu surface and the arrangement of the polyether molecule on the Cu surface may differ due to the different molecular architecture which can induce steric effects. As mentioned before, the steric hindrance effect can either contribute to improve or degrade the suppression performance [11,13]. Potential-time measurements, together with SEM analysis (not shown) were performed for copper deposition on RuTa from the base solution with 300 ppm of different polyether suppressors under investigation and at different current densities

(-2.5, -5 and -10 mA cm^{-2}). The N_p values along with the important features seen in the potential-time responses at -5 mA cm^{-2} are summarized in Table 5.4. It is interesting to follow the change in the different features (t_{coal}, b_{coal}, $\Delta\eta_{IR,\ Sup}$ and N_p) with the modification of the polyether Mw and structure. For reference, the number of attachments points, reflecting the probability to stick to the Cu surface can be seen in Table 5.1. The effect of a single alkyl end group on PEG can be seen when comparing suppressors with similar Mw (i.e. same number of ether group) but with short Methyl (-CH_3) and longer Cetyl (-$(CH_2)_{15}$-CH_3) end groups. From the table it follows that a longer end group led to shorter t_{coal}, smaller b_{coal} and higher values of $\Delta\eta_{IRSup}$ and N_p. The effect of the functional group within the repeating unit can be seen when comparing PPG Mw 725 (with only 12.5 attachment points) with PEG Mw 400 and PEG Mw 20000 (with 9 and 454.5 attachment points, respectively); the presence of the methyl group within the repeating unit of PPG induced a stronger suppression compared to PEG Mw 400 and PEG Mw 20000. Another comparison can be made for solutions containing a mixture of 50/50 PEG (Mw 1000) and PPG (Mw 725) or a block copolymer consisting 50% EO groups. It can be seen that the suppression performance is different in the two cases; i.e. longer t_{coal}, larger b_{coal} and smaller $\Delta\eta_{IR,\ Sup}$ and N_p are observed for the mixture. As mentioned before, stronger suppression can be achieved by using low Mw molecules which can provide steric hindrance. However, longer end groups or larger groups in the repeating unit may have a deteriorating effect on the suppression performance [13]. The electrochemical parameters t_{coal} and $\Delta\eta_{Sup}$ followed similar trend seen for the physical parameters N_p and b_{coal} for all polyether suppressors and at all current densities under investigation i.e. larger $\Delta\eta_{IRSup}$ and shorter t_{coal} were observed for higher N_p and smaller b_{coal}.

Solution	N_p /cm^{-2}	t_{coal} /s	b_{coal}/nm	$\Delta\eta_{Sup}$ / mV
base + PEG Mw 200	9.0×10^{8}	Was not observed	N/A	Was not observed
base + PEG Mw 400	1.5×10^{9}	259	479.6	87
base + PEG Mw 1000	3.9×10^{9}	65.3	120.9	147
base + PEG Mw 4000	9.0×10^{9}	10.8	20.0	189
base + PEG Mw 8000	1.0×10^{10}	10.5	19.4	188
base + PEG Mw 20000	1.1×10^{10}	11	20.4	192
base + Methyl PEG Mw 1000	8.8×10^{9}	11.8	21.8	188
base + Mix of 50%PPG Mw 725 50% PEG Mw 1000	1×10^{10}	11.5	21.3	194
base + Block copolymer 10R5 Mw 2000	1.3×10^{10}	10	18.5	228
base + PPG Mw 725	4.1×10^{10}	7.5	13.9	251
base + Cetyl PEG Mw 1124	2.8×10^{10}	6.2	11.2	222

Table 5.4: Cu island density, N_p, from SEM analysis, b_{coal} calculated according to Equation 5.5 and t_{coal} and $\Delta\eta_{Sup}$ from the potential-time responses. All measurements were performed in the base solution with 300 ppm of the different polyether suppressors under investigation at current density of -5 mA cm^{-2}.

5.4.6 Correlation between electrochemical parameters and Cu island density

Figure 5.12 shows the island density, N_p, for copper electrodeposited from the base solution (open symbols) and in the presence (full symbols) of the different polyether suppressors under investigation as a function of the applied current density. Only the suppression strength is indicated for clarity. Similar to the PEG (Mw 4000) case (see §5.4.3), it can be seen that N_p increases with increasing deposition current for $2.5< |i| \leq 10$ mA cm^{-2} for all the polyether suppressors under investigation. This confirms the general tendency of N_p to increase with increasing driving force for deposition [18]. A systematic increase in the island density was observed for stronger suppression.

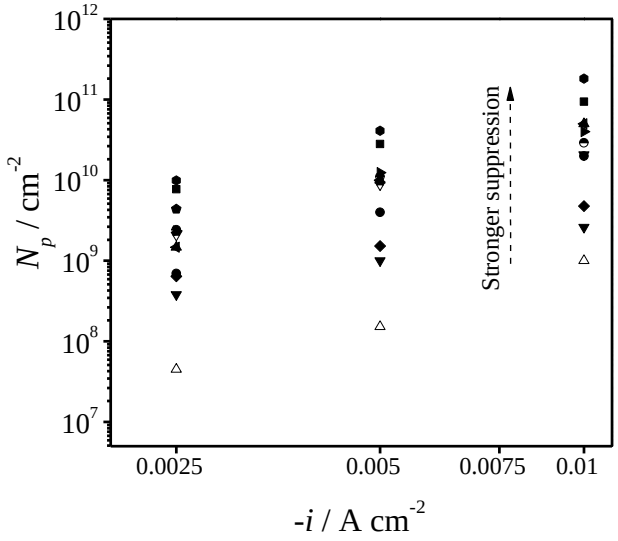

Figure 5.12: Copper island density, N_p, as a function of current density,-i. The deposition experiments were performed from the base solution and in the presence of 300 ppm of the different polyether suppressors under investigation.

In Chapter 4, the effect of cupric ion concentration and current density on island density was treated in detail. It was shown that an exponential relationship exists between N_p and -(η_{IR}-$\eta_{IR,\ Nucl}$), with $\eta_{IR\ Nucl}$ =0.025 V, independent of cupric ion concentration and current density. The N_p dependency on - (η_{IR}–$\eta_{IR\ Nucl}$) for the RuTa electrode was found to be:

Equation 5.7:
$$N_p(\eta) = 1\times10^{7}\exp\left(-32\left(\eta_{IR}-\eta_{IR\ Nucl}\right)\right)$$

Hence, with $N_{\eta,\ Nucl}$=1×10^{7} cm^{-2} and $\frac{\alpha F}{RT} = 32$ (see details in Chapter 4). To test whether this generalization holds also in the case of additives, the island density, N_p, was plotted as a function of -(η_{IR}-η_{IRNucl}) in Figure 5.13 for the base solution (open triangles) and in the presence of the different suppressors under investigation (full circles) and at different current densities (between -2.5 and -10 mA cm^{-2}). Only the suppression strength is indicated for clarity. The η_{IR} values were extracted from galvanostatic measurements such as those shown in Figure 5.5. The η_{IR} values correspond to copper deposition potentials in the plateau $\eta_{IR\ Cu/RuTa}$ (for the base solution) and in plateau $\eta_{IR\ Cu,\ Sup/RuTa}$ (for the base solution with 300 ppm of the different polyether suppressors under investigation). Note that the magnitude of the overpotential depends on the effective Cu

surface area; the overpotential shifts more positive with increase in the surface area of the Cu islands (see Chapter 4). Thus, to have fair comparison with the additive-free solutions investigated in Chapter 4, η_{IR} values that correspond to the same effective surface area of the copper islands A_{Cu} = 0.19 were selected (for detail, see Appendix). The data points, describing the dependency between N_p and -(η_{IR}-$\eta_{IR,\ Nucl}$) for the additive-free solutions with cupric ion concentrations between 0.01 M and 0.6 M from Chapter 4, are also plotted in Figure 5.13 (open squares). The island density, N_p, now follows the same exponential relationship with -(η_{IR}-η_{IRNucl}) for the RuTa substrate irrespective of Cu^{2+} concentration, suppressor type and current density (see Equation 5.7). This relationship provides a universal equation for N_p on RuTa surface. Thus, the island density can be estimated solely from the actual overpotential for copper deposition seen during galvanostatic measurements irrespective of solution composition and deposition current.

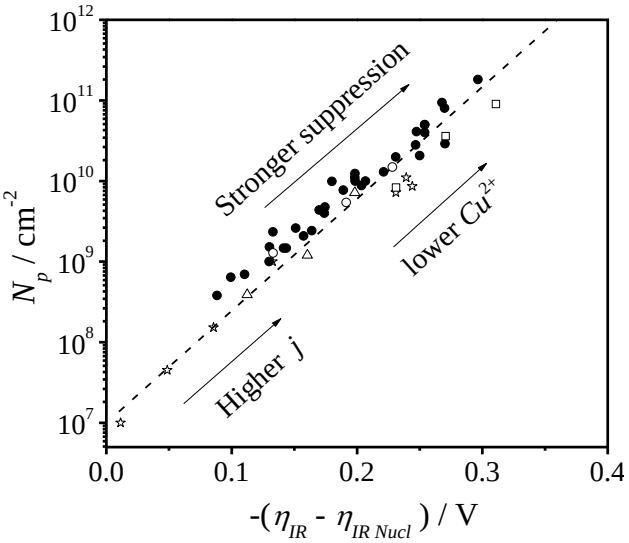

Figure 5.13: N_p as a function of the corresponding –(η_{IR}–$\eta_{IR\ Nucl}$) with η_{Nucl} = -0.025 V. The η_{IR} was determined with respect to Cu OCP and corrected for *IR* drop. The η_{IR} values were extracted from the galvanostatic measurements and correspond to copper deposition on copper islands with A_{Cu}=0.19. The deposition experiments in the absence of additives were performed from solutions of 1.8 M H_2SO_4, 1.4x10^{-3} M HCl and 0.01, 0.5, 0.1 and 0.6 M $CuSO_4$ and at different current densities (see Chapter 4). The deposition experiments in the presence of additives were performed from the base solution with the addition of 300 ppm of the different polyether suppressors under investigation. The N_p dependency on -(η_{IR}–η_{IRNucl}) for RuTa substrate is given according to the following: $N_p(\eta) = 1\times10^{7}\exp\left[-32(\eta_{IR}-\eta_{IR\,Nucl})\right]$.

5.5 Summary

The suppression performance of different polyether suppressors can be identified by analyzing the unique signature of the potential-time curves obtained during galvanostatic copper deposition on the resistive RuTa surface. The effect of current density and suppression strength is integrated in the features seen in the potential-time transients i.e. in t_{coal}, t_c and $\Delta\eta_{IRSup}$ and correspond very well with the trends seen in the physical features i.e. in N_p and b_{coal}. Analysis of the potential-time transients showed that an exponential relationship exists between the island density, N_p, and the actual deposition overpotential. Surprisingly, the same exponential dependence between copper island density and overpotential as those in the additive free $CuSO_4$ solutions was found (Chapter 4). The copper islands, however, have a flattened shape (pancakes) in the presence of suppressors, compared to hemispheres and spheres in the additive-free solutions. This study provides a general equation for determining the island density, N_p for copper deposition on a RuTa substrate based solely on the copper deposition overpotential and irrespective to solution composition and deposition current. It is concluded that high N_p can be achieved by controlling the overpotential which can be manipulated by increasing the current density, lowering the Cu^{2+} concentration and/or adding a strong suppressor to the plating solution.

[1] P.C.Andricacos, C. Uzoh, J.O. Dukovic, J. Horkans, H. Deligianni, Damascene copper electroplating for chip interconnections, IBM J. Res. DeV. 1998, 42, 567-574.

[2] R. Akolkarz and U. Landau, Mechanistic analysis of the Bottom-Up fill in copper interconnect metallization, Journal of The Electrochemical Society, 156 (2009) D351.

[3] J.J. KeIly and A.C. West, Copper Deposition in the Presence of Polyethylene Glycol I. Quartz Crystal Microbalance Study, Journal of The Electrochemical society, 145 (1998) 3472.

[4] Z.V. Feng, X. Li and A.A. Gewirth, Inhibition Due to the Interaction of Polyethylene Glycol, Chloride, and Copper in Plating Baths: A Surface-Enhanced Raman Study, The Journal of Physical chemistry B , 107, (2003) 9415.

[5] J.G. Long, P.C. Searson, and P.M. Vereecken, Electrochemical Characterization of Adsorption-Desorption of the Cuprous-Suppressor-Chloride Complex during Electrodeposition of Copper, Journal of The Electrochemical Society, 153, C258 (2006).

[6] K.R. Hebert, S. Adhikari, and J.E. Houser, Chemical Mechanism of Suppression of Copper Electrodeposition by Poly(ethylene glycol), Journal of The Electrochemical Society, 152 (2005) C324.

[7] M.E. Huerta Garrido and M.D. Pritzker, Inhibition of copper deposition by polyethylene glycol and chloride, Journal of The Electrochemical Society, 156 (2009) D36.
[8] K.R. Hebert, Role of chloride ions in suppression of copper electrodeposition by polyethylene glycol, Journal of The Electrochemical Society, 152 (2005) C283.
[9] H.M. Chen, S.J. Parulekar and A. Zdunek, Interactions of Chloride and Polyethylene Glycol in Acidic Copper Sulfate Electrolyte, Journal of The Electrochemical Society, 155 (2008) D34.
[10] T.A. Atanasova, K. Strubbe and P.M. Vereecken, Adsorption/Desorption of Suppressor Complex on Copper: Description of the Critical Potential, ECS Transactions, 33 (2011) 13.
[11] W.P. Dow, M.Y. Yen, W.B. Lin and Shih-Wei Ho, Influence of molecular weight of polyethylene glycol on microvia filling by copper electroplating, Journal of The Electrochemical Society, 152 (2005) C769.W.J. Gallaway, A.C.West, PEG, PPG, and their triblock copolymers as suppressors in copper electroplating, Journal of The Electrochemical Society, 155, (10), D632 (2008).
[12] W.J. Gallaway, A.C. West, PEG, PPG, and their triblock copolymers as suppressors in copper electroplating, Journal of The Electrochemical Society, 155, (10), D632 (2008).
[13] J. Mendez, R. Akolkar and U. Landau, Polyether suppressors enabling copper metallization of high aspect ratio interconnects, Journal of The Electrochemical Society, 156 (2009) D474.
[14] M.L. Walker, L.J. Richter, D. Josell, and T.P. Moffat, An In Situ Ellipsometric Study of Cl−-Induced Adsorption of PEG on Ru and on Underpotential Deposited Cu on Ru, Journal of The Electrochemical Society, 153,C235 (2006).
[15] A. Radisic, P. Boelen, A. Rosenfeld, J.L. Hernandez, G. Beyer and P.M. Vereecken ECS Transactions, electrochemical nucleation and growth of copper on resistive substrates, 11 (2008) 25.
[16] A. Radisic, A.C. West and P.C. Searson, Influence of additives on nucleation and growth of copper on n-Si(111) from acidic sulfate solutions, Journal of The Electrochemical Society, 149 (2002) C94
[17] M. Zheng, M. Willey and A.C. West, Electrochemical nucleation of copper on ruthenium effect of Cl-, PEG and SPS, Electrochemical and solid-state letters, 8 (2005) C151.
[18] M. Nagar, A. Radisic, K. Strubbe, P.M. Vereecken, The effect of cupric ion concentration on the nucleation and growth of copper on RuTa seeded substrates, Electrochimica Acta 92 (2013) 474.
[19] M.J. Willey, U. Emekli, A.C. West, Uniformity effects when electrodepositing Cu onto resistive substrates in the presence of organic additives, Journal of the Electrochemical Society 155 (2008) D302.
[20] M. Nagar, A. Radisic, K. Strubbe and, P. M. Vereecken, Nucleation and Growth of Copper on Ru-Based Substrates:II. The Effect of the Suppressor Additive, ECS Transactions, 41 (35) (2012) 99.
[21]http://worldaccount.basf.com/wa/NAFTA/Catalog/ChemicalsNAFTA/info/BASF/PRD/3008
[22] http://rsb.info.nih.gov/ij/docs/index.html
[23] http://www.nanotec.es/products/wsxm/index.php
[24] B.R. Scharifker and G. Hills, Theoretical and experimental studies of multiple nucleation, Electrochimica Acta 28 (1983) 879.

[25] A. Radisic, M. Nagar, K. Strubbe, S. Armini, Z. El-Mekki, H. Volders, W. Ruythooren, P.M. Vereecken, Copper plating on resistive substrates, diffusion barrier and alternative seed layers, ECS Transactions 25 (2010) 175.
[26] C. Yong-Da, D. Wei-Ping, L. Yung-Fang, L. Yuh-Lang, Y. Shueh-Lin , H. Su-Mei, Copper Underpotential Deposition on Gold in the Presence of Polyethylene Glycol and Chloride, International Journal of Electrochemical Science 6 (2011) 3416.
[27] P.M Vereecken, R.A. Binstead, H. Deligianni, P.C. Andricacos, The chemistry of additives in damascene copper plating, IBM Journal of Research and Development 49 (2005) 1.
[28]J. Vazquez-Arenas, G. Vázquez, A. M. Meléndez and I. González, The effect of the Cu2+/Cu+ step on copper electrocrystallization in acid noncomplexing electrolytes, Journal of The Electrochemical Society, 154 9 (2007) D473.
[29] T. Hurlen, G. Oven and A. Staurse, Kinetics of copper dissolution and deposition in aqueous sulphate solution, Electrochimica Acta, 23 (1978) 39.
[30] 0. R. BROWN and H. R. THIRSK, The rate-determining step in electrodeposition of copper on copper from aqueous cupric sulphate solutions, Electrochimica Acta, 10 (1965) 383.
[31] J. Shao, R.E.Baltus, Hindered diffusion of dextran and polyethylene glycol in porous membranes. AIChE Journal, 46, (2000) 1149.

CHAPTER 6: THE EFFECT OF SUBSTRATE CHARACTERISTICS ON THE ELECTROCHEMICAL NUCLEATION AND GROWTH OF COPPER.

This Chapter describes experiments and results of copper electrodeposition from acid copper sulfate ($CuSO_4$) solutions in the absence and the presence of different polyether molecules on as-received RuTa alloy substrates, electrochemically treated (EC-treated) RuTa alloys and on Pt. The main focus is on the effect of substrate properties on the nucleation and growth processes during galvanostatic deposition. The three substrates under investigation exhibited a different coverage after the formation of a Cu underpotential (UPD) layer. This, in turn, affected the island density, N_p, and the island shape. Analysis of the galvanostatic transients shows that for all three substrates an exponential relationship exists between the island density and the actual deposition overpotential. For Pt and for the as-received RuTa alloy, two general equations are proposed for determining N_p irrespective of solution composition (such as Cu^{2+} concentration and suppressor type) and deposition parameters (such as current density). Based on these general equations, it becomes possible to make a better choice of substrate for direct plating applications based only on one data point of N_p and deposition overpotential observed in the galvanostatic transient.

6.1 Introduction

Copper electrodeposition onto foreign substrates proceeds through nucleation and growth processes; i.e. either by Volmer–Weber mode (three-dimensional (3D) islands) or by Stranski-Krastanov mode (three-dimensional (2D) layer + 3D nuclei) [1,2]. The eventual growth mode is determined by the interaction energy between the copper add-atoms and the substrate, $E_{ads,Cu\text{-}S}$, and the interaction energy between copper add-atoms and the bulk copper, $E_{ads,Cu\text{-}bulk}$ [1]. In the case where $E_{ads,Cu\text{-}S} < E_{ads,Cu\text{-}bulk}$, copper nucleates directly on the substrate surface and the growth proceeds by the Volmer–Weber mode [1]. Conversely, if $E_{ads,Cu\text{-}S} > E_{ads,Cu\text{-}bulk}$ underpotential deposition (UPD) of copper leads to the formation of Cu monolayers, followed by nucleation of 3D copper islands. In that case, the growth mode follows the Stranski-Krastanov mode [1]. The Cu UPD layer serves as a wetting layer for copper nucleation, thus substrates that

exhibit small difference between $E_{ads,Cu\text{-}bulk}$ and $E_{ads,Cu\text{-}S}$ are expected to promote higher N_p [1]. The differences between $E_{ads,Cu\text{-}bulk}$ and $E_{ads,Cu\text{-}S}$ is subject to a variety of parameters related with the choice and preparation of the substrate such as lattice parameter, crystal orientation, number of active sites for nucleation, oxidation state, substrate resistivity/thickness etc. [1]. Therefore, the substrate plays a significant role in dictating the nucleation and growth mechanism of copper onto the foreign substrate, especially with respect to islands density, N_p, and the shape of the electrodeposited Cu islands.

The nucleation and growth mechanism of copper onto various substrates has been extensively studied [3-10]. Moffat *et al*. studied the electrodeposition of copper on Ru layers [4]. It was shown that copper deposition on an "oxide-free" Ru surface resulted in faster coalescence involving the formation of a Cu UPD layer. In contrast, when copper deposition was carried on an oxidized Ru surface, the oxide blocked the Cu UPD and copper deposition followed Volmer-Weber growth mode [4]. Radisic *et al*. investigated the morphology and the nucleation kinetics of copper islands during electrodeposition on gold (Au) [7], silicon (Si) [8], titanium nitride (TiN) [9] and tantalum nitride (TaN) [10]. Their results showed that the island density increased exponentially by 47, 99, 140 and 150 to 250 mV per decade for the Au, Si, TiN and TaN, respectively. These results indicate that for different substrates a different overpotential is required for the same increase in N_p. In this work, we use the term "platability" to express the substrate's capability to result in a higher N_p for the same overpotential. For example, copper platability is known to be larger for oxide-free substrates in comparison with oxide-based substrates [4]. Note that the so-called platability of a given substrate is associated to the substrate affinity to exhibit UPD behavior.

For successful void-free filling of very small features by direct plating, it is essential to have high N_p to allow fast formation of a continuous copper thin film inside the sub-30 nm features [11]. To meet these requirements, the thickness of the continuous Cu film should be 3 nm and below (corresponding to N_p of 10^{13} cm^{-2}, considering 3D hemispherical islands). The requirement for N_p can be lowered in case of quasi-2D growth of the Cu islands i.e. disk shape-like islands will lead to a thinner coalescence thickness than sphere shape-like islands [11]. In addition, high N_p and quasi-2D growth would also allow a fast propagation of the copper film across the resistive substrate (300 mm wafer) [12,13]. Therefore, since the nature of the substrate affects nucleation and growth processes, the choice of substrate is one of the key features for

direct plating applications. The choice of a suitable substrate for direct plating applications is however not obvious. Indeed, the substrate must promote high N_p and quasi-2D growth. However it also needs to be easily fabricated and integrated within the damascene process at low manufacturing cost [14,15].

Although many studies discuss copper deposition on a variety of resistive substrates, the island density is often reported as a function of applied potential but the relationship with overpotential is often ignored or considered irrelevant [3-9]. However, when comparing copper deposition on different substrates, the kinetics of the nucleation and growth processes differ, and therefore one should compare overpotentials instead of potentials. As discussed above, the mode and the kinetics of the nucleation and growth processes differ from one substrate to another. As-received RuTa, fabricated by physical vapor deposition (PVD), is typically covered with an air-formed oxide, and an electrochemical-treatment is a well-known method to reduce surface oxides [16]. On the other hand, Pt, as a noble metal, is well-known for its high chemical stability in an oxidizing atmosphere [17]. Because of this chemical stability, Pt was chosen as a model substrate, an EC-treated RuTa as an oxide-free substrate and an as-received RuTa as an oxide-based substrate to investigate the effect of surface conditions (i.e. the presence of oxide) on N_p and the island shape during galvanostatic deposition of copper. More specifically, in this Chapter, the nucleation and growth of Cu islands on as-received RuTa alloy, EC-treated RuTa alloy and Pt electrodes from acidic $CuSO_4$ solutions in the absence and the presence of different polyether suppressors was studied. The electrochemical processes at these substrates were studied using cyclic voltammetry and potentiometry. The unique signature of the current-potential and potential-time responses for copper deposition from solutions that contain polyether suppressor was used to characterize the platability of different substrates. A general description of this unique signature can be seen in Figure 6.1(a+b) (for a detailed description of these curves see also Chapter 5). Figure 6.1(a) shows typical current-potential curves for copper deposition on Cu and on a resistive substrate, such as RuTa in acid $CuSO_4$ solution in the presence of PEG. The so-called suppressor peak, measured at the RuTa electrode reflects the change of the surface during the deposition process: when most of the RuTa surface is covered with copper, the deposition current decreases due to the lower effective current density as copper and the current-potential curve joins with the *i*-U curve for copper deposition on the Cu electrode in the presence of suppressor [16]. Hence the charge associated with the suppressor peak (shown

as a gray area in Figure 6.1(a)) is a measure for the amount of copper that was deposited before the coalescence of the copper film. In Figure 6.1(b), typical potential-time responses for copper deposition on Cu and RuTa electrodes in a solution such as the one used in Figure 6.1(a) are shown. First, the potential drops from OCP to a first potential plateau (indicated as $U_{Cu/RuTa,\ sup}$) that corresponds to copper deposition on existing Cu islands. The potential remains constant for some time and then at a critical time, t_c, an additional drop to a second plateau (indicated as $U_{Cu,\ sup}$) is observed. The inflection point seen in the potential-time response on the RuTa electrode corresponds to the time when the copper islands coalesce, t_{coal}, while t_c reflects the time to achieve a fully suppressed and closed copper surface on the RuTa electrode. Once t_c is reached , the curve, measured at the RuTa electrode joins the curve at the Cu electrode in the second plateau. Indeed, we now need to look for a substrate that exhibits the smallest charge under the suppressor peak in the current-potential response and the shortest t_{coal} and t_c in the potential-time response.

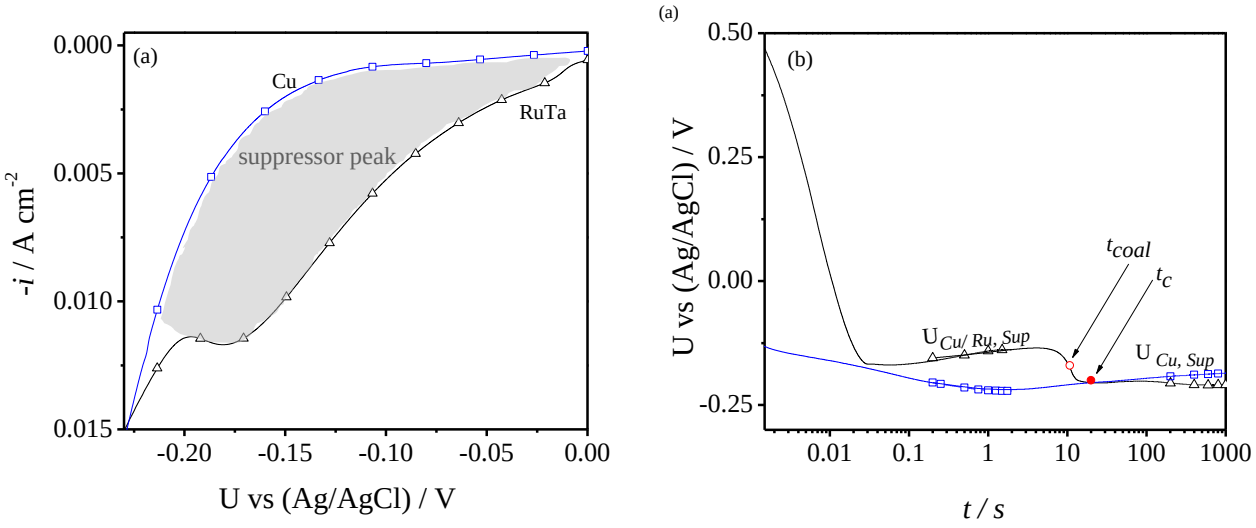

Figure 6.1: Typical (a) current-potential and (b) potential-time responses for copper deposition on (□) Cu and (Δ) RuTa electrodes in solution of 0.6 M $CuSO_4$, 1.4×10^{-3} M HCl, 1.8 M H_2SO_4 and 300 ppm PEG (Mw 4000).

6.2 Experimental details

Copper was electrodeposited onto 1.2 µm thick Cu, 5 nm thick Pt, as-received 2 nm thick RuTa and EC-treated RuTa. Details concerning the experimental set-up and substrate description can be found in Chapter 2. The electrochemical treatment on the as-received RuTa electrode was

performed in a solution that contained 10% Vol. H_2SO_4 and at current density of -10 mA cm^{-2} for 60*s*. The different substrates along with their sheet resistance values are summarized in Table 6.1. The current-potential curves in the overpotential deposition (OPD) region were obtained by changing the potential at a rate of 0.02 V s^{-1} from the open-circuit potential (OCP) to -0.5 V vs. Ag/AgCl. The copper UPD region was examined by changing the potential at a rate of 0.1 V s^{-1} from OCP value towards more negative values until $U_{(Cu^{2+}/Cu),eq}$ (0.1 V) is reached, followed by a sweep in the positive direction up to 0.7 V where he Cu UPD layer was completely removed from the electrode surface and zero anodic current was detected. The polarizations were performed at a scan rate of 0.1 V s^{-1} to allow the control of changes in the kinetics of the slow UPD processes which cannot be detected under steady state conditions i.e. at slow scan rates [18]. The copper equilibrium potentials, $U_{(Cu^{2+}/Cu),eq}$ were determined experimentally by OCP measurements in an additive-free 0.6 M $CuSO_4$ solution on the electrodes under investigation subsequent to a surface treatment in the UPD region. For the OCP measurements, the investigated solution was first purged with nitrogen for 10 min, after that the electrodes were polarized at 0.15 V for 5 min under nitrogen purge. The $U_{(Cu^{2+}/Cu),eq}$ was also measured on a Cu electrode under ambient conditions. The galvanostatic experiments were performed at a current density of -5 mA cm^{-2}. The plating solutions contained 0.6 M $CuSO_4 \cdot 5H_2O$ (>98%, Alfa Aesar), 1.4×10^{-3} M HCl (37% Assay, Baker), 1.8 M H_2SO_4 (96% Assay, Baker), and 300 ppm polyethylene glycol (PEG) with Mw 4000 (Sigma-Aldrich). The solution resistance (R_s) was determined from the slope reciprocal in the linear part of *i*-U relationship. The R_s were 4, 13, 39 and 44 Ω for the Cu, Pt, EC-treated RuTa and the as-received RuTa electrodes, respectively. The R_s values obtained from the slope reciprocal in the linear part of I-U relationship were used for the *IR* correction of the *i*-U curves and the galvanostatic transients.

Additional galvanostatic measurements were performed only at the Pt and the as received RuTa electrodes. The galvanostatic transients were further analyzed to elaborate the dependency of N_p on the deposition overpotential. As different kinetics of nucleation and growth were observed for the different electrodes, the galvanostatic deposition was performed under conditions that allowed counting the Cu islands i.e. before coalescence of the Cu islands and with varied solution composition. For the Pt electrode, we used additive-free solutions that contained 1.8 M H_2SO_4 (96% Assay, Baker), 1.4×10^{-3} M HCl (37% Assay, Baker), and 0.05, 0.1 and 0.6 M $CuSO_4 \cdot 5H_2O$ (>98%, Alfa Aesar). The additive-containing solutions contained 0.6 M

$CuSO_4 \cdot 5H_2O$, 1.8 M H_2SO_4, 1.4×10^{-3} M HCl and 300 ppm of different polyether suppressors. The suppressors' concentration was 300 ppm in all cases so that approximately the same concentration of polymer repeating units were obtained. The suppressors used were PEG with Mw 1000 g mol^{-1}, polyoxyethylene methyl ether (Methyl PEG) with Mw 1000 g mol^{-1} and polyoxyethylene cetyl ether (Cetyl PEG) with Mw 1124 g mol^{-1}. The solution resistance (R_s) was again determined from the slope reciprocal in the linear part of *i*-U curves and was 11, 11 and 13 Ω for the 0.05, 0.1 and 0.6 M $CuSO_4$ solutions, respectively. These R_s values were used for the *IR* correction of the galvanostatic transients. Description of the experimental procedure and the solution composition for the as-received RuTa electrode can be found in Chapters 4 and 7 for additive-free solutions with varied [Cu^{2+}] concentration and for additive-containing solutions with different polyether suppressors, respectively. All experiments were performed at room temperature (21° C) and without agitation. For each experiment a fresh sample was used without any further pretreatment. After copper deposition, samples were immediately removed from the solution, rinsed with de-ionized water and dried under nitrogen flow. The copper islands were examined by Scanning Electron Microscopy (SEM Nova 200, FEI). The SEM images were analyzed with Image*J* digital analysis software [19] in order to count the number of copper islands and determine the average diameter. For one data point an average of 3 images were analyzed taken at different spots near the center of the plated area.

Substrate	***Sheet resistance [Ω Sq^{-1}]***
Cu	0.14
Pt	43
EC-treated RuTa	130
As-received RuTa	200

Table 6.1: Sheet resistance values for the different working electrodes under investigation.

6.3 Current-potential characteristics:

Figure 6.2(a) shows current-overpotential curves for copper deposition on Cu, Pt, EC-treated RuTa and as-received RuTa electrodes (empty symbols) in solutions of 0.6 M $CuSO_4$, 1.8 M H_2SO_4, 1.4×10^{-3} M HCl and 300 ppm PEG at a polarization rate of 0.02 V s^{-1}. The curve for a Cu electrode in acidic 0.6 M $CuSO_4$ solution in the absence of PEG is also shown for comparison (full symbols). The overpotential values were determined with respect to the copper equilibrium

potential, $U_{(Cu^{2+}/Cu),eq}$, (0.1 V measured for the additive-free 0.6 M $CuSO_4$ solution) and corrected for the *IR* drop with R_s= 4, 13, 39 and 44 Ω for the Cu, Pt, EC-treated RuTa and as-received RuTa electrodes, respectively:

Equation 6.1:
$$\eta_{IR} = U - U_{(Cu^{2+}/Cu),eq} - IR_s$$

The current-overpotential curves for the Cu electrode in the absence and in the presence of PEG show similar behavior but are shifted with respect to each other: For the Cu electrode in the absence of PEG, the cathodic current density immediately increases strongly when sweeping V from the open-circuit potential ($U_{(Cu^{2+}/Cu),eq}$ = 0.1 V vs. Ag/AgCl) in the negative direction. In the presence of PEG, polarization of about ~ 240 mV is observed due to strong suppression of the deposition current. As a reference point for polarization, the shift in the Cu deposition potential at a current density of -2 mA cm^{-2} was used (i.e. the point where already a steep rise in *i*-U is found in all cases). For the as-received RuTa electrode, a small cathodic current wave appeared before the copper equilibrium potential at 0.1V (not shown). This prewave can be attributed to the underpotential deposition (UPD) of copper on RuTa, as well as to the partial reduction of Cu^{2+} to Cu^{+}, typically seen for noble metals such as platinum, gold and ruthenium [20,21]. As no copper is present yet, the increase in cathodic current is initially slow. The current deviates from the UPD wave (i.e. bulk copper deposition on RuTa starts) around -0.023 V, i.e. ~120 mV more negative than the copper equilibrium potential. The difference between the (steady-state) onset potential for deposition on foreign substrates and the Nernst equilibrium potential is commonly known as the nucleation overpotential, η_{Nucl}, [22]. Subsequent to the initial rise in the current, a suppressor peak appeared at -0.2 V. The charge under this so-called suppressor peak was 0.07 C cm^{-2}, equivalent to about 26 nm of deposited copper. The current-overpotential curve for the EC-treated RuTa electrode was similar in shape as compared to the curve seen for RuTa and showed an initial increase in the current followed by a suppressor peak. For this electrode, the suppressor peak appeared at -0.12 V (~80 mV more positive than the suppressor peak observed on the as received RuTa electrode). The charge under the suppressor peak was 0.025 C cm^{-2}, equivalent to about 9.5 nm of deposited copper. This observation indicated that the Cu islands coalesced faster on the oxide-free EC-treated RuTa electrode compared with the as-received RuTa electrode. The current-overpotential curve for the Pt electrode was similar to that measured at the Cu electrode

in the presence of PEG and no visible suppressor peak was observed. The potentials corresponding with the start of the steep increase in the cathodic current (determined at -2 mA cm^{-2}) along with the equivalent thickness found from the charge associated with the suppressor peak are for all electrodes under investigation, summarized in Table 6.2. The platability of the different substrates under investigation can be evaluated from the *i*-U curves (Figure 6.1). Higher copper island densities and flattening of the particles results in faster coalescence [7]. As the surface conditions affect both the island density and island shape, the shift of the i-η_{IR} curves towards the i-η_{IR} curve recorded for the Cu electrode and the charge under the suppressor peak are also a measure for the platability performance of the resistive surface i.e. substrate which exhibits better Cu platability results in smaller charge under the suppressor peak and faster overlapping of the i-η_{IR} curve for the resistive substrate with the i-η_{IR} curve for the Cu electrode [24, 25].

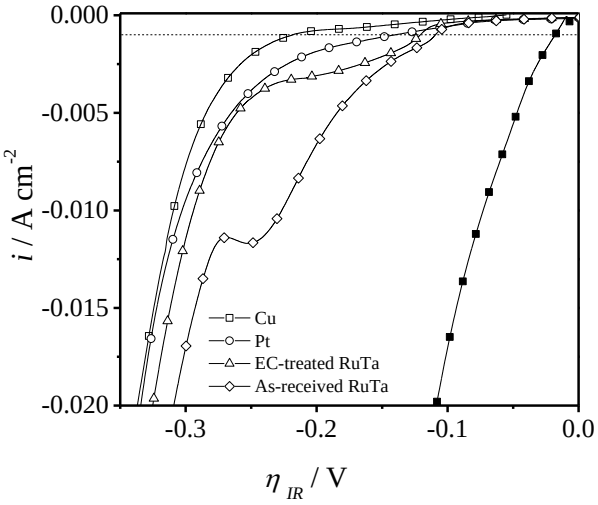

Figure 6.2: (a) Current density, *i*, versus overpotential corrected for *IR* drop, η_{IR}, curves for (□) Cu, (○) Pt, (Δ) EC-treated RuTa and (◊) as-received RuTa electrodes in solutions of 0.6 M $CuSO_4$, 1.8 M H_2SO_4, 1.4×10^{-3} M HCl and 300 ppm PEG at a polarization rate of 0.02 V s^{-1}. As a reference, the curve for a (■) Cu electrode in 0.6 M $CuSO_4$ solution in the absence of PEG is also shown. Only the forward negative scans are shown for clarity. The overpotential was corrected with R_s= 4, 13, 39 and 44 Ω for the Cu, Pt, EC-treated RuTa and as-received RuTa electrodes, respectively.

	U at -2mA cm^{-2}	*eq. thickness from the charge under the "suppressor peak" / nm*
Cu	-0.150	Was not observed
Pt	-0.100	Was not observed
EC treated RuTa	-0.040	9.5
As received RuTa	-0.023	26

Table 6.2: Copper deposition potential at -2 mA cm^{-2} (representative for the start of steep increase in the cathodic current) and equivalent copper layer thickness corresponding to the charge under the suppressor peak as obtained from the current-potential curves on the electrodes under investigation at a polarization rate of 0.02 V s-1. All measurements were performed from solutions that contained 0.6 M $CuSO_4$, 1.8 M H_2SO_4, 1.4×10^{-3} M HCl and 300 ppm of PEG (Mw 4000).

Additional current-overpotential measurements were performed in the UPD region for the Pt, EC-treated RuTa and as-received RuTa electrodes in solutions of 1.8 M H_2SO_4, 1.4×10^{-3} M HCl and 300 ppm PEG in the absence (blank solution) and the presence of 0.6 M $CuSO_4$ (Figure 6.3(a-c)). For the as-received RuTa electrode, no significant anodic or cathodic currents were observed in the blank solution (Figure 6.3(a)) indicating that the electrode is inert within this potential range and no significant reduction/oxidation or adsorption/desorption reactions occur on the air-formed oxide. The polarization in the 0.6 M $CuSO_4$ solution revealed a small cathodic current wave (-0.15 mA cm^{-2}) from 0.02 V on towards $U_{(Cu^{2+}/Cu),eq}$. In the reverse scan, no significant anodic currents were observed. Polarization of the EC-treated RuTa electrode in the blank solution (Figure 6.3(b)) resulted in higher cathodic currents in the forward negative scan compared with the as-received RuTa electrode. As no symmetrical anodic currents were observed in the reverse scan, these cathodic currents can be attributed to a reduction rather than to an adsorption reaction. Note that adsorption reactions typically exhibit symmetrical peaks in the reverse scan due to a fixed amount of adsorbed species [23]. Polarization in the blank solution subsequent to a nitrogen purge for 10 min (not shown) resulted in a decrease in the cathodic current density. This indicates that these currents can be attributed to oxygen reduction on the oxide-free EC-treated electrode. The polarization from the 0.6 M $CuSO_4$ solution revealed a bigger cathodic current wave (-0.6 mA cm^{-2}) which appeared 50 mV more positive compared with the as-received RuTa electrode. In the reverse scan, higher anodic currents were observed compared with the as-received RuTa electrode. As no such currents were observed in the reverse scan from the blank solution, these currents can be attributed to stripping of the Cu UPD layer formed in the forward scan on the oxide-free EC-treated electrode. Similar to the EC-treated

RuTa electrode, polarization of the Pt electrode in the blank solution resulted in higher cathodic currents ascribed to oxygen reduction. In the reverse scan higher anodic currents compared with the blank solution were observed that can be ascribed to stripping of the Cu UPD layer. Integration of the cathodic charge after subtracting the cathodic currents observed in the blank solutions for these electrodes yields a charge of 0.36, 0.4 and 0.008 mC cm^{-2} for the Pt, EC-treated RuTa and as-received RuTa electrodes, respectively. Previous studies on Cu UPD on monocrystalline Pt and Ru electrodes reported on charges of 0.42 and 0.6 mC cm^{-2}, assigned to close-packed monolayers (ML) of Cu(111)/Pt(111) and Cu(111)/Ru(0001), respectively [24,25]. Note that the number of ad-atoms in the monolayer is equal to that of surface atoms of the support. This explains the higher charge that is found with the hexagonal close-packed (hcp) structure of Ru than with the face-centered cubic (fcc) structure for Pt [20]. The electrodes under investigation have a polycrystaline structure. In this work, the charge related with deposition of 1 ML on a monocrystalline surface is taken as a reference value to evaluate the coverage of the Cu UPD layer. The charge obtained from integration of the cathodic currents in Figure 6.3(a-c) was hence normalized to the charge assigned with 1 ML. With this reference, monolayers of *ca.* 0.85, 0.68 and 0.02 ML were found for the Pt, EC-treated RuTa and as-received RuTa electrodes, respectively. Figure 6.3(d) shows Cu OCP curves as a function of time for all the electrodes under investigation in additive-free 0.6 M $CuSO_4$ solution subsequent to polarization at 0.15 V for 5 min in solution of 0.6 M $CuSO_4$, 1.8 M H_2SO_4, 1.4×10^{-3} M HCl and 300 ppm PEG under nitrogen purge. For comparison, OCP measurements for Cu and as-received RuTa electrodes (dashed lines) in the additive-free 0.6 M $CuSO_4$ solution are also shown. All electrodes revealed an OCP of 0.1 V vs. Ag/AgCl, indicating a Faradaic component. For the as-received RuTa, the OCP was stable for ~0.3*s* and then immediately increased again to 0.6 V indicating that the deposited copper dissolves in the acid $CuSO_4$ solution. The OCP on the EC-treated RuTa electrode was stable for ~100*s* while the OCP on the Pt electrode was stable for ~320*s*. These observations imply that on the Pt electrode the Cu UPD layer covered a larger fraction compared with the EC-treated RuTa electrode while the Cu UPD coverage for the as-received RuTa electrode was poor. As the Cu UPD layer serves as a wetting layer for bulk Cu deposition, the i-η_{IR} curves shown in Figure 6.2(a) are affected accordingly i.e. higher UPD coverage resulted in polarization of the i-η_{IR} curves and faster coalescence of the Cu islands.

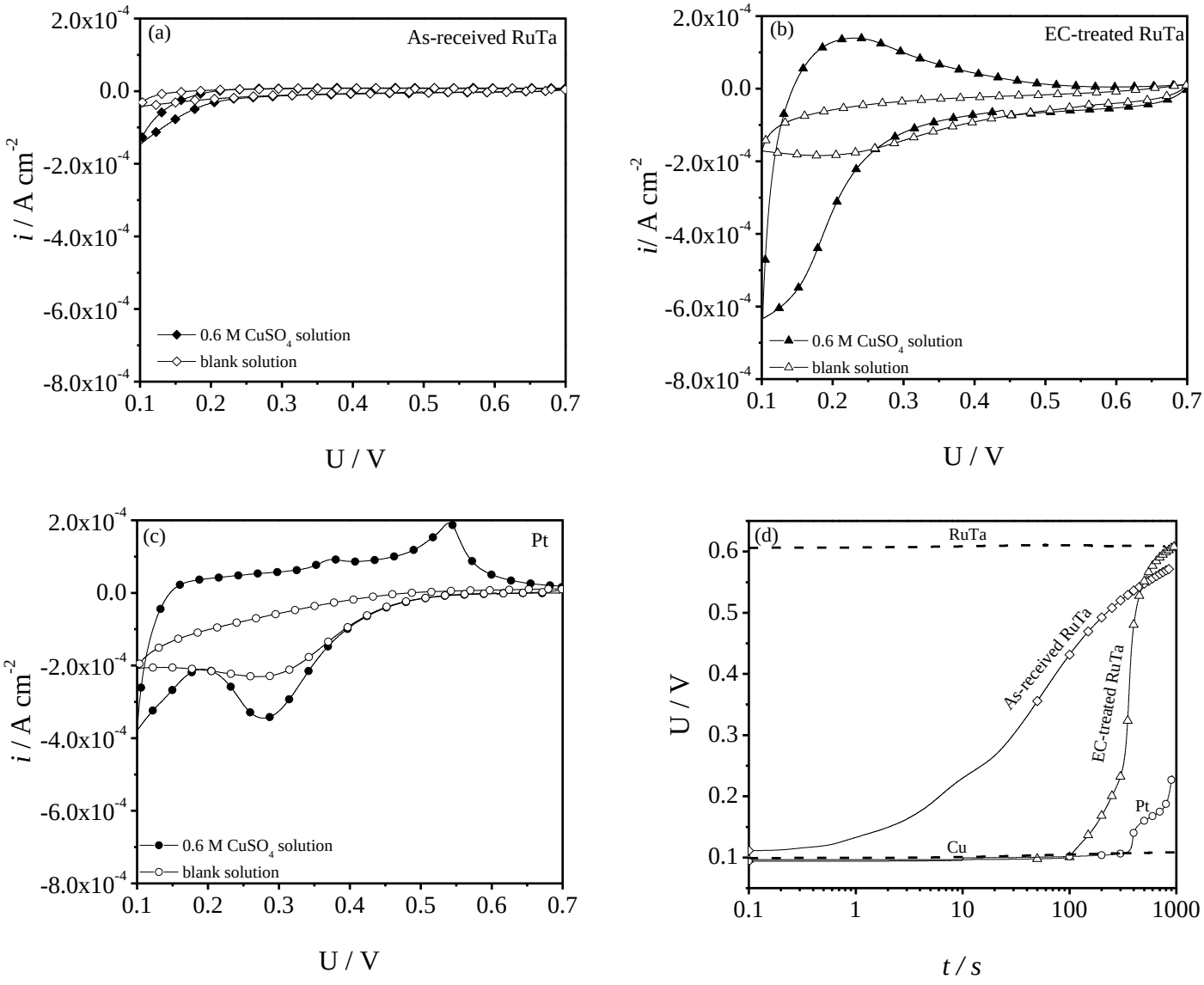

Figure 6.3: Current density, *i*, versus potential for (a) as-received RuTa (b) EC-treated RuTa and (c) Pt electrodes in solutions of 1.8 M H_2SO_4, 1.4×10^{-3} M HCl and 300 ppm PEG in the absence (blank solution) and the presence of 0.6 M $CuSO_4$ at polarization rate of 0.1 V s^{-1} (d) Cu OCP as a function of time for all the electrodes under investigation in an additive-free 0.6 M $CuSO_4$ solution subsequent to polarization at 0.15 V under nitrogen purge for 5 min in a solution of 0.6 M $CuSO_4$, 1.8 M H_2SO_4, 1.4×10^{-3} M HCl and 300 ppm PEG. For comparison, OCP measurements on Cu and on as-received RuTa electrodes (dashed lines) in the additive-free 0.6 M $CuSO_4$ solution are also plotted.

6.4 Galvanostatic deposition

Figure 6.4 shows the overpotential corrected for *IR* drop, η_{IR}, as a function of time during galvanostatic copper deposition, measured at the as-received RuTa, EC-treated RuTa and Pt electrodes in solutions of 0.6 M $CuSO_4$, 1.4×10^{-3} M HCl, 1.8 M H_2SO_4 and 300 ppm PEG (Mw 4000) at current density of -5 mA cm^{-2}. For comparison, a transient recorded at the Cu electrode is also plotted. For the as-received RuTa, the overpotential dropped from OCP to a first potential value, $\eta_{Cu/RuTa,\ Sup}$. The potential remained there for about ~10*s* after that time an additional drop to a second plateau, at a potential $\eta_{Cu,\ Sup}$ was observed. In this second plateau the transient coincided with the transient recorded at the Cu electrode. The transient, recorded at the EC-treated RuTa electrode exhibited similar behavior as the as-received RuTa electrode, however shorter residence time was observed in the $\eta_{Cu/RuTa,\ Sup}$ plateau (~0.4*s*). For the Pt electrode, the potential dropped immediately after applying the current and no visible residence time in $\eta_{Cu/RuTa,\ Sup}$ plateau was observed. The inflection points in the transients, occurrig after a time t_{coal}, (empty circles in Figure 6.4) were observed at 10.8, 1.8 and 0.2*s* resulting in a q_{coal} of 54, 9 and 1 mC cm^{-2} (corresponding with equivalent thickness of 20, 3.3 and 0.4 nm) for the as-received RuTa, EC-treated RuTa and Pt electrodes, respectively. The critical time, t_c, (full circles in Figure 6.4) at which a closed Cu film is achieved, decreased from 20 to 4.3 and 1.1*s*, and corresponded with a closed Cu film with thickness of 37, 6.7 and 2 nm for the as-received RuTa, EC-treated RuTa and Pt electrodes, respectively.

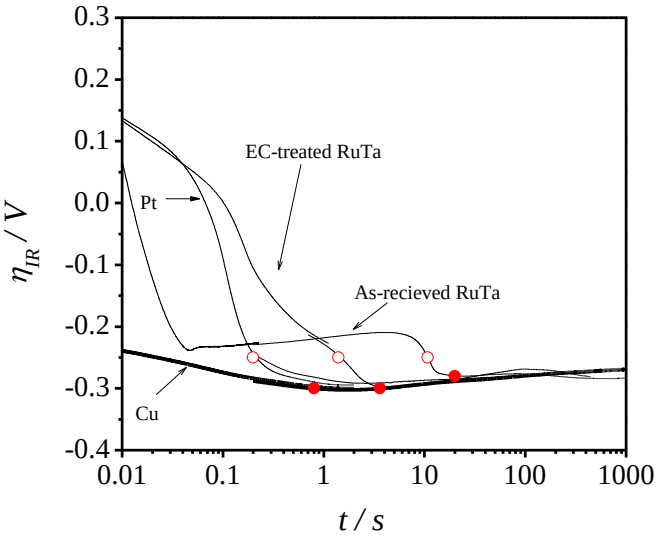

Figure 6.4: η_{IR}-time curves for galvanostatic copper deposition on as-received RuTa, EC-treated RuTa and Pt electrodes in solutions of 0.6 M $CuSO_4$, 1.8 M H_2SO_4, 1.4×10^{-3} M HCl and 300 ppm PEG Mw 4000 at current density of -5 mA cm^{-2}. For comparison, a transient recorded at the Cu electrode is also plotted. t_{coal} and t_c are marked as empty and full circles, respectively. The η_{IR} is given with respect to the copper equilibrium potential (0.1 V vs. Ag/AgCl) for the 0.6 M $CuSO_4$ additive-free solution and corrected for IR_s drop with R_s = 4, 13, 30 and 44 Ω for the Cu, Pt, EC-treated RuTa and as-received RuTa, respectively.

Figure 6.5 shows top-down SEM images of Cu islands electrodeposited on the as-received RuTa, EC-treated RuTa and Pt electrodes from a solution of 0.6 M $CuSO_4$, 1.8 M H_2SO_4, 1.4×10^{-3} M HCl and 300 ppm PEG (Mw 4000) at a current density of -5 mA cm^{-2} for a deposition charge density of 0.01 C cm^{-2}. For the as-received RuTa electrode, the island density was 9×10^{9} cm^{-2} and flattened-shaped (x > 12) islands were observed. The EC treatment of the as-received RuTa electrode resulted in a significant increase in the island density and most of the RuTa surface was covered with copper. Note that the SEM images for the EC-treated electrode were obtained after 2*s*, this is around t_{coal} as observed from the η_{IR}-t transient for the EC-treated RuTa in Figure 6.4. At the Pt electrode, no visible islands were observed. In the inset of Figure 6.5(c), a top-down SEM image is shown of Cu islands electrodeposited on the Pt electrode at a lower current density of -2.5 mA cm^{-2} but for the same deposition charge. The Cu islands, with average diameter of ~15 nm covered most of the Pt surface. As an increase in the current density leads to an increase in the number of nucleation sites and smaller islands it follows that at a current density of -5 mA cm^{-2} the islands (with diameter smaller than 15 nm) already coalesced

and the closed Cu film with small roughness could not be observed with our SEM, having 10 nm resolution.

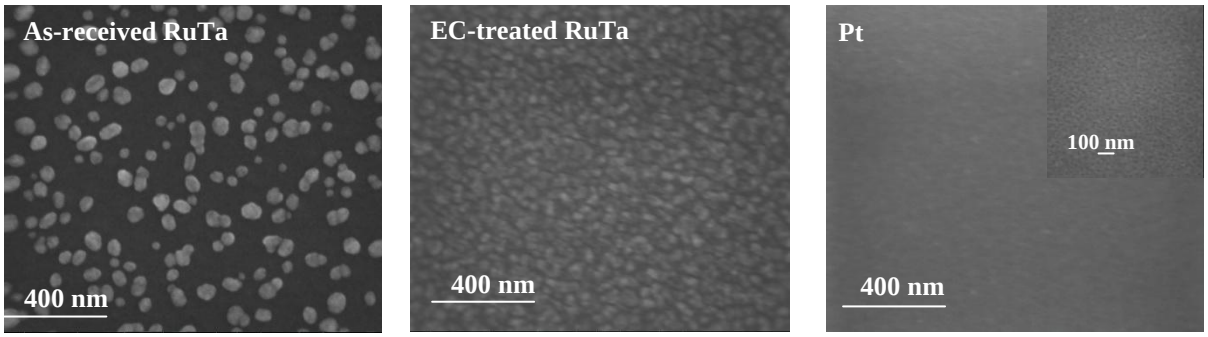

(a) (b) (c)

Figure 6.5: Top-down SEM images of Cu islands electrodeposited on (a) as-received RuTa (b) EC-treated RuTa and (c) Pt from solution of 0.6 M $CuSO_4$, 1.8 M H_2SO_4, 1.4×10^{-3} M HCl and 300 ppm PEG (Mw 4000) at current density of -5 mA cm^{-2} for deposition charge density of 0.01 C cm^{-2}. In the inset of Figure 6.5(c), a top-down SEM image of Cu islands electrodeposited on the Pt electrode at current density of -2.5 mA $cm^{-2\ 2}$ for deposition charge density of 0.01 C cm^{-2}, illustrating the coalescence of the Cu islands.

Figure 6.6 shows cross-sectional SEM images of electrodeposited Cu islands on the as-received RuTa, EC-treated RuTa and Pt electrodes. Since coalescence in the PEG-containing solution occurs fast on the Pt electrode (Figure 6.5) the deposition was performed from an additive-free solution to have a clear view on the island shape. The deposition experiments were therefore performed from a solution of 0.6 M $CuSO_4$, 1.8 M H_2SO_4 and 1.4×10^{-3} M HCl at a current density of -2.5 mA cm^{-2} for deposition charge of 0.01 mC cm^{-2}. From Figure 6.6(a) it can be seen that spherical-like islands were observed on the as-received RuTa surface. The EC treatment resulted in hemispherical islands (Figure 6.6(b)) while flattened islands were observed on the Pt surface (Figure 6.6(c)). Indeed, the presence of a Cu UPD layer can promote not only nucleation but also allows lateral growth of the Cu islands.

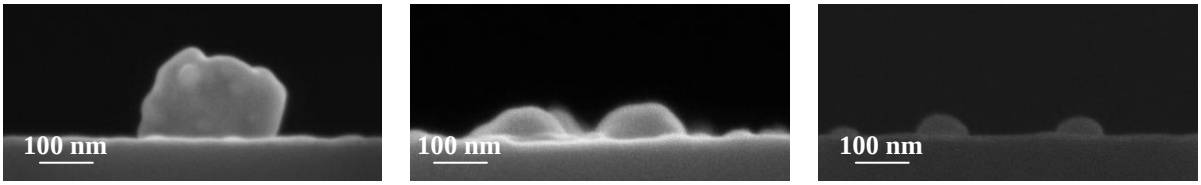

(a) (b) (c)

Figure 6.6: Cross-sectional SEM images of Cu islands electrodeposited on (a) as-received RuTa (b) EC-treated RuTa and (c) Pt from a solution of 0.6 M $CuSO_4$, 1.8 M H_2SO_4 and 1.4×10^{-3} M HCl at current density of -2.5 mA cm^{-2} for deposition charge density of 0.01 C cm^{-2}.

6.5 Correlation between electrochemical parameters and Cu island density

In Chapter 4, it was shown that for the as-received RuTa electrode an exponential relationship exists between N_p and -(η_{IR}-η_{IRNucl}), independent of cupric ion concentration and current density. In Chapter 5, it was shown that this relationship holds also in the case where different polyether suppressors are present in the plating solution. The general equation describing the relationship between N_p and -(η_{IR}-η_{IRNucl}), is given by:

Equation 6.2:
$$N_p(\eta) = N_{\eta_{IR},Nucl}\exp\left(-\frac{\alpha F}{RT}\left(\eta_{IR}-\eta_{IR\,Nucl}\right)\right)$$

where η_{IRNucl} is the steady-state overpotential for nucleation, $N_{\eta IR,Nucl}$ is the pre-exponential factor assigned to the island density at $\eta=\eta_{Nucl}$ and $\frac{\alpha F}{RT}$ relates to the electrode kinetics [11].

The relationship between N_p and -(η_{IR}-η_{IRNucl}), found for the as-received RuTa electrode was:

Equation 6.3:
$$N_p(\eta) = 1\times10^{7}\exp\left(-32\left(\eta-\eta_{Nucl}\right)\right)$$

Note that the value of -0.025 V refers to the steady state overpotential for nucleation as obtained from a current-potential scan on the as-received RuTa electrode at a polarization rate of 0.001 V s^{-1}. This relationship provides a general equation for N_p as a function of the overpotential on the as-received RuTa electrode, irrespective of Cu^{2+} concentration, nature of the suppressor and current density. This hence means that, the island density can be estimated solely from the actual

overpotential for copper deposition, seen during galvanostatic measurements, and irrespective of the solution composition and the deposition current. This N_p dependency on -(η_{IR}-η_{IRNucl}) is shown in Figure 6.7 (line b). In order to test whether this generalization also holds in the case of other substrates, the island density, N_p, was plotted as a function of -(η_{IR}-η_{IRNucl}) for the Pt electrode. The result can be seen in Figure 6.7 (line a) with η_{IRNucl} = -0.010 V. Note that the value of -0.010 V refers to η_{IRNucl} as obtained from the current-potential curve at the Pt electrode at a polarization rate of 0.001 V s^{-1}. The η_{IR} values were extracted from the potential-time curves such as those shown in Figure 6.4 for copper deposition on Pt from solutions with different composition (different Cu^{2+}, different current densities and different polyether molecules). The η_{IR} values correspond to the copper deposition potential in the plateau $\eta_{Cu/RuTa}$ (for the additive-free solutions with different Cu^{2+} concentrations) and in the plateau $\eta_{Cu,\ Sup/RuTa}$ (for solutions that contained different polyether molecules). Note that the overpotential shifts towards more positive values when the effective surface area of the copper islands increases i.e. during growth [5]. The effective copper surface area is affected by the island shape (Figure 6.6) as well as by the number of nuclei (Figure 6.5) which can be different from one substrate to another [11]. Thus, to have a fair comparison between different substrates, one should consider the overpotential after taking into account the effective copper surface area [11]. Therefore, to have fair comparison between the data on Pt and the data, extracted for the as-received RuTa electrode, η_{IR} values that correspond to the same effective surface area of copper islands A_{Cu}=0.19 were selected (for detail, see Appendix). It was found that, similar to the as-received RuTa electrode, also at the Pt electrode, the island density, N_p, followed an exponential relationship with -(η_{IR}-η_{IRNucl}), irrespective of solution composition and current density. Thus, also for the Pt electrode, the island density can be estimated solely from the actual overpotential for copper deposition seen during galvanostatic measurements and irrespective of solution composition and deposition current. Interestingly, the linear relationship between lnN_p and -(η_{IR}-η_{IRNucl}), found at the Pt electrode, had the same slope as the as the lnN_p and -(η_{IR}-η_{IRNucl}) curve, measured at the as-received RuTa electrode with $\frac{\alpha F}{RT}$=32. However, the pre-exponential factor, $N_{\eta IR,Nucl}$ increased by a factor of 88: from 1.0×10^{7} cm^{-2} for the as-received RuTa to 8.8×10^{8} cm^{-2} at the Pt electrode. Since copper deposition proceeds on the existing Cu islands, the electrode kinetics are expected to be similar on the two substrates. Also the increase in $N_{\eta IR,Nucl}$ is expected for substrates with

smaller η_{IRNucl} i.e. which can promote Cu nucleation (higher N_p). Two additional data points (empty squares marked in a gray area and indicated with an arrow from line b to line a) are added for the RuTa electrode EC-treated in a solution of tetrafluoroboric acid (HBF_4). The pretreatment step with tetrafluoroboric acid (HBF_4) led to a significant increase in the island density [26]. For example, for 0.1 and 0.6 M $CuSO_4$ solutions, the island density was 1.8×10^9 and 5.6×10^8 cm^{-2} for galvanostatic deposition at -2.5 mA cm^{-2} which corresponded to an overpotential of 0.078 and 0.046 V, respectively. i.e. to $-(\eta_{IR}- \eta_{IRNucl})$ of 0.068 and 0.036 with η_{IRNucl} of -0.01 V. The position of these two data points next to line a, describing the N_p dependency on the overpotential for Pt, confirms that surface treatment of the RuTa surface before electrodeposition can lead to nucleation kinetics that are similar to those on Pt. Choosing the right preparation for the RuTa surface can thus be beneficial for DP applications.

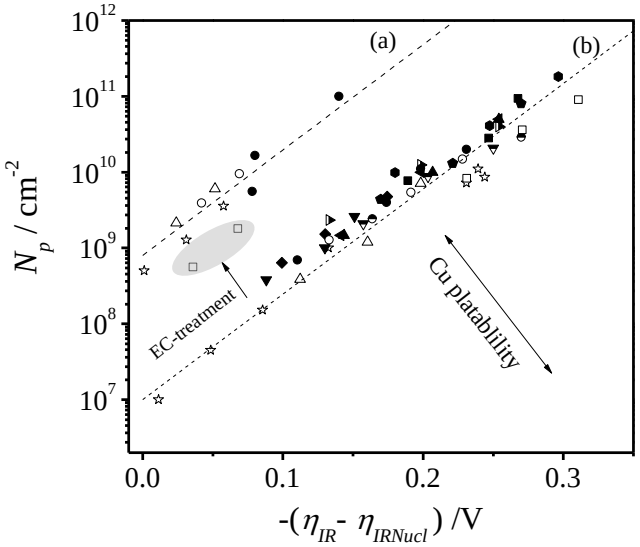

Figure 6.7: Cu island density, N_p, as a function of the corresponding $-(\eta_{IR}-\eta_{IR\ Nucl})$ with η_{Nucl} = -0.01 V for Pt (line a) and η_{Nucl} = -0.025 V for RuTa (line b). The η_{IR} was determined with respect to copper OCP and corrected for *IR* drop. η_{IR} was determined from the galvanostatic transients for A_{Cu}=0.19. The deposition experiments were performed from solutions with varied composition (see experimental part of this of Chapters 4 and 5). Note that the empty symbols relate to deposition from additive-free solutions while full symbols relate to deposition from solutions that contained different polyether molecules. The N_p dependency on $-(\eta_{IR}- \eta_{IRNucl})$ is given according to the following: $N_p(\eta) = 1\times10^7 \exp(-32(\eta-\eta_{Nucl}))$ for as-received RuTa and $N_p(\eta) = 8.8\times10^8 \exp(-32(\eta-\eta_{Nucl}))$ for Pt.

6.6 Summary

The platability of as-received RuTa alloy, EC-treated RuTa alloy and Pt electrodes in copper containing solutions was studied using cyclic voltammetry and potentiometry. The three substrates under investigation exhibited different nucleation and growth kinetics. It was found that a higher coverage of the electrode surface after Cu UPD resulted in higher N_p, lateral island growth and consequently to a faster coalescence of the Cu islands. The coalescence of the Cu islands on the electrodes can be captured in the current-potential and potential-time responses, recorded in the solutions with suppressor additive. Combination of the potentials observed in the galvanostatic transients and the nucleus densities, determined with SEM analysis allowed to determine the relationship between N_p and the overpotential for the Pt and the as-received RuTa substrates, after taking into account the effective copper surface area. This relationship provides a general equation that allows to estimate N_p at a given overpotential for a given substrate, irrespective to solution composition and deposition parameters. Importantly, this equation allows to estimate the platability of different substrates with respect to Pt and as-received RuTa substrates based solely on the overpotential seen in the galvanostatic transient.

[1] J.A. Venables, G.D.T. Spiller, M. Hanbucken, Nucleation and growth of thin films, Reports on Progress in Physics 47 (1984) 399.

[2] E. Budevski, G. Staikov, W.J. Lorenz, Electrocrystallization Nucleation and growth phenomena, Electrochimica Acta 45 (2000) 2559.

[3] G. Oskam, P.M. Vereecken, P.C. Searson, Electrochemical deposition of copper on n–Si/TiN, Journal of the Electrochemical Society 146 (1999) 1436.

[4] T.P. Moffat, M. Walker, P.J. Chen, J.E. Bonevich, W.F. Egelhoff, L. Richter, C. Witt, T.Aaltonen, M. Ritala, M. Leskel, D. Josella, Electrodeposition of Cu on Ru barrier layers for damascene processing, Journal of the Electrochemical Society 153 (2006) C37.

[5] D. Grujicic, B. Pesic, Electrodeposition of copper: the nucleation mechanisms, Electrochimica Acta 47 (2002) 2901.

[6] N. Jourdan, L. Carbonell, N. Heylen, J. Swerts, S. Armini, A. Maestre Caro, S. Demuynck, K. Croes, G. Beyer, Z. Tökei, S. Van Elshocht, E. Vancoille, Evaluation of metallization options for advanced Cu interconnects application, ECS Transactions 34 (2011) 515.

[7] A. Radisic, P.M. Vereecken, P.C. Searson, F.M. Ross, The morphology and nucleation kinetics of copper islands during electrodeposition, Surface Science 600 (2006) 1817.

[8] A. Radisic, A. C.West, and P. C. Searson, Influence of additives on nucleation and growth of copper on n-Si (111) from acidic sulfate solutions, Journal of the Electrochemical Society, 149(2), (2002) C94.

[9] A. Radisic, J. G. Long, P. M. Hoffmann, and P. C. Searson, Nucleation and growth of copper on TiN from pyrophosphate solution. Journal of The Electrochemical Society, 148(1) (2001) C41.
[10] A. Radisic, Y. Cao, P. Taephaisitphongse, A.C. West, P.C. Searson, Direct Copper Electrodeposition on TaN Barrier Layers, Journal of the Electrochemical Society 150 (2003) C362.
[11] M. Nagar, A. Radisic, K. Strubbe, P.M. Vereecken, The effect of cupric ion concentration on the nucleation and growth of copper on RuTa seeded substrates, Electrochimica Acta 92 (2013) 474.
[12] P. Andricacos, H. Deligianni, W.J. Horkans, K.T. Kwietniak, M. Lane, S.G. Malhotra, F.R. McFeely, C. Murray, K.P. Rodbell, P.M. Vereecken, U.S. Patent Application Pub. No. US20050199502 A1.
[13] P.M. Vereecken, P. Andricacos, H. Deligianni, K.T. Kwietniak, C. Andricacos, U.S. Patent Application Pub. No. US2006/0163055 A1.
[14] N. Jourdan, L. Carbonell, N. Heylen, J. Swerts, S. Armini, A. Maestre Caro, S. Demuynck, K. Croes, G. Beyer, Z. Tökei, S. Van Elshocht, and E. Vancoille, Evaluation of Metallization Options for Advanced Cu Interconnects Application, ECS Transactions, 34 (1) (2011) 515.
[15] Y.K. SIEW, J. Versluijs, E. Kunnen, I. Ciofi, W. Alaerts, H. Dekkers, H. Volders, S. Suhard, A. Cockburna, E. Sleeckx, E. Van Besien, H. Struyf, M. Maenhoudt, A. Noorib, D. Padhib, K. Shahb, V. Gravey , G. Beyer, Integration of 20 nm half pitch single damascene copper trenches by spacer-defined double patterning (SDDP) on metal hard mask (MHM), In Interconnect Technology Conference (IITC), IEEE, (2010) 1.
[16] A. Radisic, M. Nagar, K. Strubbe, S. Armini, Z. El-Mekki, H. Volders, W. Ruythoorena, and P. M. Vereecken, Copper Plating on Resistive Substrates, Diffusion Barrier and Alternative Seed Layers, ECS Transactions, 25 (27) (2010) 175.
[17] M. Nayak, S. Ezhilvalavan, T.Y. Tseng, In Handbook of thin film materials, Nalwa H.S. Ed. Academicpress. San Diego, 2001 Vol.3, p121.
[18] A.I. Danilov, E.B. Molodkina, Yu.M. Polukarov, V. Climent, J. Feliu, Active centers for Cu UPD–OPD in acid sulfate solution on Pt(111) electrodes, Electrochim. Acta 46 (2001) 3137.
[19] http://rsb.info.nih.gov/ij/docs/index.html.
[20] Herrero, E., Buller, L. J., & Abruna, H. D. (2001). Underpotential deposition at single crystal surfaces of Au, Pt, Ag and other materials. Chemical Reviews,101(7), 1897-1930.
[21]Y. Zhang, L. Huang, T. N. Arunagiri, O. Ojeda, S. Flores, O. Chyan and R. M. Wallace, Underpotential deposition of copper on electrochemically prepared conductive ruthenium oxide surface, Electrochemical and solid-state letters, 7(9) (2004) C107.
[22] B. R. Scharifker and G. Hills, Theoretical and experimental studies of multiple nucleation**,** Electrochimica Acta 28 (1983) 879.
[23] Instrumental methods in electrochemistry, D. Pletcher Ed. (2001) P 207.
[24] E. Herrero, L. J. Buller and H. D. Abrun, Underpotential Deposition at Single Crystal Surfaces of Au, Pt, Ag and Other Materials, Chem. Rev., 101, (2001) 1897.
[25] C. Nguyen, Van Huong and M. J. Gonzalez-Tejera, Underpotential deposition of copper and silver on polycrystalline ruthenium electrodes, Journal of Electroanalytical Chemistry and Interfacial Electrochemistry, 244 (1) (1988) 249.
[26] A. Radisic, P.M. Vereecken, U.S. Patent Application Pub. No. US2010/0273323 A1.

PART 2: FILLING OF 20 NM FEATURES BY DIRECT PLATING.

CHAPTER 7: IN-SITU FORMATION OF THE CU SEED LAYER WITH SIMULTANEOUS FEATURE-FILL OF 20 NM FEATURES.

This Chapter describes experiments and results of copper deposition on a Pt blanket wafer and on a RuTiN patterned wafer with 20 nm trenches from an optimized low Cu^{2+} concentration solution. The focus is on the formation of a Cu seed layer followed by the filling of 20 nm trenches from the same solution. Results from TOF-SIMS and AFM measurements show that a closed Cu film with thickness of about ~2.5 nm is obtained on a Pt blanket wafer subsequent to copper deposition from the low Cu^{2+} concentration solution. Successful filling of the 20 nm trenches was achieved by a two-steps galvanostatic deposition process where first ~2.5 nm thick Cu seed was formed at current density of -5 mA cm^{-2} followed by filling of the trenches at a constant current density of -1.2 mA cm^{-2}.

7.1 Introduction

The principle, requirements and challenges of the direct plating (DP) process were extensively described in the previous Chapters. In order to implement DP in the damascene process for the filling of sub-30 nm features, the coalescence of the nuclei into a continuous copper layer (in-situ formed wet seed) should be fast, followed by bottom-up copper fill of the features which is indistinguishable from feature fill with a conventional copper seed layer. Since the first condition for successful implementation of the DP is the formation of an in-situ Cu seed, the plating bath composition was first optimized to enable fast coalescence of the Cu islands (i.e. high island density, N_p, and quasi 2D growth) occurs. In Chapters 3-5, it was demonstrated that the formation of a thin continuous Cu film is highly dependent on the composition of the plating bath and on the deposition parameters. The results presented in these Chapters showed that high N_p, and thus fast coalescence, is achieved with high current densities (between -5 and -10 mA cm^{-2}) and acidic 0.01 M $CuSO_4$ solutions (pH = -0.2). In addition, it appeared that there was an optimal concentration of Cl^- ions and suppressor, for which the best suppression performance was obtained.

In Chapter 6, it was shown that the addition of polyether molecules to the plating bath resulted in even higher values of N_p. The best performance in terms of high N_p and fast coalescence was achieved with the addition of polyoxyethylene cetyl ether (Cetyl PEG) to a 0.6 M $CuSO_4$ solution (see Chapter 6). Note that the concentration of 0.6 M $CuSO_4$ was chosen to be able to visualize features such as t_{coal} and t_c in the galvanostatic transients (since the nucleation rate for the solutions with a low Cu^{2+} concentration is fast, these features are not visible in the galvanostatic transient in these solutions). However, since the effect of Cu^{2+} concentration on the N_p does not change with the addition of polyether molecules (see Chapter 5) it is expected that even faster coalescence will be achieved in the acidic 0.01 M $CuSO_4$ solution with Cetyl PEG added. From Chapters 3-6 it was concluded that the optimal composition for the plating bath is: 0.01 M $CuSO_4$ 0.14×10^{-3} HCl, 1.8 M H_2SO_4 and 500 ppm of Cetyl PEG. In what follows, we call this the optimized low Cu^{2+} concentration solution. However, not only the bath chemistry affected N_p but also the condition of the RuTa surface. In Chapter 7 we demonstrated that electrochemical (EC) treatment of the RuTa surface resulted in a significant increase in N_p and faster coalescence.

The scope of this Chapter is to investigate the seed formation and the filling capability of the optimized low Cu^{2+} concentration solutions with different additives. The work is divided into two parts: in the first part, the minimum thickness of a closed Cu film that can be obtained from the low Cu^{2+} concentration solution is investigated. For this purpose, Pt was used as a model substrate (i.e. to resemble a treated surface with no native oxide layer). It must be noted that the determination of the minimum thickness of such a thin layer, obtained from low Cu^{2+} solutions on a pre-treated surface with no native oxide layer, is challenging since these small thicknesses cannot be detected with SEM (having 10 nm resolution). These small thicknesses also cannot be determined by electrochemical techniques since t_{coal} and t_c are not observed in the galvanostatic measurements). In the second part of this Chapter, copper deposition experiments were performed on the patterned RuTiN wafer. The deposition experiments were performed within a range of current densities to allow both formation of in-situ seed (-0.8 to -10 mA cm^{-2}) and the fill of the 20 nm trenches (-0.8 to -1.6 mA cm^{-2}).

7.2 Experimental details

Copper was electrodeposited onto 5 nm Pt blanket wafers and patterned RuTiN wafers with 20 nm trenches (patterned SD20). Details concerning the experimental set-up and substrate description can be found in Chapter 2. For the first part of the experimental work; copper was deposited on a 5 nm Pt electrode from a solution that contained 0.01 M $CuSO_4 \cdot 5H_2O$ (>98%, Alfa Aesar), 0.14×10^{-3} M HCl (37% Assay, Baker), 1.8 M H_2SO_4 (96% Assay, Baker) and commercial Via-Form (VF) additives (suppressor, accelerator and leveler) provided by Enthone. The additive concentration was 4 ml l^{-1} VF suppressor, 8.5 ml l^{-1} VF accelerator and 2.5 ml l^{-1} VF leveler. The galvanostatic experiments were performed at current densities between -2.5 and -10 mA cm^{-2}. The charge, associated with copper deposition was determined subsequent to the galvanostatic deposition by polarizing the potential at a rate of 0.02 V s^{-1} from 0 V towards 0.7 V vs. Ag/AgCl. At this potential, all the deposited Cu was removed from the electrode surface and the anodic current was zero. TOF-SIMS measurements were performed in order to determine the minimum thickness, needed to obtain a closed Cu film. The TOF-SIMS data was obtained using an IONTOF IV instrument. Surface spectra were recorded in both positive and negative ion detection modes using a bunched 15kV Ga analysis beam (~0.7pA) rastered over an 200×200 μm^2 area. AFM measurements were performed in order to determine the roughness of the electrodeposited copper layer on the Pt surface. The AFM measurements were performed with a Bruker Dimension Icon-PT atomic force microscope with Peak Force Tapping mode. The RMS values were determined with WSxM digital analysis software [1] subsequent to AFM measurement scanning areas of 5 µm × 5 µm. Details concerning the mode of operation and working principle of TOF-SIMS and AFM can be found in Chapter 2.

The experiments concerning the seed formation were performed on a RuTiN patterned wafer from a solution containing 0.01 M $CuSO_4$, 0.14×10^{-3} M HCl, 1.8 M H_2SO_4, 500 ppm Cetyl PEG and 1 ppm SPS at current densities of -0.8, -2.5, -5 and -10 mA cm^{-2} for charge density of 0.0068 C cm^{-2} (equivalent Cu film thickness of 2.5 nm). Prior to copper deposition, the sample was treated with 10%Vol. H_2SO_4 at a current density of -10 mA cm^{-2} for 60*s*. The filling experiments were performed at low current densities, ranging between -0.5 and -1.6 mA cm^{-2} from solutions of 0.01 M $CuSO_4$, 0.14×10^{-3} M HCl, 1.8 M H_2SO_4 1 ppm SPS and 500 ppm polyethylene glycol (PEG) Mw 1000 and Cetyl PEG Mw 1124.

7.3 Minimum Cu island coalescence thickness-part I

Figure 7.1 shows tilted SEM images of Cu islands electrodeposited on 5 nm Pt at current densities of -2.5 and -10 mA cm^{-2}, for a charge corresponding to an equivalent thickness of 2.5 nm. At -2.5 mA cm^{-2}, the N_p was 5×10^{10} cm^{-2} and Cu islands with average diameter of about ~ 20 nm were observed on the Pt surface. At -10 mA cm^{-2} no visible islands were observed. From the former Chapters, it could be concluded that an increase in the current density leads to an increase in the number of nucleation sites and smaller islands. As such, at a current density of -10 mA cm^{-2} the islands are expected to coalesce. In an attempt to observe islands at deposition current of -10 mA cm^{-2}, deposition was performed at different times , corresponding to equivalent thicknesses of 0.7 and 3.8 nm. However, the Cu islands were still not visible with SEM (not shown), having 10 nm resolution capability. Since the Cu islands deposited at -10 mA cm^{-2} were not visible with SEM, other techniques, such as TOF-SIMS and AFM were used in order to determine at which thickness the Cu islands coalesced and a closed Cu film was obtained on the Pt surface.

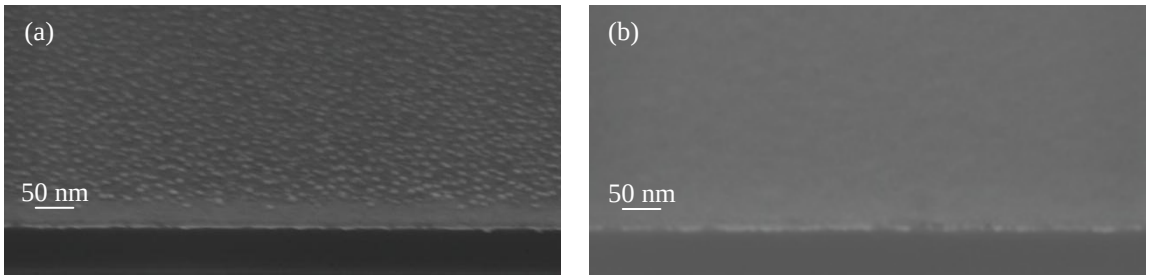

Figure 7.1: Tilted SEM image of Cu islands electrodeposited on 5 nm Pt from solution of 0.01 M $CuSO_4$, 1.8 M H_2SO_4, 0.14×10^{-3} M HCl and VF additives (suppressor, accelerator and leveler) at current density of (a) -2.5 mA cm^{-2} and (b) -10 mA cm^{-2} for deposition charge density of 0.01 C cm^{-2}.

Figure 7.2 shows TOF-SIMS mass spectrum in negative mode for Cu electrodeposited on Pt for different thicknesses. The negative secondary ions, coming from the uppermost surface (10 Å) of the Cu/Pt samples, provide indication for the surface composition. Thus, the TOF-SIMS mass spectrum shown in Figure 7.2 can confirm the thickness at which a closed Cu film was obtained on the Pt surface (for more information on the TOF-SIMS technique see Chapter 2). The TOF-SIMS measurements were performed subsequent to copper deposition of different

Cu thicknesses of 0.7, 2.5, 3.8 and 20 nm on top of the 5 nm Pt electrode from the solution of 0.01 M $CuSO_4$, 1.8 M H_2SO_4, 0.14×10^{-3} M HCl and VF additives (suppressor, accelerator and leveler) at a current density of -10 mA cm^{-2}. The intensity of negative secondary ions only for the bare Pt electrode is added as a reference. For this reference Pt electrode, two ^{195}Pt isotope peaks were observed at *m/z*= 194.3 and 194.7 [2]. Deposition of 0.7 nm Cu on top of the Pt electrode resulted in a decreased Pt signal and a ^{63}Cu isotope peak appeared at *m/z*= 63.9 [3]. After deposition of 2.5 and 3.8 nm Cu on top of the Pt electrode the peak for ^{63}Cu was again observed, whereas a small signal associated with the Pt substrate was still observed. Further increase of the thickness of the deposited Cu layer to 20 nm revealed a peak for ^{63}Cu only, while no signals were recorded for the Pt substrate. It must be remarked that with a copper layer of 3.8 nm, deposited at lower current density of -5 mA cm^{-2} most of the Pt surface was covered and Cu islands with an average diameter of about ~10 nm were observed on the Pt surface (SEM image is not shown). Therefore, the small signals observed for the Pt substrate for the 2.5 and 3.8 nm thick Cu layer, deposited at -10 mA cm^{-2}, may be due to the roughness created during the coalescence of the Cu islands (see schematic illustration in Figure 7.3(b). In order to investigate this hypothesis we conducted AFM measurements to follow the roughness profile for different copper thicknesses.

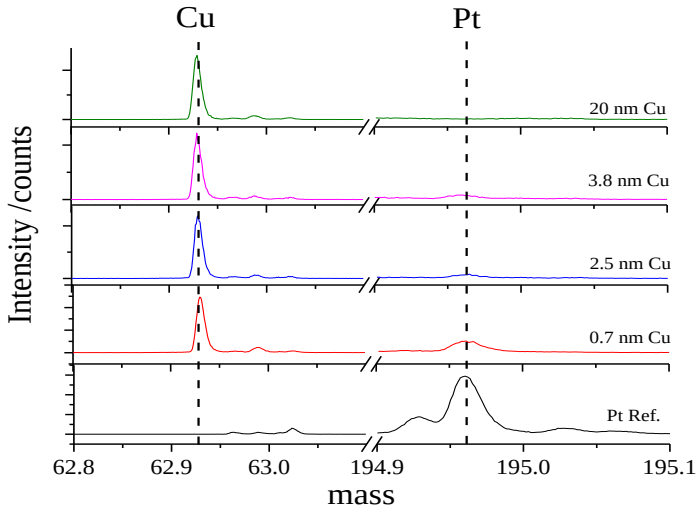

Figure 7.2: TOF-SIMS mass spectrum in negative mode for Cu electrodeposited on Pt for different Cu thicknesses. The measurements were performed subsequent to copper deposition on top of a 5 nm Pt electrode from a solution of 0.01 M $CuSO_4$, 1.8 M H_2SO_4, 0.14×10^{-3} M HCl and VF additives (suppressor, accelerator and leveler) at a current density of -10 mA cm^{-2} for Cu thicknesses of 0.7, 2.5, 3.8 and 20 nm.

Figure 7.3(a) shows the RMS values of Cu layers with different thickness (such as those shown in Figure 7.2), electrodeposited on Pt. An RMS of 0.8 nm was found for the reference Pt electrode. Deposition of 0.7 nm Cu led to an increase in the RMS value to 1.3 nm for the Cu/Pt surface. Further increase of the Cu thickness to 2.5 and 3.8 nm resulted in a decrease in the RMS values to 1 and 0.9 nm respectively. Figure 7.3(b) shows a schematic illustration of the Cu/Pt surface to explain the complementary results obtained from the AFM and TOF-SIMS measurements. The RMS of the sample with 0.7 nm Cu increased compared to the Pt reference surface, because 3D Cu islands were deposited on the Pt surface. These Cu islands did not coalesce yet (Figure 7.3(b2)) and thus a Pt signal was detected during the TOF-SIMS measurements (Figure 7.2). The RMS values for the Cu layers with thickness of 2.5 nm and 3.8 nm confirmed that under these circumstances the Cu islands coalesced and grew decreasing the roughness of the layer. The small Pt signals that are still observed for these thicknesses can then result from areas where the effective Cu thickness is low (note that 1 nm~ 4 monolayers). The roughness profile of the Cu/Pt surface, together with the TOF-SIMS measurements confirm that a closed Cu film was already obtained with 2.5 nm thick layers.

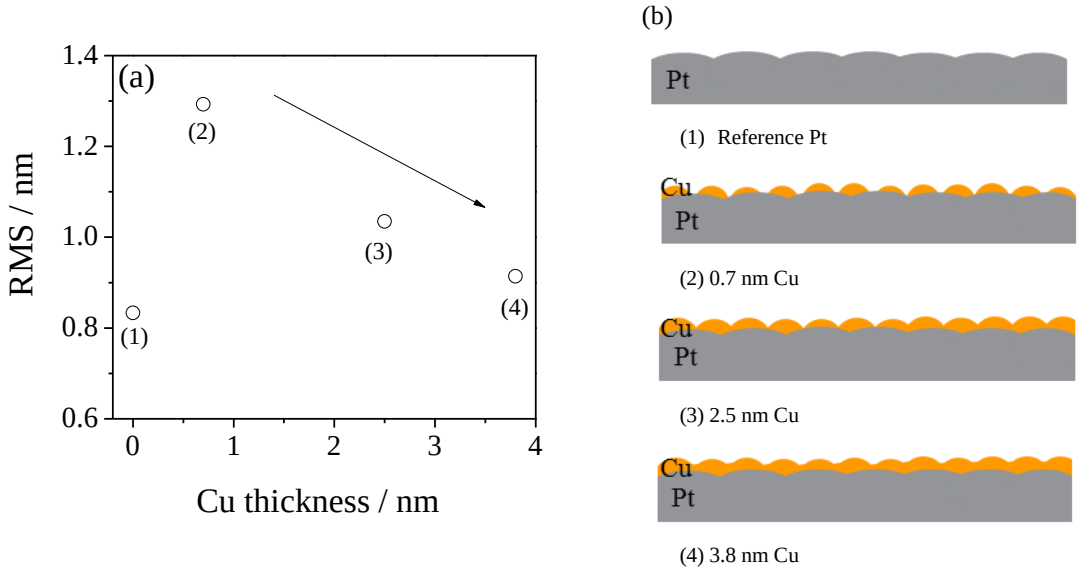

Figure 7.3: (a) RMS values versus thickness of the Cu layer on Pt (b) schematic presentation of the Cu/Pt surface roughness for deposited Cu layers with thicknesses of 0.7, 2.5 and 3.8 nm.

7.4 Formation of the seed layer and the filling of 20 nm features-part II

7.4.1 Optimum conditions for in-situ seed formation

Seed formation experiments were performed on the patterned RuTiN wafer from a solution of 0.01 M $CuSO_4$, 0.14×10^{-3} M HCl, 1.8 M H_2SO_4, 500 ppm Cetyl PEG and 1 ppm SPS at current densities of -0.8, -2.5, -5 and -10 mA cm^{-2} . The seed layer had an equivalent thickness of 2.5 nm. Prior to copper deposition, the sample was treated with 10%Vol. H_2SO_4 at current density of -10 mA cm^{-2} for 60*s*. Figure 7.4 shows tilted SEM images for 20 nm and 60 nm space lines, subsequent to deposition of 2.5 nm seed at current densities of -0.8 mA cm^{-2} and -2.5 mA cm^{-2}. The seed formation at -0.8 mA cm^{-2} resulted in visible Cu islands with average diameter of about ~25 nm that covered the whole sample surface (i.e. high N_p). The deposition at -0.8 mA cm^{-2} did not result in the formation of a continuous Cu seed layer. Consequently, the Cu islands blocked the 20 nm trenches and prevented further fill. For the seed formation at -2.5 mA cm^{-2}, fast coalescence inside the 20 nm trenches was likely achieved as no islands were observed on the surface with SEM. The seed formation at current densities of -5 and -10 mA cm^{-2} exhibited similar behavior i.e. no Cu islands were visible subsequent to the seed formation (not shown). Therefore, the seed formation should occur within this current range if one wants to have void-free filling.

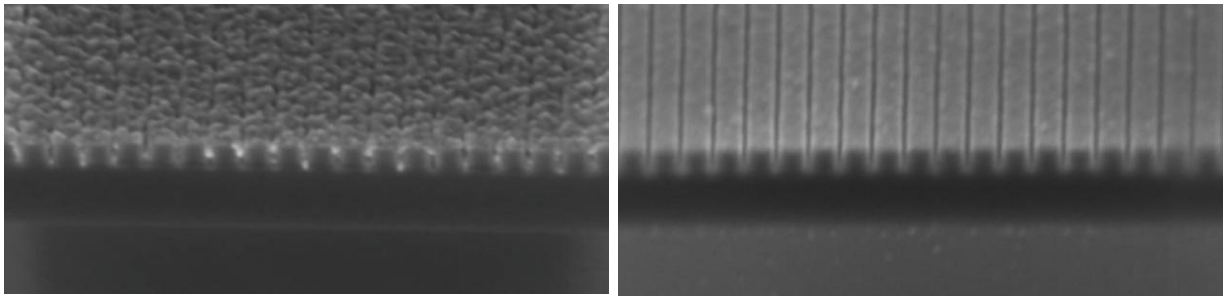

(a) (b)

Figure 7.4: Tilted SEM images of a RuTiN surface with 20 nm wide trenches with 60 nm spacing subsequent to deposition of 2.5 nm seed at (a) -0.8 mA cm^{-2} and (b) -2.5 mA cm^{-2}. Before deposition, an electrochemical clean of the RuTiN surface was performed with 10%Vol. H_2SO_4 at -10 mA cm^{-2} for 60*s*. Deposition experiments were performed from a solution of 0.01 M $CuSO_4$, 0.14×10^{-3} M HCl, 1.8 M H_2SO_4, 500 ppm Cetyl PEG and 1 ppm SPS.

Figure 7.5 shows the current efficiency for copper deposition as a function of the thickness of the electrodeposited Cu layers. The theoretical diffusion-limited current as a function of time can be calculated from the Cottrell equation:

Equation 7.1:
$$i = \left(\frac{nFD^{1/2}C_b}{\pi^{1/2}t^{1/2}} \right)$$

where $n=2$ for the number of electrons in the reaction, $F=96485$ C mol^{-1} for Faraday's constant, C_b is the bulk concentration (1×10^{-5} mol cm^{-3}) and D is the diffusion coefficient (7.52×10^{-5} mol cm^{-3} for 1×10^{-5} mol cm^{-3} Cu^{2+} given by the empirical relationship found by Quickenden and Jiang [4]). From simulated current–time responses obtained from Equation 7.1 (not shown), the transferred charge can be calculated by integrating the area under the curve for partial copper deposition current. The current efficiency can then be calculated theoretically by dividing the charge for copper deposition by the partial charge for copper deposition as obtained from Cottrell equation. At -0.8 mA cm^{-2} the current efficiency for deposition of 2.5 nm Cu is 100% . However, as shown in the SEM image in Figure 7.4(a) the current density of -0.8 mA cm^{-2} did not result in the formation of a continuous Cu seed layer. At a current density of -10 mA cm^{-2} it is very likely that an in-situ seed of 2.5 nm can be formed. However, from Figure 7.5 it follows that the current efficiency is very low at this current density. For this reason, the current densities of -2.5 and -5 mA cm^{-2} were selected for seed formation.

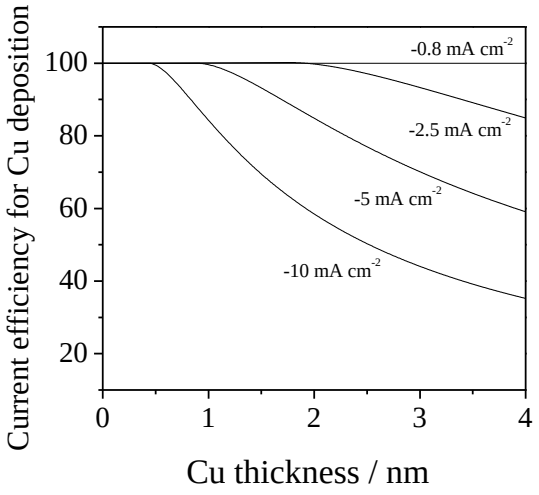

Figure 7.5: Current efficiency for copper deposition as a function of Cu thickness..

7.4.2 Optimum conditions for filling

Filling experiments were performed subsequent to seed formation at current densities of -2.5 and -5 mA cm^{-2} (for equivalent Cu film thickness of 2.5 nm). Prior to the seed formation, the sample was treated with 10%Vol. H_2SO_4 at a current density of -10 mA cm^{-2} for 60*s*. The filling experiments were performed from the same bath used for the seed formation (see §7.4.1) in the current density range between -0.5 and -1.6 mA cm^{-2}. This density range was chosen to assure 100% deposition efficiency (see Figure 7.5) and to avoid copper depletion inside the 20 nm features. From SEM measurements (not shown), it appeared that the filling experiments performed subsequent to the seed formation at current density of -2.5 mA cm^{-2} failed and defects and voids were present in the 20 nm features. Figure 7.6 shows cross-sectional SEM images of the 20 nm trenches, subsequent to a deposition of 2.5 nm seed at -5 mA cm^{-2}, that was followed by filling at current densities of (a) -1.2 mA cm^{-2} and (b) -1.6 mA cm^{-2}. From the figure it can be seen that voids are observed when a current density of -1.6 mA cm^{-2} was applied, while at -1.2 mA cm^{-2} void-free filling of the 20 nm features was achieved. These observations imply that the seed layer, formed at -2.5 mA cm^{-2}, was not continuous or too rough. Hence, the filling experiments subsequent to the seed formation at -2.5 mA cm^{-2} failed while the filling experiments subsequent to the seed formation at -5 mA cm^{-2} resulted in formation of an in-situ seed layer that allowed void-free filling.

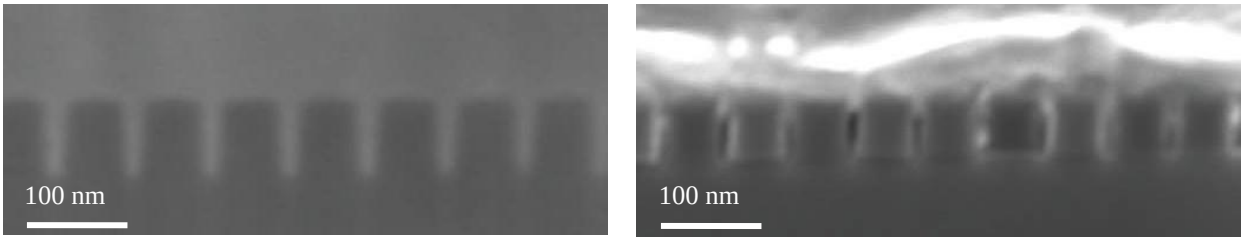

(a) (b)

Figure 7.6: Cross-sectional SEM images of a RuTiN surface with 20 nm wide trenches with 60 nm spacing, subsequent to deposition of 2.5 nm Cu seed at -5 mA cm^{-2} followed by fill at (a) -1.2 mA cm^{-2} and (b) -1.6 mA cm^{-2}. Deposition experiments were performed from a solution of 0.01 M $CuSO_4$, 0.14×10^{-3} M HCl, 1.8 M H_2SO_4 1 ppm SPS and 500 ppm Cetyl PEG Mw 1124. Before the experiments, an electrochemical clean of the RuTiN surface was performed with 10% Vol. H_2SO_4 at -10 mA cm^{-2} for 60*s*.

7.4.3 The effect of the suppressor additive

In order to investigate the contribution of the suppression to the seed formation and to the fill of the 20 nm trenches, additional seed formation and filling experiments were performed, similar to those described above but with PEG Mw 1000 added to the solution (instead of Cetyl PEG). Figure 7.7 shows cross-sectional SEM images of the 20 nm trenches subsequent to deposition of 2.5 nm seed at -5 mA cm^{-2} followed by filling at -1.2 mA cm^{-2} from a solution of 0.01 M $CuSO_4$, 0.14×10^{-3} M HCl, 1.8 M H_2SO_4 1 ppm SPS and 500 ppm (a) PEG Mw 1000 or (b) Cetyl PEG Mw 1124. The suppressors have similar Mw which corresponds to the same number of ether groups and thus possible anchor or attachment points to the copper surface through chloride bridges – see Chapter 5) but with no end group (in the case of PEG) and a longer cetyl ($-(CH_2)_{15}-CH_3$) end group (in the case of Cetyl PEG). It was observed that the fill of the 20 nm trenches, performed with the solution that contained PEG (Mw1000) failed in this respect that severe defects were observed. From the SEM images it was seen that most of the trenches were not filled and that most of the deposition occurred outside the trenches. This implies that the experiment failed already in the early stage of seed formation. Deposition with Cetyl PEG (with an alkyl end group) however resulted in void-free filling. These results confirm the need of strong suppression for both the seed formation and the fill of small features by direct plating (see also Chapter 5).

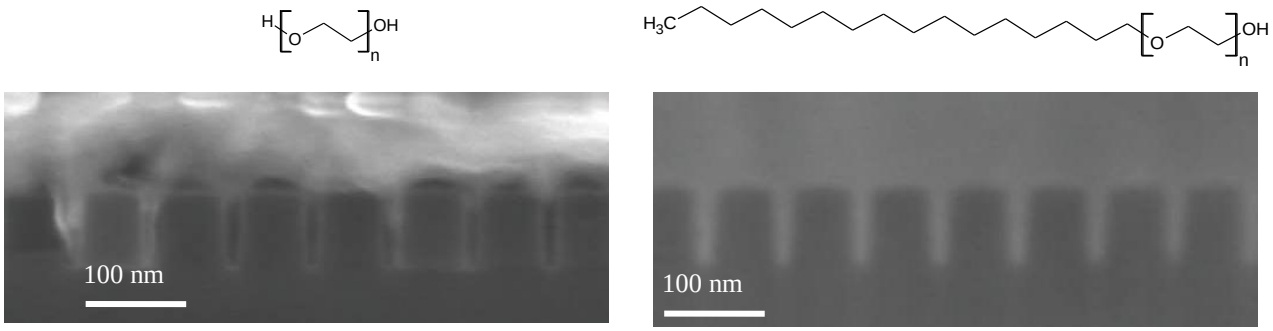

Figure 7.7: Cross-sectional SEM images of a RuTaN surface with 20 nm wide trenches with 60 nm spacing, subsequent to deposition of 2.5 nm seed at -5 mA cm^{-2} followed by fill at -1.2 mA cm^{-2}. Deposition experiments were performed from a solution of 0.01 M $CuSO_4$, 0.14×10^{-3} M HCl, 1.8 M H_2SO_4 1 ppm SPS and 500 ppm (a) PEG Mw 1000 and (b) Cetyl PEG Mw 1124. Before the experiments, an electrochemical clean of the RuTiN surface was performed with 10% Vol. H_2SO_4 at -10 mA cm^{-2} for 60*s*.

7.5 Summary

The seed formation and filling capability of the optimized low Cu^{2+} concentration solutions was investigated. Different surface techniques, applied subsequent to deposition experiments on Pt from the optimized solution, showed that the minimum thickness to obtain a closed Cu film was 2.5 nm. Deposition experiments performed on the patterned RuTiN wafer demonstrated that formation of a continuous thin in-situ seed is essential for efficient further filling. Filling experiments in the presence of different suppressors demonstrated the need to have strong suppression for effective seed formation and fill. From the work presented in this Chapter it is concluded that successful filling of 20 nm trenches can be achieved with a low Cu^{2+} concentration solution that contained Cetyl PEG. The global process of seed formation and filling was performed in two deposition steps and occurred with the same solution. Optimal conditions for in-situ seed formation were found to be a deposition current of -5 mA cm^{-2}, and a layer thickness equivalent to 2.5 nm while the optimal condition for filling corresponded to a current density of -1.2 mA cm^{-2}.

[1] http://www.nanotec.es/products/wsxm/index.php
[2] T. Laiho and J.A. Leiro, TOF-SIMS study of 1-dodecanethiol adsorption on Au, Ag, Cu and Pt surfaces. Surface and Interface Analysis, 40(1), (2008) 51.
[3] X. Zeng and S. Bruckenstein, Polycrystalline gold electrode redox behavior in an ammoniacal electrolyte: Part II. A parallel RRDE, EQCM and TOF-SIMS study of copper underpotential deposition, Journal of Electroanalytical Chemistry, 461(1) (1999) 143.
[4] T.I. Quickenden and X. Jiang, Electrochimica Acta 29 (1984) 693.

SUMMARY AND PERSPECTIVES

The main goal of the present work was to perform a fundamental study on the electrochemical nucleation and growth of copper on RuTa in order to gain insight in the conditions in which direct plating can be implemented in the damascene process. The study covers : technical as well as scientific aspects of the process. In the technical part, the conditions that allow fast coalescence of the Cu islands into a continuous < 3nm Cu film are optimized. This optimizing involved first of all modifying the concentration of the inorganic components (Cu^{2+}, H_2SO_4 and Cl^-) in the solution, studying their individual contribution to the nucleation and growth process and following their contribution to the nucleation and growth processes in the presence of other components. For example, the Cl^- ions revealed dual contribution to the nucleation and growth processes in the absence and the presence of an organic additive. Besides the effect of inorganic compounds, The effect of different polyether molecules was also studied. In this part of the thesis, it was demonstrated how the suppression strength can be modified by changing the molecular weight and structure of the organic compounds. Further, the effect of the condition of the RuTa surface on the nucleation and growth processes was studied. It appeared that a surface pre-treatment of the substrate results in an oxide-free surface, which in turn promotes nucleation and is hence beneficial for direct plating applications. After optimizing the conditions under which a high N_p can be achieved it was demonstrated that, on a Pt surface, the coalescence thickness can be as low as 2 nm when deposition occurs from a low Cu^{2+} concentration solution. Note that the Pt substrate, having a native oxide-free surface, resembles a pre-treated RuTa surface. This observation implies that filling by direct plating would be feasible on pre-treated Ru-based substrates, even for 10 nm features. In this study, the filling of 20 nm features from the same acidic plating bath by direct plating was also demonstrated.

In the scientific part of this thesis, the electrochemical deposition of copper on RuTa, Pt and Cu from acidic $CuSO_4$ solutions under galvanostatic conditions was investigated. The potential-time responses were recorded and analyzed for different bath composition (different Cu^{2+} and polyether suppressors), different current densities and for different surface conditions. To be able to compare between so many parameters, such as different bath composition, different surface conditions or deposition currents, we needed to consider overpotential and not potential. It was demonstrated that the overpotential for deposition is related to the effective surface area of

the Cu islands and thus changes in time due to the growth of the copper nuclei. It should be noted that for a given experiment, performed under different conditions, the effective Cu surface area is different due to different N_p and island shape. It was therefore necessary, to find a reference point that, for all the experiments, corresponds to the same effective Cu surface area. It was shown that for all cases, and irrespective of the deposition current and composition of the bath composition, an exponential relationship exists between the N_p and the overpotential if the same surface area is considered. The correlation between the island density and the overpotential is one of the most fascinating observations in this work. Two general equations, one for Pt and one for RuTa are presented. These equations demonstrate that the density of the copper islands is a function of the overpotential only (even though the experiments were performed under different conditions). This overpotential, for a given substrate, can be manipulated by the bath composition or by the deposition parameters in order to better control the N_p. In addition, it was shown that the relationship between $\ln N_p$ and overpotential for different substrates such as Pt and RuTa followed the same slope, $\frac{\alpha F}{RT}$, while the value of the pre-exponential factor, $N_{\eta,Nucl}$ was higher. Since the slope, $\frac{\alpha F}{RT}$, refers to the electrode kinetics (i.e. copper deposition on copper), it is expected the N_p-η relationship for other substrates would show a similar behavior i.e. a same value of $\frac{\alpha F}{RT}$ and different $N_{\eta,Nucl}$. These equations are unique and beneficial for direct plating as they enable to predict the N_p based solely on the overpotential, determined from the galvanostatic transients.

This work provides valuable insight into the nucleation and growth processes of copper on RuTa and covers technical as well as scientific aspects. However, there are still some challenges to overcome when bringing the process to a wafer scale. The real challenge in the implantation of DP in the damascene process lays in the combination of the terminal effect and the nucleation and growth of copper into a coalesced or closed film across the whole 300 mm wafer. Since the overpotential changes with wafer radius, N_p is also dependent on the wafer radius. Once N_p is high enough and the Cu islands coalesce, a copper ring with a nucleation front sweeps over the surface from the wafer edge (where the electrical contact is) to the center of the wafer. In this research, the formation of an in-situ Cu seed layer and the fill of 20 nm features from the same solution (i.e. with the optimized low Cu^{2+} concentration solution) was demonstrated on a coupon

scale. In order to implement DP in the damascene process, additional experiments on a wafer scale should be performed. These experiments should involve optimization of the current wave in order to find the plating conditions in which ‘in-situ’ Cu seed is formed followed by void-free fill of the small features across the whole wafer.

SAMENVATTING EN BESLUIT

Wegens de continue miniaturisering in de IC technologie werd bij de productie van geïntegreerde schakelingen (IC) aluminium als verbindingsmetaal recent vervangen door koper. Deze integratie van koper gebeurt via zgn. dual damascene plating, een proces waarbij kopermetaal elektrochemisch wordt afgezet op een dunne koperen kiemlaag (ook seed layer genoemd) die op voorhand op het substraat werd aangebracht. Vandaag blijkt echter dat, wegens de steeds verder afnemende dimensies binnen de IC technologie, ook het tot nu gebruikte dual damascene plating proces aan de grenzen van zijn mogelijkheden zit. Er is daarom nood aan alternatieve productieschema's waarin de koperen kiemlaag volledig kan worden geëlimineerd en koper ofwel rechtstreeks wordt afgezet op het substraat of waarbij gebruik gemaakt wordt van alternatieve kiemlagen. Eén van deze alternatieve benaderingen is zgn. "direct plating" (DP) waarbij koper rechtstreeks elektrochemisch afgezet wordt op een dunne, resistieve barrière of op een kiemlaag die bestaat uit alternatief materiaal, en dus niet op een koperen kiemlaag zoals gebruikelijk in het damascene proces.

De elektrodepositie van koper op een niet-koper substraat is een welgekend proces en er is reeds een ruime hoeveelheid informatie voorhanden. Wanneer men binnen de IC technologie de elektrodepositie van koper wil laten doorgaan op wafer-niveau, zijn er echter nog verschillende uitdagingen die moeten worden overwonnen. De elektrodepositie van koper op een niet-koper substraat omvat zowel kiemvormings- als kiemgroeiprocessen en beide spelen een belangrijke rol wanneer op een wafer aanwezige karakteristieke structuren met afmetingen kleiner dan 30 nm moeten worden gevuld. Om dergelijke structuren void-free (zonder holtes) te kunnen opvullen moeten deze structuren allereerst - in-situ – bedekt worden met een dunne, continue koperen film en dit over het gehele oppervlak van de 300 mm wafer. Op deze in-situ gevormde laag kan vervolgens koper elektrochemisch worden afgezet en kunnen de structuren void-free worden gevuld. Een dunne, continue koperen film kan echter slechts bekomen worden wanneer de kiemdichtheid groot genoeg is en wanneer de groei van de kiemen nagenoeg tweedimensionaal doorgaat. Een goede controle over de kiemdichtheid en de kiemgroei is dus essentieel voor een efficiënt direct plating proces.

Om meer inzicht te krijgen in de mogelijkheden om direct plating te implementeren in het damascene process, werd in dit doctoraat een fundamentale studie verricht naar de kinetiek en

het mechanisme van de elektrochemische nucleatie en groei van koper op RuTa elektroden. Deze studie bevat zowel een fundamenteel wetenschappelijk luik als een onderzoek naar meer technische en toepassingsgerichte aspecten van het proces.

In het meer toepassingsgerichte deel van de thesis werd nagegaan wat de optimale omstandigheden zijn voor de vorming van een continue koperfilm met dikte < 3nm op het RuTa substraat. Dit onderzoek spitste zich eerst toe op de invloed van de concentratie van de anorganische componenten (Cu^{2+}, H_2SO_4 en Cl^-) die in het plating bad aanwezig zijn. Nadat de individuele bijdrage van deze componenten op het nucleatie- en groeiproces eerst afzonderlijk werd bestudeerd, werd onderzocht hoe ze reageerden in aanwezigheid van andere reagentia. Zo bleek bv. de invloed van Cl^- ionen sterk verschillend naargelang er wel of geen organisch additief aan het bad was toegevoegd. Nadat het effect van de anorganische bestanddelen op de elektrochemische afzetting was onderzocht werd de rol nagegaan van verschillende polyether moleculen (die optreden als suppressor). Hier bleek dat de suppressiesterkte afhankelijk was van de moleculaire massa en de structuur van de organische verbindingen. Ook de toestand van het RuTa oppervlak bleek een grote rol te spelen in mechanisme en kinetiek van de nucleatie- en groeiprocessen: een voorbehandeling waarbij een oxidevrij RuTa oppervlak verkregen werd gaf de grootste kiemdichtheden en is bijgevolg aangewezen voor direct plating. Nadat de omstandigheden waaronder een hoge nucleatiedichtheid N_p kan verkregen worden waren afgebakend werd aangetoond dat, op een platina oppervak, omstandigheden konden gecreëerd worden waarbij de dikte van de continue koperlaag kon worden gereduceerd tot 2nm. Omdat een oxidevrij Pt oppervlak zich analoog gedraagt als een oxidevrij RuTa oppervlak volgt hieruit dat, mits de geschikte voorbehandeling, direct plating op een RuTa gebaseerd substraat mogelijk is zelfs voor structuren met afmetingen van 10 nm. In dit werk werden effectief structuren van 20 nm void-free gevuld. Dit gebeurde via een twee staps-proces waarbij in de eerste stap koper werd afgezet met een hoge nucleatiedichtheid en in een tweede stap de structuren elektrochemisch werden gevuld. Beide stappen gingen door in hetzelfde plating bad.

In het meer fundamenteel-wetenschappelijk gerichte deel van dit werk werd de elektrochemische afzetting van koper op RuTa, Pt en Cu vanuit zure oplossingen bestudeerd door middel van galvanostatische metingen. De potentiaal-tijd curven werden geanalyseerd voor oplossingen met verschillende samenstelling, voor verschillende aangelegde stroomdichtheden en voor verschillende voorbehandelingen van het elektrode-oppervlak. Om de gegevens onder

verschillende reactieomstandigheden te kunnen vergelijken was het noodzakelijk om de overpotentialen voor nucleatie te beschouwen in plaats van, zoals doorgaans gebeurt, de potentialen. In dit werk werd aangetoond dat de nucleatieoverpotentiaal in relatie staat met het effectieve oppervlak van de koperkiemen tijdens het afzettingsproces. Wegens de groei van de koperkiemen verandert dit effectieve oppervlak in functie van de tijd. Omdat het effectieve oppervlak geassocieerd is met de dichtheid en de vorm van de koperkiemen, en deze laatste sterk afhangen van de experimentele condities, was het in dit werk noodzakelijk een referentiepunt te definiëren dat, voor de verschillende experimenten, correspondeert met een zelfde effectieve koperoppervlak. Er werd aangetoond dat wanneer dezelfde effectieve oppervlakte wordt beschouwd onder alle omstandigheden een exponentieel verband bestaat tussen de kiemdichtheid N_p en de overpotentiaal. De algemeenheid van het verband is één van de meest opzienbarende resultaten die tijdens deze thesis werden vastgesteld.

Zowel voor Pt als voor RuTa wordt het kwantitatief verband uitgedrukt d.m.v. een generieke vergelijking waarmee de kiemdichtheid kan worden berekend bij een gegeven overpotentiaal, onafhankelijk van de omstandigheden waarin de afzetting gebeurt. Aangezien de overpotentiaal waarbij de nucleatie doorgaat voor een gegeven substraat kan worden gemanipuleerd door middel van variaties in de elektrolytsamenstelling en/of de afzetparameters, kan de waarde van de kiemdichtheid tijdens depositie worden gemanipuleerd. Daarnaast werd aangetoond dat wanneer $\ln N_p$ wordt uitgezet ten opzichte van de overpotentiaal, voor de twee substraten Pt en RuTa een zelfde helling, $\frac{\alpha F}{RT}$, werd gevonden, terwijl de waarde van de pre exponentiële factor $N_{\eta,Nucl}$ hoger was in het geval van Pt. Aangezien de helling, $\frac{\alpha F}{RT}$, in verband staat met de elektrodekinetiek (i.e. koper afzetting op koper) wordt een analoog $\ln N_p$-η verband verband verwacht voor andere substraten, nl. eenzelfde waarde $\frac{\alpha F}{RT}$ maar een verschillende waarde voor $N_{\eta,Nucl}$. Deze vergelijkingen zijn enorm belangrijk voor de praktische toepassing van direct plating, omdat ze toelaten om de kiemdichtheid te voorspellen, louter op basis van de overpotentiaal bepaald uit galvanostatische transiënten.

Alhoewel dit werk zowel vanuit fundamenteel als technologisch standpunt waardevolle informatie biedt over het proces van elektrochemische nucleatie en groei van koper op RuTa, zijn er toch nog enkele belangrijke uitdagingen wil men het proces upgraden naar wafer-schaal.

De grootste uitdaging voor het toepassen van direct plating tijdens het damascene process ligt in de combinatie van het zogenaamde terminal effect en de elektrochemische vorming van een gesloten koperfilm over het volledige oppervlak van een 300 mm wafer. Aangezien de overpotentiaal verandert met de straal van de wafer, hangt N_p ook hier van af. Op het ogenblik dat de kiemdichtheid voldoende groot is opdat de koperkiemen overlappen, beweegt een koperen ring met een nucleatiefront over het oppervlak van de rand van de wafer (waar de elektrische contacten zijn) naar het centrum van de wafer. In dit onderzoek werd aangetoond dat het voor relatief kleine oppervlakken mogelijk is in-situ en vanuit dezelfde oplossing kleine structuren met afmetingen van 20 nm te bedekken met een koperen kiemlaag en deze structuren vervolgens void-free te vullen. Om direct plating te implementeren in het damascene proces, is het echter noodzakelijk om ook op wafer schaal de nodige experimenten te verrichten die toelaten de juiste omstandigheden af te bakenen waaronder kleine structuren efficiënt kunnen worden gevuld, maar nu over het volledig waferoppervlak van een 300 mm wafer.

APPENDIX

The partial charge density, q_{Cu} (C cm^{-2}), associated with copper deposition is obtained from Faraday's law:

[A-1] $$q_{Cu} = \frac{nF\rho}{Mw} V_p N_p$$

with ρ=*8.96* g cm^{-3} for the density of dense metallic copper and V_p (cm^{-3}) the volume of a single copper island; $V_p = \frac{\pi d^3}{x}$ where d is the island diameter (cm) and x is a dimensionless factor indicating the shape of the island: x=6 for spherical, x=12 for hemispherical islands and x>12 for flattened shaped islands (Figure A-1), and N_p (cm^{-2}) is the island density determined from SEM analysis.

x=6 x=12 x>12

Figure A-1: Schematic illustration of the shape factor, x, for spherical x=6, hemispherical x=12 and for flattened shaped islands x>12 at coalescence.

The relationship between partial copper charge density and diameter is then given by:

[A-2] $$q_{Cu} = Kd^3 N_p \quad \text{with} \quad K = \left(\frac{\pi nF\rho}{xMw}\right)$$

The geometrical surface area of a single copper island:

[A-3] $$A_{P\ (Cu)} = \frac{6\pi}{x} d^2$$

Substitution of d from [A-2] into [A-3] gives:

[A-3] $$A_{P\ (Cu)} = \frac{6\pi}{x}\left(\frac{q_{Cu}}{KN_p}\right)^{2/3}$$

The effective surface area of total deposited copper i.e. the cumulative area of copper islands per cm^2 of the planar electrode area (effectively dimensionless):

[A-4] $$A_{Cu} = A_{p(Cu)}N_p = \frac{6\pi}{x}N_p^{\ 1/3}\left(\frac{q_{Cu}}{K}\right)^{2/3}$$

The total effective electrode area per cm^2 of planar electrode surface (effectively dimensionless) is the sum of the cumulative area of copper islands (per cm^2 of the planar electrode area) and the area of exposed RuTa (i.e. not covered by copper) per cm^2 of the planar electrode area:

[A-5] $$A_{eff} = (1 - \pi\frac{d^2}{4}N_p) + A_{Cu}$$

The effective surface area of total deposited copper (A_{Cu}) refers only to the surface area of the copper islands while the total effective electrode area includes both deposited and non-deposited areas.

When assuming hexagonal packing (Figure A-2), the coalescence charge density, q_{coal} (C cm^{-2}), can be related to the copper island density, N_p, through:

[A-6] $$N_p^{-1} = \frac{\sqrt{3}}{2}d_{coal}^2$$

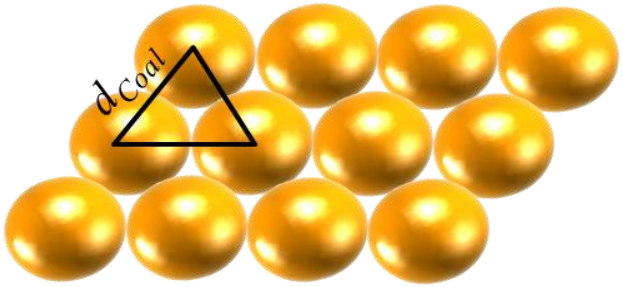

Figure A-2: Cu island diameter at coalescence in case of hexagonal packing.

Substitution of equation [A-2] into [A-6] gives:

[A-7] $$q_{coal} = \frac{n\pi F\rho}{xMw\sqrt{N_p}}$$

The coalescence charge is directly proportional to the coalescence time, t_{coal}, when the current density is kept constant as $q_{Cu} = i \times t$.

The theoretical Cu coverage, θ_{Cu}, (assuming hexagonal packing) can be calculated until t_{coal} is reached according to:

[A-8] $$\theta_{Cu} = N_p^{1/3} \cdot A_{prog,p}$$

Substitution of [A-7] into [A-8] gives:

[A-9] $$\theta_{Cu} = \frac{\pi}{4} \cdot N_p^{1/3} \cdot \left(\frac{q_{Cu}}{K}\right)^{2/3} = \frac{\pi}{4} \cdot N_p^{1/3} \cdot \left(\frac{i}{K}\right)^{2/3} t^{2/3} \quad \text{for } q_{Cu} < q_{coal}$$

and:

[A-10] $$\theta_{Cu} = \frac{\pi}{4} \quad \text{for } q_{Cu} < q_{coal}$$

For the case of flattened hemisphere, the shape factor *x*, can be calculated as following:

[A-11] $$x = \frac{24y^3}{3y^2 + 4} \qquad \text{with} \qquad y = \frac{d_{coal}}{h}$$

where *h* is the particle height and *y* is the fraction of its diameter, as illustrated in Figure A-3.

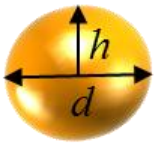

Figure A-3: Schematic illustration of a flattened hemispherical island with height, *h*, and diameter, *d*.

THANK YOU…BEDANKT…..תודה

Assuming that you've been reading the whole thesis[1], I thank you for that and hope you've found it fascinating. If you still have unresolved questions[2], please feel free to contact me[3]. You deserve some of my time in exchange for your time in reading this thesis.

Completing a thesis is a challenge, thanking all those who contributed to it, is even a greater one. Many people were involved in shaping this thesis. I would like to thank them all, including those who are not mentioned here by name.

First, I would like to thank Prof. Dr. Philippe Vereecken. Thanks for believing in my work and me, thanks for your scientific guidance and your valuable advice. Through You, I've learned the importance of understanding things at the fundamental level[4]. It helped me shaping this thesis and enhanced my professional growth tremendously. Deep gratitude is also given to my other two supervisors: Dr. Aleksandar (Alex) Radisic and Prof. Dr. Katrien Strubbe. Alex gave me the freedom to define my own scientific research path. He was always there for me, pushing up, believing and not giving up on me during difficult times. Thanks Alex. Thanks for your patience, your sincere care and your understanding. Katrien gave me a great support, helping me to deal with administrative and scientific issues. I enjoyed having conversations with her and I learned a lot from her great determination and effectiveness. I was so lucky to have three supervisors who allowed me to take what I needed from each one of them to have myself the perfect supervisor. Not many PhD students have such freedom and I am grateful for that. I Thank all the three of You for all You did for me during this journey!

I would also like to thank the persons that, in different ways, contributed to this work: Moussa Alain for the AFM measurements, Dr. Franquet Alexis for the TOF-SIMS measurements and Rudy Caluwaerts for the FIB cuts. I greatly appreciate their professional help.

I would like to thank Gent University for providing me a grant, IMEC for extending it and all the innocent taxpayers for their contribution to research. I would like to thank the members of the examination committee for the time and effort they spent in reading my thesis. I sincerely hope that it was worth your time.

[1] Did you?
[2] I have some myself
[3] maginagar@gmail.com
[4] Very fundamental

I would like to thank the wonderful ECAT group members: Alex, Nancy, Henny, Patrick, Tinne, Liu, Harold, Sofie, Fumihiro, Greet, Mia, Zaid, Kristof, Silvia, Yiting, Lieve, Diana, Kevin and Herbert. How lovely it is that you can come to work with a smile. Each one of them contributed to the final outcome of this thesis with a smile, help in training, giving feedback, providing materials, laughing, telling jocks, giving professional and friendly support. Thanks guys.

I would like also to thank 'Belgium' for introducing me to lekkere frietjes, blauwe chimay[5], mayonaise as a main dish, green fields, minus 20 degrees and walking on snow. The last ~5 years in Belgium made me realize that home is exactly where you, surrounded by people who truly care about You. A huge thanks to all the friends I met along the way who made it unforgettable and special period for me: To Sara (A.K.A. Miss Pina), thanks for your true friendship, for letting me to be myself, for your great sense of humor, for crazy/funny/sad/joy-able night talks. To Hari, for funny moments in the lab, for ice creams and spicy Indian food, for philosophical discussions on science and karma. To Ruth, for her super fantastische vriendschap, for walks in the park, for hope and dreams. To Johan, who lost a lot of "Taki"[6] games and still didn't learn how to lose. To Bertos and Raquelita for their sincere friendship. To Regieneke, my crazy Dutch teacher who became a dear friend, for her comforting words, love and support. To Johannes, thanks for sharing with me the passion for science. For funny mails with Samson en Gert episodes and writing songs together[7]. Thanks to the ladies from 'the ladies' night club[8], Marianna, Elisabeth, Severine, Joelle and Emma, for lovely hanging around together and nice dinners. To my "core" Belgian friends: Hanske, Hilde and Jo. To funny nights, dinners, trips, drinks and laughs. You always smiled to me and were good friends along the way.

Thanks to my "home" friends Ayelet, Shlomit, Noa, Liroz and Julia for their unconditional love. Despite the distance they always hugged me and encouraged me to be a better person. Thanks for your unconditional love and for always being interested in my happiness and wellbeing. A very special mention for Yoni shmucher, who will always have a place in our heart.

Thanks to Kim and the beloved Baumans Family, Lucien, Jose, Dirk, Melissa and Joy who opened their door for me, for being my family, for their love and care throughout good and less good periods. To Dizzy, who shared with me scary nights in the woods, being a truthful friend.

[5] Going to take couple of packs with me
[6] Israeli cards game, you should try it!
[7] With the hits "have you seen Filip?" and " I want to die"
[8] Strong independent women

Last but definitely not the least my family. They say that you don't choose a family. Yet, if I needed to choose one I would have choosen You to be mine. Thanks to my beautiful sisters Nomi, Yafit and Ortal, my wonderful brothers in law Igal and Avi and my sweet nephews Bar, Nuni, Shaked and Rotem for their endless love and support who has been a great source of strength all through this period.

To my parents Shoshana and Zohar. Thanks for allowing me the freedom to choose my own path in life, knowing that this path keeps me away from You[9]. Despite the distance I know that you're proud of me and happy for me that I live my own life. Mom, I've learned a lot from your strength and inner peacefulness. Dad, I hope you're smiling to me, I miss you dearly. You two spared no effort to provide me with the best education and values possible, and for that I will be eternally grateful.

[9] Only physically as we are chained

“I'd rather regret the things I've done than regret the things I haven't done.”

- Lucille Ball (1911-1989)